UNIVERSITÉ DE STRASBOURG

ÉCOLE DOCTORALE DES SCIENCES DE LA VIE ET DE LA SANTE

Institut de Génétique et Biologie Moléculaire et Cellulaire

THÈSE

présentée par :

Samantha CARRILLO-ROSAS

soutenue le : **30 octobre 2017**

pour obtenir le grade de : **Docteur de l'université de Strasbourg**

Discipline/ Spécialité : Aspects moléculaires et cellulaires de la biologie

Etude du rôle de l'Ataxine-7 dans le développement de l'œil et son impact dans la compréhension des pathologies de l'œil et de l'ataxie spinocérébelleuse de type 7.

THÈSE dirigée par :

Dr TROTTIER Yvon	Directeur de Recherche, IGBMC, Inserm U964, UMR 7104 CNRS, Université de Strasbourg

RAPPORTEURS :

Dr HAZAN Jamilé	Directrice de Recherche, Neuroscience Paris Seine
Dr HUMBERT Sandrine	Directrice de Recherche, GIN, Inserm U1216 University Grenoble

---

AUTRES MEMBRES DU JURY :

Dr DEVYS Didier	MCU-PH, IGBMC, Inserm U964, Université de Strasbourg
Dr TORRIGLIA Alicia	Directrice de Recherche, Inserm U872

A mi madre,

A mi abuela,

A Dios

Los tres pilares en mi vida

Les dedico esta Tesis

Acknowledgements

I would like to begin by dedicating this first line to Yvon, my PhD supervisor. I want to thank you for the guided freedom that you gave during the development of this project. Thank you for teaching, helping and challenging me in the past four years.

I also thank my thesis committee: Dr. Sandrine Humbert, Dr. Jamilé Hazan, Dr. Alicia Torriglia and Dr. Didier Devys for accepting to evaluate my work, and taking time out of their busy schedules to read through this manuscript.

Thanks to the Dr. Philippo del Benne, and Dr. Julien Vermot, the jury on my mid-thesis committee, for evaluating my work at pivotal time in my thesis. Their comments helped me to decide the path to pursue for this project and go further.

I would like to thank our engineer Chantal for all the technical support that she provided during the development of this project. I would especially like to thank Chan-Chan because in addition to the technical support (really appreciated) as the engineer, you were also my lawyer, my accountant, my guarantor, my translator but above all you were my FRIEND, and I literally wouldn't be here without you. Thank you Chan Chan ♥!

I am very grateful to all the people that helped me during the development of the project. Thanks to all the lab members (present and former), for the nice discussions we had and all what I learned from you! I would also like to include the members of the team Vermot, especially Stéphane, Emily and Marina for all the advice, help and for sharing protocols and ideas. Last but not least, a gigantic thank you to Cristelle Golzio, your guidance for the CRISPR-Cas9 was key and I really appreciate it.

Thanks to the IGBMC Imaging & Microscopy platform for all the help provided. Thanks to Nadia for the beautiful electron microscopy and your contagious enthusiasm. To Yves for all the advice. A huge thanks to Pascal for his help and patience, to create 3D figures of my fish and for encouraging me to pursue a singing career ☺.

I also acknowledge the “zebrafish staff” Sandrine, Sylvie and Norbert for their help, for keeping our fish happy and healthy and for my small French lessons, Merci!

To the students and PIs of the Translational Medicine and Neurogenetics department – thank you for creating a wonderful and stimulating scientific environment.

On a personal note I would like to thank the most amazing person I met during this PhD. Damy, I am not sure of the right words to thank you, you have always been there for me (except when I first asked to be flat mates but you said no…). I can't remember a laugh without you, a tear that you didn't comfort, a beef that you didn't share, a pray that you didn't say. Thank you so much for sharing this experience with me (all but the goat, yes I still complain about the goat) and your friendship. I will always be grateful for having crossed paths with you, and girl I aint going anywhere ☺. P.S. See you in the kitchen in 5.

To the Company. Fran and Lorraine: "Laugh is the language of the soul" Girls, you have then amazing souls. I can't let this opportunity pass without thanking you for the lunch-laughs so many amazing crazy ideas and for all your support. To Tiphaine, thank you for your support all along the PhD, sometimes simple phrases have the most impact, your "I believe in you", helped me a lot!

To the president of the Fat-ass club, also known as my chicken translator☺. Girl this wouldn't have been the same without you! Thank you so much for all your help, and support you always say it's normal, well if it is, I hope I keep normally finding amazing people like you!

To Fabulous-Fab, thanks for all the personal and professional advises that you gave me. It was always nice to have a good life discussion with you. And also Mims, you are the sweetest, thanks for caring about me!

I feel truly blessed for the people I met during my PhD, all of you. Thank you!

Finalmente quisiera agradecer a mi gente en México, que a distancia estuvieron cerca de mí. A los vástagos y las niñas que después de más de 15 años siguen apoyándome y echándome porras desde donde están. A Paco por no desesperarse con todos mis quejidos a distancia y por hacerme reír en los momentos en que necesitaba. A Ceci, por seguir ahí chismeando conmigo y compartiendo alegrías y ciencia. A la comunidad de la iglesia, por siempre tomar el tiempo para preguntar por mí y ofrecer una oración. A todos Gracias!

A mi familia, tíos, tías, primos y primas que desde el momento en que les anuncie que había obtenido una beca me han hecho sentir su orgullo y cariño. En especial; Alberto, por cuidar de mis peques y siempre mantenerme al tanto de ellos, gracias. A los que no están en cuerpo pero espero estén orgullosos de mí desde el cielo (Malila, Martin y Felipe). Y finalmente a mi familia perruna (Fran, Lore y Gogy) por llenar mi vida de risas, amor y pelos!

A mi abuelita, Martiux, Gracias por estar siempre al pendiente, por procurar hacer mis postres preferidos cuando voy, por todas tus oraciones por proveerme de abrazos llenos de orgullo y cariño. Por estar conmigo aun estando lejos.

Finalmente quiero agradecer y dedicar esta tesis a mi madre, Lety. No estoy segura de las palabras adecuadas para agradecer todo el apoyo que me has brindado a lo largo de los años. Por siempre impulsarme a ser la mejor versión que pudiera de mi misma. Por recorrer este ya largo camino académico conmigo, siempre mirándome con orgullo. Por ser mi fan número uno. Ahora que llegamos al final, espero haber haberlo logrado y que estés orgullosa de mi, tanto como yo de ti.

Table of Contents

List of Tables

List of Figures Introduction

List of Figures Results

Abbreviations

ADCAs	Autosomal Dominant Cerebellar Ataxias
AR	Androgen Receptor
ATXN7	ATAXIN-7 gene
ATXN7	ATAXIN-7 protein
CAG	Cytosine-Adenine-Guanine
CBP	CREB-Binding Protein
CIC	Capicua
CNS	Central Nervous System
COXVb	Cytochrome C Oxidase Subunit Vb
CRDs	Cone-Rod Dystrophies
CRX	Cone-Rod Homeobox
CTD	C-terminal domain
D-D	Dorso-Distal
DHH	Desert Hedgehog
DRPLA	Dentatorubral Pallidoluysian Atrophy
DUB	Deubiquitination Module
D-V	Dorsal-Ventral
ERG	Electroretinogram
FGF	Fibroblast Growth Factor
HAT	Histone Acetyl Transferase
HD	Huntington's Disease
Hh	Hedgehog
hpf	Hours Post Fertilization

HPRT	Hypoxanthine-Guanine Phosphoribosyltransferase
IHH	Indian Hedgehog
INL	Inner Nuclear Layer
IPL	Inner Plexiform Layer
IS	Inner Segments
KO	Knock-Out
LCL	Lymphoblastoid Cell Lines
mATXN7	Mutant ATXN7
Nr2E3	Nuclear Receptor Subfamily 2, Group E, Member 3
NRL	Neural Retina Leucine Zipper Protein
NTD	N- Terminal Domain
OC	Optic Cup
ONL	Outer Nuclear Layer
OP	Optic Primordia
OPL	Outer Plexiform Layer
OS	Outer Segments
OTX2	Orthodenticle Homeobox 2
OV	Optic Vesicle
PAX2	Paired Box Gene 2
PAX6	Paired Box Gene 6
P-D	Proximal-Distal
PIC	Pre-Initiation Complex
PLK4	Polo Like Kinase 4
Pol II	RNA polymerase II transcription
PolyQ	Polyglutamine

PR	Photoreceptor
RBM17	RNA Binding Motif Protein17
RCC	Renal Cell Carcinoma
RGCs	Retinal Ganglion Cells
RPE	Retinal Pigmented Epithelium
RX	Retinal Homeobox
SAGA	Spt-Ada-Gcn5 Acetyltransferase
SBMA	Spinal And Bulbar Muscular Atrophy
SCA7	Spinocerebellar Ataxia Type 7
SHH	Sonic Hedgehog
smu	Mutant Of Smoothened
STAGA	SPT3-TAF9–GCN5 Complex
syu	Sonic-You
TBP	TATA-Binding Protein
TFTC	TBP-free TAFcontaining complex
TGF-β	Transforming Growth Factor Beta
twhh	Tiggy- Winkle Hedgehog
VAX	Ventral Anterior Homeobox
ZnF	Zinc-Finger

INTRODUCTION

Chapter 1

Introduction

I. Spinocerebellar Ataxia Type 7

1. Polyglutamine repeat disorders

Spinocerebellar ataxia type 7 (SCA7) belongs to the family of polyglutamine (polyQ) diseases, which are neurodegenerative disorders caused by an abnormal and unstable expanded cytosine-adenine-guanine (CAG) repeat in their corresponding causative gene. The expanded CAG repeat is consequently translated into an abnormally expanded polyQ tract in the disease protein. Apart SCA7, this group is composed of five other types of SCAs (type 1-3, 6, and 17) and three non-SCA including: Huntington's disease (HD), spinal and bulbar muscular atrophy (SBMA) and dentatorubral pallidoluysian atrophy (DRPLA) (Zoghbi and Orr, 2000) (Table 1).

SCA7 and other polyQ diseases are clinically and genetically heterogeneous, however they share a number of common features. They are dominantly inherited, with the exception of SBMA, which is linked to a mutation in a gene located on the X chromosome, they are all progressive, adult onset and have a relationship between the number of CAG repeats on expanded alleles and the age of onset and severity of the disease, a prominent feature of all polyQ disorders named anticipation (Schols et al., 2004).

These diseases have their own causative gene in different chromosomes and present a variable threshold number of repeats (Table 1). Interestingly the nine proteins associated with these disorders share no sequence or structural homology except for the unstable PolyQ tract. Additionally, although the altered associated proteins are widely expressed in the central nervous system (CNS), each present specific populations of vulnerable neurons resulting in defined patterns of neurodegeneration and clinical features (Zoghbi and Orr, 2000) (Figure 1).

The synthetized proteins that bear an abnormal expanded polyQ appear to take on an atypical configuration resulting in the formation and deposition of insoluble polyQ aggregates that subsequently accumulate in neurons forming nuclear or cytoplasmic inclusions, which are neuropathological hallmarks in these diseases (Perutz et al., 2002; Ross and Poirier, 2004).

Multiple common mechanisms of neurodegeneration have been identified in the polyQ disorders, including: autophagy, Ca^{2+} homeostasis/signaling alterations, transcription alteration, disruption of axonal transport and vesicle trafficking, mitochondrial impairment, alteration of proteasome degradation as well as caspase activation and aggregation, amongst others, all leading to early synaptic neurotransmission deficits, that will progressively cause cell death (He et al., 2010; Matilla-Duenas et al., 2014; Shao and Diamond, 2007). Alterations in the protein configuration, formation of insoluble polyQ aggregates, as well as proteolytic cleavage of the expanded polyQ proteins have been suggested as enhancers of cell toxicity (Shao and Diamond, 2007).

Understanding how different proteins share pathological features has become one of the main interests for researchers. Identification of the steps in the pathogenic cascade leading to the onset and progression of the disease is likely to be cross-beneficial for developing effective therapies.

Disease	Gene[1]	Gene locus[1]	Protein [2]	Putative Normal Function [2]	Normal repeat length [3]	Pathogenic repeat length [3]
SCA1	*ATXN1*	6p22.3	ataxin-1	Chromatin-binding factor that acts as corepressor.	6-39	45-91
SCA2	*ATXN2*	12q24.12	ataxin-2	Epidermal growth factor trafficking. RNA metabolism.	14-31	35-500
SCA3	*ATXN3*	14q32.12	ataxin-3	Deubiquitinating enzyme. Transcription and degradation of misfolded chaperone substrates.	11-44	61-87
SCA6	*CACNA1A*	19p13.13	α1A voltage-dependent calcium channel subunit	Mediate the entry of calcium ions into excitable cells. Involved calcium-dependent processes.	4-18	20-33
SCA7	*ATXN7*	3p14.1	ataxin-7	Component of the STAGA transcription coactivator-HAT complex. Microtubule and cytoskeleton stabilization.	4-35	36-460
SCA17	*TBP*	6q27	TATA box binding protein	General transcription factor. Core of multiprotein factor TFIID.	25-42	49-66
HD	*HTT*	4p16.3	huntingtin	Microtubule-mediated transport or vesicle function. Transcription factor binding.	9-35	>40
DRPLA	*ATN1*	12p13.31	atrophin-1	Transcriptional corepressor.	6-35	49-93
SBMA	*AR*	Xq12	androgen receptor	Steroid-hormone activated transcription factor.	9-34	38-62

Table 1 Polyglutamine disorders, their associated gene, gene locus, protein and function, and the CAG repeat thresholds.

1 Gene information is in accordance with information provided by NCBI.

2 Protein abbreviation and function is in accordance with UniProt.

3 CAG repeat threshold in accordance with information from SCAbase website or NCBI.

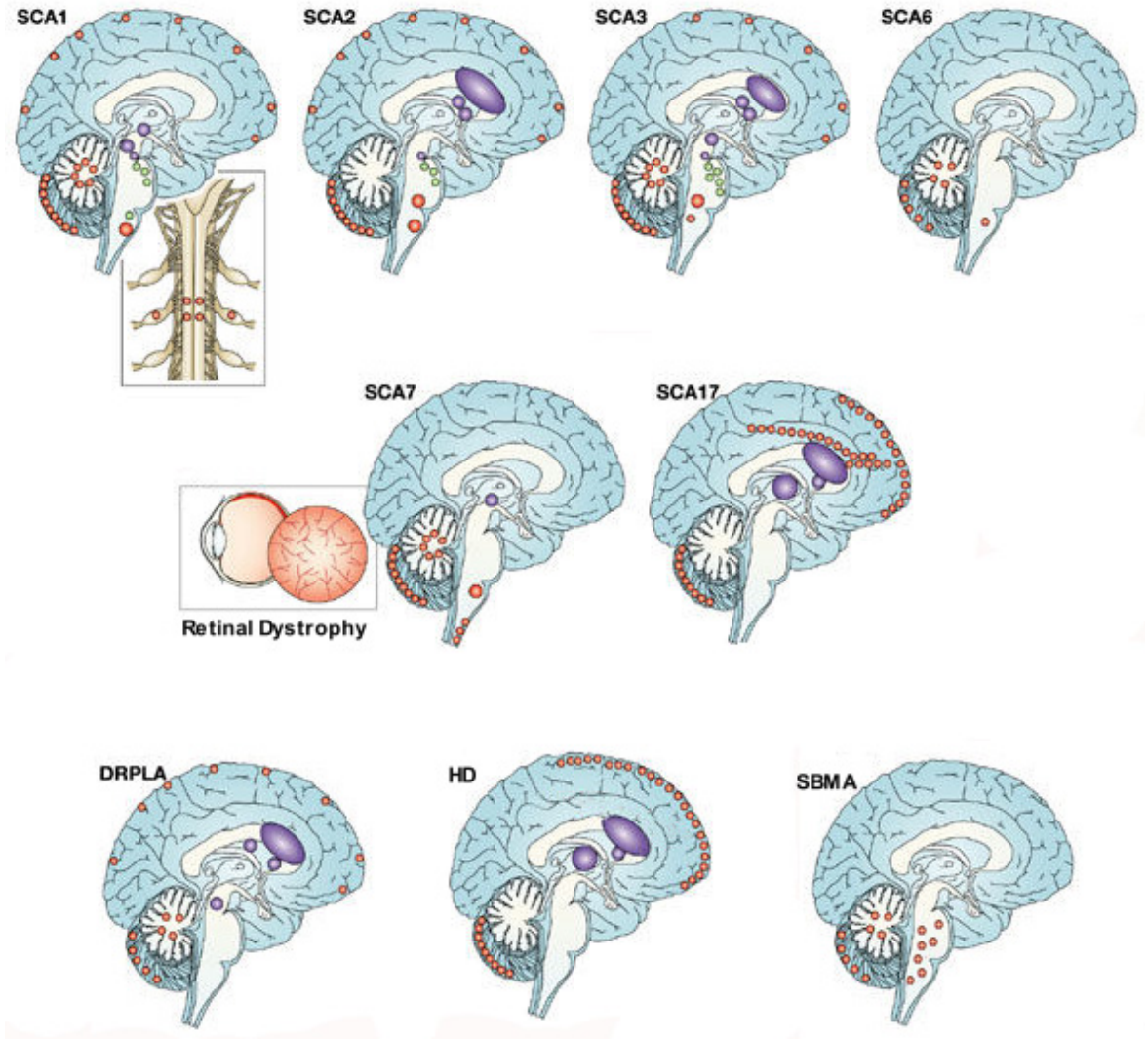

Figure 1 Affected brain regions in PolyQ disorders (adapted from (Taroni and DiDonato, 2004))

a. Gain vs loss of function.

The mechanisms underlying polyQ diseases are complex. Different experiments have revealed that PolyQ disorders might be acting in two different but not mutually exclusive ways: a gain of toxic function and a partial loss of the normal protein function.

It is noteworthy to mention that while PolyQ expansion is classified as a dominant mutation, there is not a pure complete or 50% loss of the normal function for the protein. Evidence for this has been shown in multiple studies performed with various levels of mutant huntingtin. A complete huntingtin Knock-Out (KO) in HD mouse led to embryonic lethality (Nasir et al., 1995; Zeitlin et al., 1995). Furthermore, neuropathological findings from heterozygote and homozygote patients for HD showed that homozygote patients present an increase in the rate of disease progression without changes in age of onset, suggesting that the mutant protein is able to execute the normal protein function at least until the disease onset (Squitieri et al., 2003). Moreover, huntingtin hemizygous inactivation does not cause HD disease symptoms despite the reduction of expression to half normal in humans and mice (Ambrose et al., 1994; Duyao et al., 1995; Persichetti et al., 1996). Additionally, deletion of one huntingtin allele does not result in HD (Housman, 1995).

The toxic gain of function is supported by the fact that expression of different expanded chains of polyQ peptides alone are intrinsically cytotoxic and cause neuronal degeneration in fly (Marsh et al., 2000) and in *C.elegans* (Morley et al., 2002). The concept of gain of toxic function is further supported by experiments where an expanded form of polyQ in the hypoxanthine-guanine phosphoribosyltransferase (HPRT), a protein unrelated to the known polyQ diseases-causing proteins, induces neurotoxicity and mice develop a similar phenotype to the CAG repeat disorders (Ordway et al., 1997), while HPRT knock-out mice develop a different phenotype.

However, there is growing evidence showing that the protein context is critical. In fact, in some cases, expansion of the polyQ tract by itself is not sufficient for disease (Chen et al., 2003; Emamian et al., 2003), pointing out that partial loss of normal protein function occurs alongside the pathogenesis. For example, conditional KO of normal huntingtin in a large proportion of neurons has been shown to decrease the survival and phenotypic stability of CNS cells along with, motor phenotypes and premature death (Dragatsis et al., 2000; O'Kusky et al., 1999). Moreover, overexpression of wild type form of huntingtin can lessen the mutant huntingtin effect (Leavitt et al., 2001; Van Raamsdonk et al., 2006). Furthermore, functions such as vesicular and mitochondrial trafficking or the Neuron Restrictive Factor (NRSF) regulation are

impaired in huntingtin KO mice (Dragatsis et al., 2000; Trushina et al., 2004) . Thus, deficits in trafficking observed in HD models probably represent a loss-of-function feature of polyQ huntingtin.

Similarly, studies in *Drosophila*, have demonstrated that neurodegeneration caused by the expanded form of ataxin-3 can be rescued by the normal ataxin-3, suggesting that at least in this model, the neurodegenerative phenotype might be due to the loss of ataxin-3 function (Warrick et al., 2005). Additionally, it was found that loss-of-function of ataxin-1 in mice is sufficient to cause many transcriptional changes common to the SCA1 knock-in mice, a model that faithfully replicates many features of the disease, suggesting that several molecular changes could be attributed to loss of ATXN1 function in SCA1(Crespo-Barreto et al., 2010). More recently, downregulation of key factors involved in calcium homeostasis were observed in the ataxin-2 KO. Interestingly, some of them also occurred in SCA2. For example, the transporter ITPR1 was depleted from soluble fractions in both mutants, suggesting a partial loss-of function in SCA2 (Halbach et al., 2017).

Nonetheless, the mechanisms underlying the loss of function are not clear. The polyQ expansion could cause the loss of function of the mutant protein and/or act negatively on the functions of the normal one.

It has been proposed that huntingtin expression levels is reduced along the pathology, as HD transgenic mice presented decreased levels of endogenous huntingtin, suggesting an alteration in the stability of the protein (Cattaneo et al., 2001).

It is known that at least two distinct large native protein complexes are associated with ATXN1: one containing the Capicua (CIC) transcription factor, and the other RNA binding motif protein17 (RBM17). In SCA1, expansion in ataxn1 causes increased interaction with RBM17 and a loss of interaction with the CIC, altering the proportion of the mutant protein participating in the formation of these complexes *in vivo*. This suggests that this alteration could at least partially account for SCA1 pathogenesis (Fryer et al., 2011; Lim et al., 2008). Likewise, proteins differentially interact with the normal or polyQ androgen receptor (AR). The N- terminal domain (NTD) of AR contains a transactivation domain that participates in multiple protein–protein interactions with general transcription factors and co-regulatory proteins. Thus, changes in the AR NTD induced by polyQ expansion can potentially strengthen or diminish the interaction of the polyQ AR with these proteins, implicating different pathways in SBMA pathogenesis (Beitel et al., 2013). For example, cytochrome c oxidase subunit Vb (COXVb) interacted more strongly with normal AR than polyQ AR in a hormone-dependent manner (Beauchemin et al., 2001). On the contrary, polyQ AR –and not normal AR- specifically interacted with PTIP (Pax

Transactivation-domain-interaction Protein), a protein that functions in DNA repair, suggesting the polyQ AR may attenuate the DNA damage response (Xiao et al., 2012).

Therefore, it is becoming important to study the interplay between gain and loss of function. The full impact on cellular functions mediated by novel or altered interactions between the polyQ mutant proteins and other proteins is still being explored. Knowing the context and the normal functions of the implicated proteins for each disease can contribute to a better understanding of the pathogenesis that they cause.

b. Developmental component

PolyQ disorders are classified as adult or late onset disorders, which means symptoms appear in middle adulthood (variable for each disorder and depending on the size of the expansion). Several studies have focused on changes present right before, or during the disease onset and progression. However, studies in SCA2, SCA3, SCA6, and HD are challenging and changing this approach, showing that alterations during development could serve as the biological base for the programming and the vulnerability of adult onset disorders that they cause. Supporting this view, recent studies in non-symptomatic patients have shown subtle developmental brain differences that may account for susceptibility and neurodegeneration are present in these diseases (Lee et al., 2012; Nopoulos et al., 2011).

Mice null mutation in huntingtin leads to an early embryonic death (Nasir et al., 1995; Zeitlin et al., 1995). This can be rescued by providing wild-type extraembryonic tissue (Dragatsis et al., 1998). While low levels of huntingtin may rescue the lethality phenotype, huntingtin insufficiency causes abnormal brain development and mild movement abnormalities (Auerbach et al., 2001). Interestingly, decreased level of wild-type huntingtin followed by a later reconstitution, resulted in progressive striatal and cortical degeneration and motor coordination (Arteaga-Bracho et al., 2016). Similarly, mutant huntingtin has been shown to cause changes in the developing cortex along with defects in the proliferation of neuroprogenitors, or lead to perinatal death (Auerbach et al., 2001; Molina-Calavita et al., 2014). Furthermore, Molero et al. (2016) showed that when mice are selectively exposed to mutant HTT 97Q until postnatal day 21, they recapitulate a HD-like phenotype including neuropathology and motor deficits (Molero et al., 2016). More recently, it was shown that the loss of huntingtin during embryonic development has an impact in the dendritic morphology in young adults (Barnat et al., 2017).

All these studies have shown that variations in the levels of expression of either normal or mutant huntingtin, during the embryonic development is sufficient for generate neurological phenotype in mice. Moreover, huntingtin knockdown in zebrafish led to a variety of developmental defects, including hypochromic blood, associated to alteration in iron metabolism; loss of olfactory and lateral line sensory neurons and the presence of massive apoptosis of neuronal cells with enlarge in the ventricle area (Diekmann et al., 2009; Henshall et al., 2009; Lumsden et al., 2007), suggesting that huntingtin appears to be important for vertebrate development.

In the case of SCA3, injection of mutant *ataxin-3* mRNA into the zebrafish embryos led to p53-dependent apoptosis, which occurred mainly in the central nervous system of zebrafish at early development stage (Liu et al., 2016). Additionally, using RNA interference for Ataxin-2, *C.elegans* embryos showed arrest in different stages of development, indicating an essential role of ataxin-2 for early embryonic development (Kiehl et al., 2000). On the contrary, null mutation in mouse ataxin-2 didn't display obvious defects until adult stage, when they presented obesity and subtle rotarod defect (Kiehl et al., 2006). These differences present between both organisms during development could relate to the presence of orthologs and redundant mechanisms that may rescue the function.

Recently, it was shown that SCA6 mice presented alterations during early development (P10-13) in the maturation of Purkinje cells, which suggests impaired function. Notably, no motor deficit was detected. Moreover, the development alterations were transient and no longer observed at later stages (P21-24), showing that changes in the developing cerebellar circuit can occur without detectable motor abnormalities, and that changes in cerebellar development may not necessarily remain persistent into adulthood (Jayabal et al., 2017).

Put together, these studies provide new insight into polyQ disorders, showing that the pathogenesis present in these diseases might be more complicated and multiple approaches are needed to understand the pathological mechanisms involved in each disease. The role of loss of normal function of the polyQ proteins can be readdressed in light of their role during development as a complementary strategy to understand the pathological mechanisms involved. Recognizing the molecular changes that precede the neuronal death, as well as the alterations that provide susceptibility and predisposal to later pathophysiology could be of great value to identify putative therapeutic targets that might prevent, delay or cure determined polyQ diseases.

2. Autosomal Dominant Cerebellar Ataxias

SCA7 also belongs to the group of Autosomal dominant cerebellar ataxias (ADCAs), which are late onset heterogeneous neurodegenerative disorders. This group had been described in multiple families worldwide and in 1982 it was first proposed a classification system for them. By 1993 was refined and grouped the ADCAs into three main categories based on clinical presentation that is still a guideline in clinical practice (Harding, 1982, 1993). Characterized by progressive ataxia but also often associated with a broad spectrum of neurological or other clinical findings (Table 2). Currently, ADCAs are classified under different genetic subtypes known as SCAs. It is noteworthy that Spinocerebellar Ataxia type 7 (SCA7) is the only type of ADCA type 2, which is characterized by progressive cerebellar ataxia and retinal degeneration.

ADACA type	**ADCA I**	**ADCAII**	**ADCAIII**
Clinical presentation	Cerebellar syndrome with ophtalmoplegia/pyramidal/extrapyramidal signs/cognitive impairment/peripheral neuropathy	Cerebellar syndrome with pigmentary retinopathy	Pure cerebellar syndrome
Neuropathology	Degeneration of the cerebellum, and of the basal ganglia/cerebral cortex/ optic nerve/pontomedullary systems/spinal tracts/peripheral nerves	Cerebellar and pigmentary retinal degeneration	Cerebellar degeneration
SCA	1, 2, 3, 4, 8, 10, 12, 13, 17, 18, 19/22, 20, 21, 23, 24, 25, 27, 28, 32, 33, 34, 35, 36	7	5, 6, 11, 14, 15/16, 26

Table 2: Modified Harding's classification of ADCAs (adapted from (Duenas et al., 2006)).

The SCAs are clinically and genetically heterogeneous. Clinically they are characterized by progressive loss of coordination in gait and limb movements. They are also associated with variable additional symptoms, including cerebellar dysarthria, dysphagia, extrapyramidal movement disorders, peripheral neuropathy, sphincter disturbances, cognitive impairment, epilepsy and dementia (Rub et al., 2013; Schols et al., 1997).

To date, 39 types of SCAs have been identified and are classified as SCA1 through SCA43 (no record for SCA33 or 39), most of which are autosomal dominant (except SCA24 and 28) and were categorized according to ADCA types (OMIM database 2017 https://omim.org/ (Amberger et al., 2015)). Moreover, ~80% have found and associated gene, however a large group of pedigrees with ADCA have still not found a determined loci, suggesting that the number could increase (Matilla-Duenas, 2012).

Interestingly, the increasing number of SCAs have shown multiple and different mechanisms that ultimately lead to ataxia clinical symptoms (Matilla-Duenas et al., 2014). Rising the question if there are unifying or converging pathways for these SCA.

Among all these ADCAs and polyQ disorders, SCA7 represents an interesting pathology. It present a unique retinal degeneration in addition to the cerebellar degeneration.

3. Major features of SCA7

a. Clinic-genetic

Efforts to identify the genetic cause of SCA7 began in the mid 90's. In 1995, the causative mutation of SCA7 was identified (Trottier et al., 1995). By 1998, through positional cloning the *ATAXIN-7* gene (*ATXN7*) was identified and was shown to contain a polymorphic CAG repeat making SCA7 the eighth disease to be classified as a polyglutamine disorder (David et al., 1998).

The wild-type alleles of *ATXN7* have between 4-35 CAG repeats, while SCA7 alleles have typically 36-460 repeats (Table 1). Among CAG/polyQ disorders, SCA7 CAG repeats show the highest tendency to expand upon transmission, explaining the strong anticipation observed in families (mean 19 ± 13 years) (David et al., 1998; Michalik et al., 2004). Interestingly individuals with 25-35 repeats are asymptomatic, but they clearly gave rise to an SCA7 expansion in the next generation. This would explain why, despite the extreme anticipation observed in SCA7, the disease has not disappeared (Stevanin et al., 1998).

There is a significant negative correlation between the size of the CAG expansion and the age of onset and disease duration. This correlation is independent on the sex of the patient. While SCA7 alleles with ranges between 36-55 CAG repeats are responsible for the classical adult-onset form,(Michalik et al., 2004), >70 CAG repeats typically result in juvenile-onset forms with accelerated disease course. The repeat length also influences the symptoms at onset:, large repeat expansions are typically associated with early onset and cause visual loss before

cerebellar ataxia, while shorter expansions with later onset cause ataxia symptoms before visual loss (David et al., 1998; Giunti et al., 1999). Extremely large CAG expansions (>100 CAG) cause infantile forms with multisystem disorders such as failure to thrive, hypotonia, myoclonic seizures and non-central nervous systems dysfunctions like congestive heart failure, patent ductus arteriosus, renal failure, and muscle atrophy, and lead to death within few years or months (Ansorge et al., 2004; Benton et al., 1998; Giunti et al., 1999; Trang et al., 2015; van de Warrenburg et al., 2001; Whitney et al., 2007).

b. Cerebellar pathology.

SCA7 progressive cerebellar ataxia is manifested by the inability to coordinate balance, gait, and speech. Additional neurological deficits include slow saccades, opthalmoplegia, dysphagia, as well as pyramidal signs (David et al., 1998; Giunti et al., 1999). Variable levels of cerebellar and pontine atrophy are observed by magnetic resonance imaging (Alcauter et al., 2011; Bang et al., 2004; David et al., 1998; Horton et al., 2013; Michalik et al., 2004). Neuropathologically, the neuronal loss is substantial in the cerebellum (Purkinje cell layer and in the dentate nuclei), thalamus, nuclei of the basal ganglia, in the inferior olivary nuclei and brainstem (in basis pontis), which is associated with the atrophy of spinocerebellar and pyramidal tracts and milder changes are present in the granule cell layer (Horton et al., 2013; Michalik et al., 2004; Rub et al., 2005). Atrophy or loss of myelin is observed in the cerebellar white matter and extra cerebellar associated structures (Martin et al., 1999; Rub et al., 2013). In the classical adult-onset form, the disease progresses over several decades until death, due to dysphagia and other motor bulbar problems, most of the patients die of bronchopneumonia.

As previously mentioned SCA7 is the only type of ADCA type 2, characterized by retinal degeneration in addition to the progressive cerebellar ataxia.

c. Retinopathy.

The retina is the neurosensory part of the eye and is a simple system of the central nervous system, and because of this a study of neural processes operant in the retina could assist in an understanding of the intricate mechanisms involved in the workings of the brain.

The vertebrate retina is a multilayered structure and composed of seven main cell types: rod and cone photoreceptors, horizontal cells, bipolar cells, amacrine cells, ganglion cells, and

Müller glia, which are each found in a specific layer of the organ (Thoreson, 2008) (see Figure 2).

Behind the neurosensory retina is a monolayer of pigmented epithelial cells known as the retinal pigmented epithelium (RPE) that forms part of the blood/retina barrier along with the Bruch's membrane and the choriocapillaris. As a layer of pigmented cells the RPE absorbs the light energy focused by the lens on the retina but as well assists in support and maintenance of the neural retina, by transporting ions, water, metabolic products and recycling photo pigments generated during the visual cycle. The RPE also phagocytoses shed photoreceptor membranes to assist in constant renewal of outer segments (OS) (Strauss, 2005).

Basal to the RPE it is located the rod and cone photoreceptor (PR) layer, which is subdivided into the OS and the inner segments (IS). Rod and cone photoreceptors are light sensing cells. Cone photoreceptors are responsible for color vision and perception in bright light, and in humans are concentrated in the central macular region of the retina, decreasing in number towards the periphery of the eye. Three cone subtypes with different spectral sensitivities are found in primates: short-wavelength (S or blue-sensitive) cones, middle-wavelength (M or green-sensitive) cones, and long-wavelength (L or red sensitive) cones. This difference in spectral sensitivity arises from the presence of different cone opsins. Rod photoreceptors aid in perception in low light conditions, and outnumber cone cells 18-20:1 in humans (Swaroop et al., 2010).

The outer nuclear layer (ONL) contains the cell bodies of rod an cone photoreceptors, cone pedicles and rod spherules are synaptic upon various bipolar cell and horizontal cell types in the outer plexiform layer (OPL). The inner nuclear layer (INL), of the retina, contains cell bodies of three varieties: horizontal, bipolar and amacrine cells. Synaptic contact among bipolar, amacrine and ganglion cells are made in the inner plexiform layer (IPL). Anterior to the IPL, closer to the front surface of the retina is the ganglion cell layer (GCL), which contains cell bodies of the retinal ganglion cells (RGCs). Axons form retinal ganglion cells join together as they exit the eye to form the optic nerve, which projects to higher visual centers. Müller glia cell body is located in the INL, however, extension of the cell spans in every layer as these glial cells role is to protect and repair retinal neurons as well as act as architectural support (Thoreson, 2008) (Figure 2).

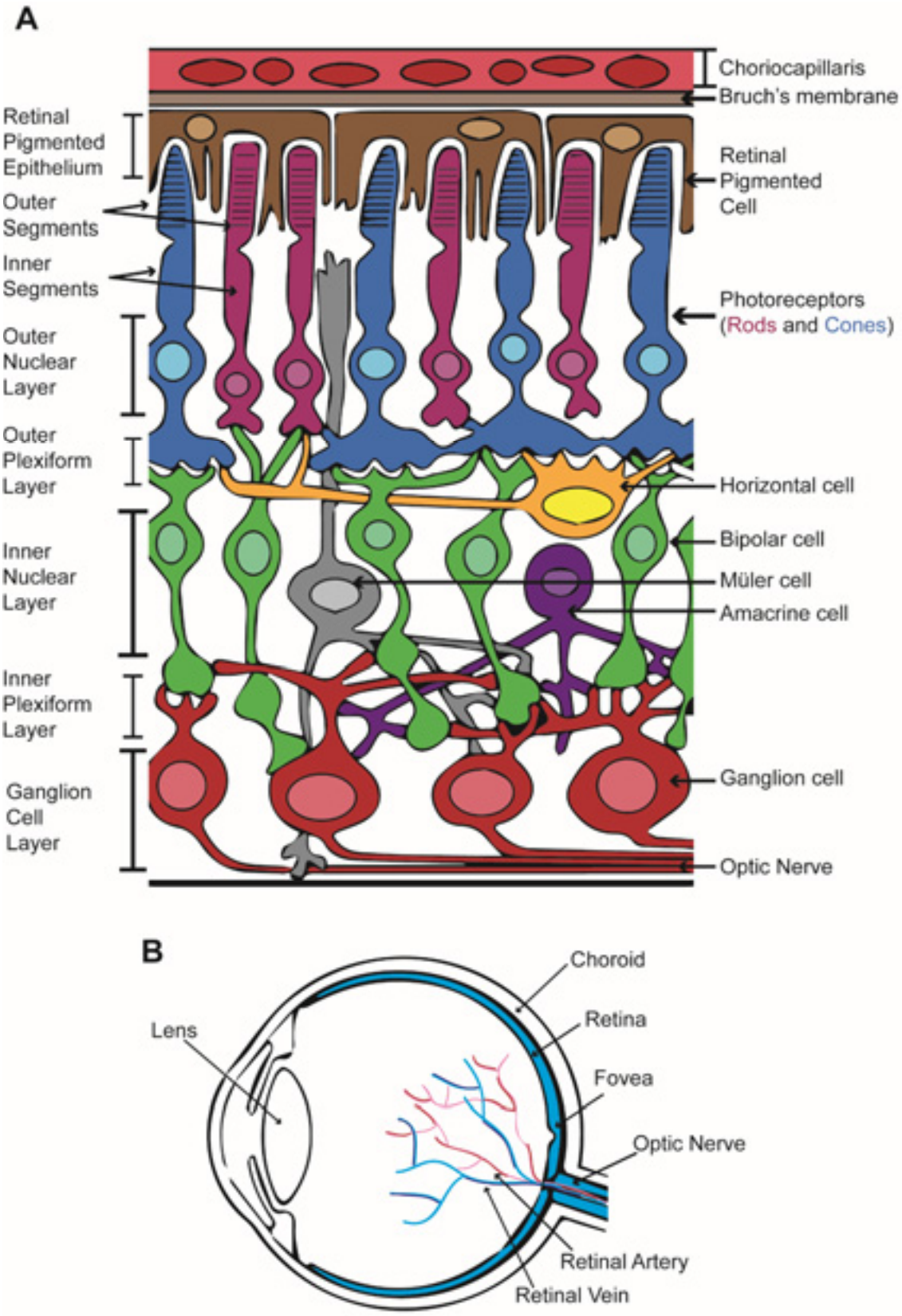

Figure 2 . Eye and retina diagram.

(**A**) Cellular structure of human retina (**B**) Human eye anatomy

> "In Family 3, cerebellar ataxia was associated with retinal degeneration in 2 of the affected individuals; the others had visual failure but no further clinical details were available. In the patient seen by the author, there was **extensive pigmentary degeneration involving most of the retina.** Saccadic eye movements were virtually absent but he could slowly follow movements of his own hand. This particular patient had **symptoms of visual impairment** before the development of ataxia, as did his relatives."
>
> *(Harding, 1982)*

This was the first classification of SCA7 as a distinct type of ADCA. The characteristic presence of retinopathy indicated that SCA7 was genetically distinct from other SCAs (Table3).

The retinal disease begins with an initial deterioration of the central vision affecting first cone photoreceptors, manifested by the loss of blue/yellow color discrimination (dyschromatopsia) and of visual acuity (due to loss of cone function); and then progresses toward a cone-rod dystrophy, this is manifested by the loss of peripheral visual fields (due to loss of rod function). This progressively spreads out to the whole retina, declining toward complete blindness. (Enevoldson et al., 1994; Gouw et al., 1994; Thurtell et al., 2009).

SCA7 patients may present visual impairments either before or after the onset of ataxia. Fundoscopy examination shows atrophic macula with granular pigmentation, pale areas with pigmentary atrophy and poor vasculature (Gouw et al., 1994; Michalik et al., 2004) (Figure 3A-B).

Post-mortem retinal histological examinations reveal almost complete loss of photoreceptors and substantial loss of the bipolar and ganglion neurons, associated with a severe thinning of the nuclear and plexiform layers especially in the foveal and parafoveal regions (Aleman et al., 2002; Michalik et al., 2004; Rub et al., 2008) (Figure 3C-D). In addition, damages in the Bruch's membrane, retinal pigmentary epithelium and hypomyelinisation of the optic nerve have also been reported (Enevoldson et al., 1994; Gouw et al., 1994; Horton et al., 2013; Rub et al., 2008).

Despite the accumulated knowledge from imaging studies of SCA7 patients and the examinations of post-mortem retinal tissue, we are still lacking information regarding the temporal and spatial degeneration in the SCA7 patient retina.

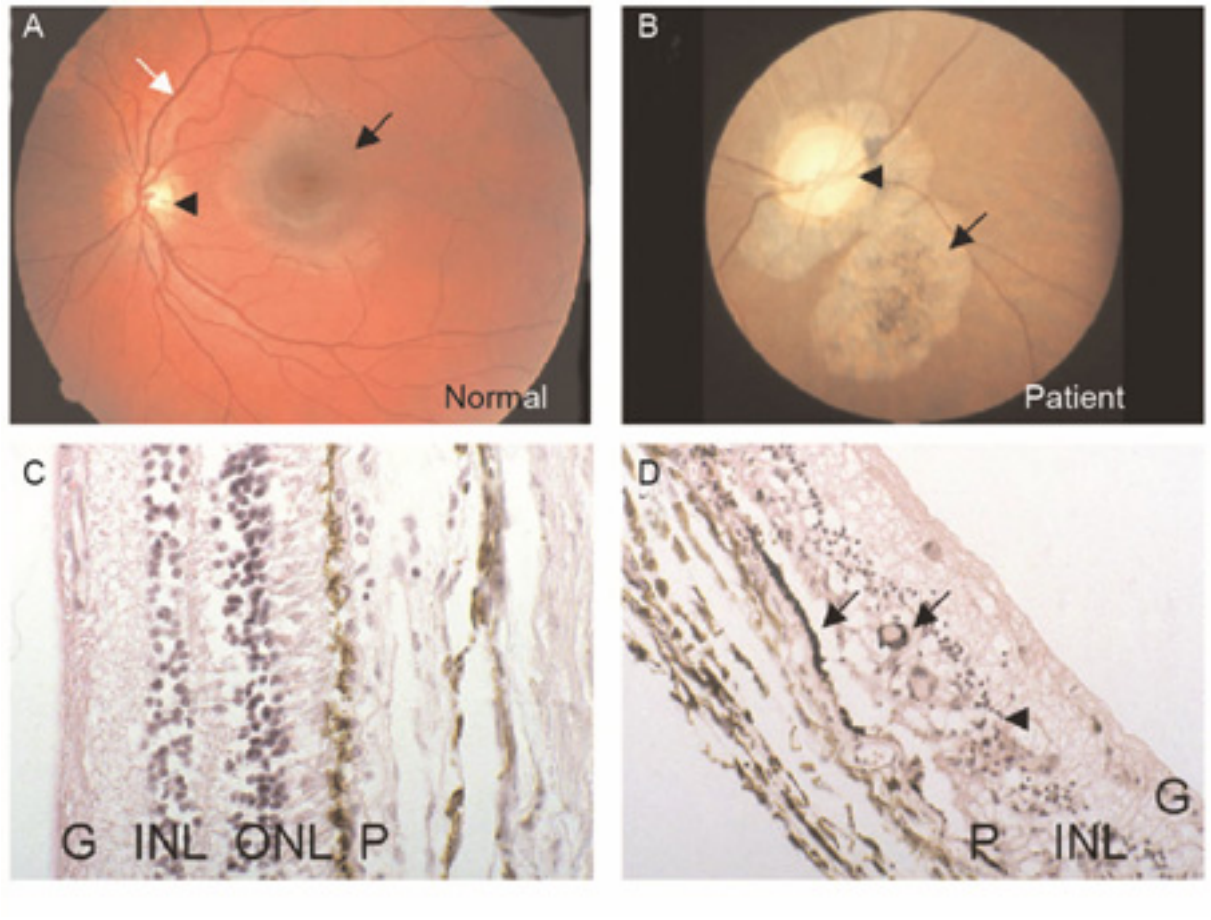

Figure 3 Hallmarks of SCA7 human retinopathy.

(**A, B**) Fundoscopy images of a normal (**A**) and SCA7 patient (**B**) retinae. The SCA7 retina displays an extremely pale optic disc (arrowhead), atrophy of the pigmentary epithelium and choroid layer (arrow) as compared to the normal retina that shows normal macula (black arrow) and optic disc (arrowhead) and well-developed vasculature (white arrow).

(**C, D**) Histological sections of normal (**C**) and SCA7 patient (**D**) retinae. The normal retina (**C**) shows a proper organization of the retinal layers: the pigment epithelium (P), nuclei of rods and cones within the outer nuclear layer (ONL), the nuclei of bipolar, horizontal and amacrine neurons within the inner nuclear layer (INL) and the ganglion cell layer (G). In contrast, the retina of the SCA7 patient (**D**) is severely degenerated, and displays complete loss of photoreceptor segments and nuclei, disorganization of the INL (arrowhead) and migration of the melanin pigment (P) deep into the atrophic retina (arrows).

Adapted from (Michalik et al., 2004)

II. Ataxin-7 gene

The ATAXIN-7 (ATXN7*)* protein harbors a polymorphic polyQ stretch in the amino-terminus and it also presents three conserved domains that are shared with three paralogs, ATXN7L1, L2 and L3: a typical C2H2 zinc-finger (ZnF) motif, an atypical Cys-X9–10–Cys-X5–Cys-X2-His motif, known as SCA7 domain, and a third domain absent in ATXN7L3 (Figure 4) (Helmlinger et al., 2004b). *ATXN7* mRNA and protein are widely expressed in neural and non-neural tissues and has been shown to be regulated by SUMOylation and acetylation (Duncan et al., 2013; Einum et al., 2001; Janer et al., 2010). ATXN7 appears predominantly in the nucleus (Kaytor et al., 1999). However, it has been reported that the intracellular distribution of ATXN7 dynamically changes and that ATXN7 distribution frequently shifts from the nucleus to the cytoplasm (Nakamura et al., 2012; Taylor et al., 2006) . Nuclear localization of ATXN7 is essential for transcription function while cytoplasmic ATXN7 has microtubule associating and stabilizing properties(Nakamura et al., 2012). There is no apparent correlation between cellular or subcellular localization and level and the vulnerability of neurons to degeneration in SCA7.

ATXN7 and its yeast ortholog *sgf73* are core components of SAGA complexes (Spt-Ada-Gcn5 Acetyltransferase) involved in chromatin remodeling (also known in human as the TBP-free TAF containing complex (TFTC) and the SPT3-TAF9–GCN5 complex (STAGA) (Helmlinger et al., 2004b; Palhan et al., 2005; Sanders et al., 2002; Scheel et al., 2003).

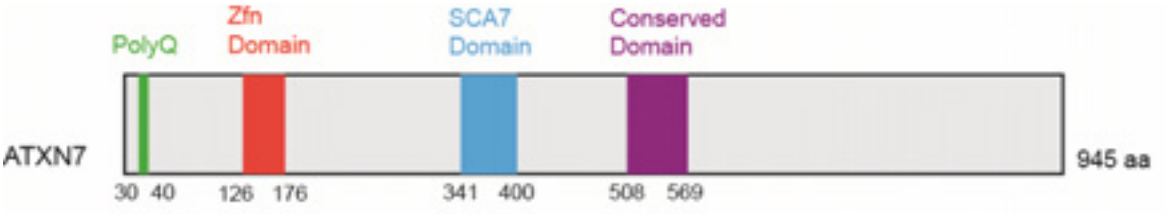

Figure 4 Modular structure of human ATXN7 protein.

1. SAGA complex

SAGA is a multi-protein chromatin modifying complex that performs histone modifications and acts as co-factor for RNA polymerase II transcription (Pol II) (Bonnet et al., 2014). It is conserved between yeast and humans and can be subdivided in four modules (Table 3). Two enzymatic modules: the histone acetyl transferase (HAT) module that acetylates histone H3

through GCN5 activity and deubiquitination module (DUB) that deubiquitinates histone H2B through USP22 activity. And two modules implicated in pre-initiation complex assembly and architecture (TBP-associated factor (TAF) and SPT modules) (Koutelou et al., 2010). *ATXN7* belongs to the DUB together with the human ubiquitin protease USP22, ATXN7L3 and ENY2.

a. SAGA in Transcription

Gene expression is a complex process that requires the participation of various enzymatic complexes and is regulated at different levels. It involves two main stages: transcription and translation. Being transcription a key stage since it ensures the RNA synthesis based on a DNA template. Characterization of the yeast SAGA complex has revealed its involvement in various steps in the transcription process, including initiation and elongation; histone ubiquitination and interactions with the TATA-binding protein (TBP) (Koutelou et al., 2010; Wyce et al., 2004).

An initial step in the transcription process involve the chromatin remodeling in order to recruit the transcription machinery to the DNA. This remodeling is the consequence of histone modification. The HAT module of SAGA catalyzes the histone acetylation that ultimately will open up the chromatin allowing the formation of the pre-initiation complex (PIC) (Bhaumik, 2011). Additionally studies in yeast have revealed the complex involvement in the transcriptional activation through the recruitment of TBP by the ySpt3 subunit (Mohibullah and Hahn, 2008). Moreover, the activity of the DUB module has been shown to be necessary for switching from the initiation to the elongation stage allowing the recruitment of the Ctk1 kinase, an important catalytic subunit, which hyperphosphorylates the C-terminal heptapeptide repeat domain (CTD) of the largest RNA polymerase II subunit (Wyce et al., 2007).

Additional non transcriptional roles include mRNA export, DNA repair and telomere maintenance (Atanassov et al., 2009; Guo et al., 2011; Rodriguez-Navarro et al., 2004). Moreover SAGA complex can acetylate non-histone chromatin proteins like specific transcription activators such as c-Myc and Polo Like Kinase 4 (PLK4) (Fournier et al., 2016; Patel et al., 2004).

Component	Yeast	Drosophila	Zebrafish	Human
HAT module	yGcn5	dGcn5	zGcn5	GCN5
(Histone acetyl transferase)	yAda2b	dAda2b isoform a dAda2b isoform b	zAda2b	ADA2B
	yAda3	dAda3	zTada3l	ADA3
	ySgf29	CG30390	zSgf29	SGF29
DUB module	yUbp8	Nonstop	zUsp22	USP22
(Deubiquitination)	**ySgf73**	**Dmel\dAtxn7**	**zAtxn7**	**ATXN7**
	ySgf11	dSgf11	zAtxnL3	ATXN7L3
	ySus1	dE(y)2	zEny2	ENY2
TAF module	yTaf5	Wda	zTaf5	TAF5L
	yTaf6	dSAF6	zTaf6	TAF6L
	yTaf9	dTaf9	zTaf9	TAF9
	yTaf10	dTaf10b	zTaf10	TAF10
	yTaf12	dTaf12	zTaf12	TAF12
SPT module	yTra1	Nipped-A	zTrrap	TRRAP
	ySpt8	-	-	-
	yAda5/Spt20	dSpt20	zSupt20	SPT20
	ySpt7	CG6506	zSupt7L	SUPT7L
	ySpt3	dSpt3	zSupt3h	SPT3
	yAda1	dAda1	zTada1	TADA1

Table 3. Components of SAGA in yeast, drosophila, zebrafish and human (Adapted from (Wang and Dent, 2014)).

b. SAGA role in development.

Development requires the precise control of gene expression during different stages. This can range from regulation of changes of transcript levels in both space and time up to the maintenance of constant levels of expression for extended periods. Knowing that SAGA complex plays an important role in the regulation of gene expression is no surprise that components of this complex have shown involvement in events during development.

The member of the HAT module, Gcn5, was shown to be essential for the development of different organisms. *Drosophila* mutant revealed that while *Gcn5* is not required for early larval life it does impede the metamorphosis prior to larvae death (Carre et al., 2005). This lethal phenotype is as well present in *Gcn5*-null mice that die as consequence of apoptosis of mesoderm cells (Xu et al., 2000). Moreover, levels of expression seem to be crucial for a proper mouse development, as mice with catalytically inactivated *Gcn5* presented severe neural tube closure defects and died in mid-gastrulation (Bu et al., 2007) while reduced *Gcn5* expression causes homeotic transformations in lower thoracic and lumbar vertebrae as well as exencephaly (Lin et al., 2008). Other two members of the HAT module, *Ada2* and *Ada3*, present in *Drosophila* similar phenotypes to that of *Gcn5* mutant larvae, with metamorphosis defect and lethality (Qi et al., 2004).

Components of the deubiquitinating module are also involved in development. *usp22*-null mutation is lethal in mouse due to an elevated p53 transcriptional activity (Lin et al., 2012). The *Drosophila* homologues nonstop and Sgf11 mutants result in defects in neuronal connectivity in the developing visual system as well as aberrant development of photoreceptor cells (Ma et al., 2016; Mohan et al., 2014). Finally, downregulation of the zebrafish *usp22* orthologue showed the presence of hydrocephaly (Tse et al., 2009).

Thus far no members from the TAF module have been linked to a developmental phenotype, while only the drosophila homologue Nipped A from the SPT module has shown participation in the wing development acting as a coactivator of the protein mastermind (Gause et al., 2006).

Up to now few subunits of the SAGA have been characterized for developmental defects. Additional studies are needed to understand how these genes function as part of the SAGA complex or independently. Understanding the role of these proteins during development may presage important implications in human diseases.

c. SAGA complex and disease.

Besides SCA7, which is caused by a member of the deubiquitinating module of SAGA, other members have been linked to disease, particularly with hallmarks of cancer, including DNA damage repair, cell cycle regulation and post translational regulation.

SAP130 and DDB1, two proteins associated to the human SAGA complex have shown to be involved in DNA repair (Brand et al., 2001; Martinez et al., 2001). Interestingly results obtained in yeast equally support the role of SAGA with DNA damage repair co-transcriptionally or independent of transcription (Ferreiro et al., 2006; Yu et al., 2005).

Three subunits of the DUB module have been linked with cancer. *USP22* has been identified as a component of an 11-gene signature associated with poor prognosis of diverse types of cancer, it has been hypothesized that USP22 could regulate tumorigenesis by inducing histone modifications (Zhang et al., 2008b). Moreover, USP22 is required for the activation of target gene transcription by MYC, lack of USP22 alters MYC functions and ultimately results in a specific G1 phase cell arrest while the USP22 recruitment allows certain essential cell cycle genes to be transcriptionally activated (Zhang et al., 2008a; Zhang et al., 2008b). ATXN7, has been reported to be associated with susceptibility with breast cancer and prognosis of renal cell carcinoma (RCC) (Gotoh et al., 2014; Milne et al., 2014). Finally, the ENY2 protein member as well of the DUB module, might be defined as a diagnostic marker for primary breast cancer (Armakolas et al., 2012).

On the other hand, the HAT module member, *GCN5* has been related to different types of cancer including lung, liver and colon. Alteration in the levels of expression is responsible for cell cycle progression arrest and apoptosis.GCN5 has been shown regulates the expression of cyclin D1, and cyclin E1 (cell growth and the G1/S phase transition), E2F1 (transcription factor that can induce both proliferation and apoptosis.) and $p21^{Cip1/Waf1}$ (cell cycle inhibitor). (Chen et al., 2013; Majaz et al., 2016; Yin et al., 2015).

In summary, ATXN7 is a member of the SAGA complex. This complex consist of distinct modules that participate at different levels in the transcription mediated by Pol II. The composition of these modules is now well known, however, much information regarding their biological functions remains to be elucidated. Moreover, for now multiple SAGA members are linked to disease and to multiple stages in development, rising questions of their specific roles in such biological processes.

III. Pathogenesis of SCA7 retina phenotype

Different models have been used in order to study the SCA7 disease. Current information is the result of years of biochemical, molecular and organismal studies. This section will focus on the *in vivo* and *in vitro* models that have been generated to better understand the underlying pathomechanisms of the SCA7 disease.

1.Cell-based Models

In vitro models have provided important insights about the SCA7 pathogenesis; however there are important challenges present with their use. First, SCA7 is an adult onset neurodegenerative disorder which means long-time cultures are required in order to properly model the late onset of the disease. Additionally, there is a lack of specific affected cell types such as neurons and photoreceptors patient-derived appropriate for *in vitro* studies. Regarding to the latter one; while is possible to culture from post mortem tissue derived from brain (Verwer et al., 2003) or retina (Kim and Takahashi, 1988; Marita, 2011; Mayer et al., 2005) a major drawback is the limited time for establishing these cultures (less than 48 hours after patient death). Because of this, efforts have focused on using other cell types derived from SCA7 patients, such as skin derived fibroblasts (Luo et al., 2012; Scholefield et al., 2014) or lymphoblastoid cell lines (LCL) (Tsai et al., 2005). This lines give the advantage having a genetic accurate disease background, however these cells are normally unaffected by the pathology and have a limited culture life span *in vitro*.

For those reasons the most common method has been to transfect established cell lines with different ATXN7 expression vectors. Providing valuable information regarding interactors, toxicity, patterns of expression, among others. Summarized in Table 4.

Patient derived cell lines			
Cell line	Design	Contribution	Reference
FIB (patient and control fibroblast)	Individuals with 55 or 150Q	Expression of atxn7 and the antisense non-coding RNA SCAANT1.	(Sopher et al., 2011)
	Patient with 45 Q	Generation of induced pluripotent stem (iPS) cells.	(Luo et al., 2012)
	Individuals with 57 Q	Allele-specific siRNA silences the mutant transcript more efficiently than the wild-type.	(Scholefield et al., 2014)
LCL (lymphoblastoid cell lines)	Individuals with 41 and 100Q	Expanded ataxin-7 significantly impaired the expression of the heat shock proteins Hsp27 and Hsp70.	(Tsai et al., 2005)
	Individuals with 10,51,59 or 66Q	Increased expression of ataxin-7 sense transcript levels.	(Sopher et al., 2011)
Human Non-Patient derived cell lines			
Hek293 (Human Embryonic Kidney 293 cells)	Transfected full length *ATXN7* (10/100Q)	shRNA decreased numbers of cells with mutant protein aggregates.	(Scholefield et al., 2009)
	FLAG-tagged full length *ATXN7* (10/60Q)	Normal and mutant ATXN7 equally interacted with the TFTC subunits TRRAP, GCN5 and TAF10.	(Helmlinger et al., 2004b)
	Full length *ATXN7* (10/100Q) and truncated form	Heat-shock proteins, subunits of the proteasome, transcription factors and activated caspase-3 were detected in a subset of inclusions.	(Zander et al., 2001)

HeLa (Cervical Cancer Cell line)	FLAG-tagged full-length or truncated *ATXN7* (10/65Q)	Small increase in NOX1 expression, p53 co-aggregates with mutant ATXN7 and the p53 transcriptional activity is reduced.	(Ajayi et al., 2015)
Non-Human Cell lines			
Cos-1 (Monkey kidney – fibroblast like)	Transfected full length *ATXN7* (10/52/75Q)	ataxin-7 localization to the nucleus is dependent on the function of an arginine-lysine nuclear localization signal (NLS)	(Kaytor et al., 1999)
Cos-7 (Monkey kidney – fibroblast like)	Transient transfection *ATXN7* (10/72Q)	Inclusions were highly enriched in Hsp70, 19S proteasome, and ubiquitin.	(Janer et al., 2010)
	Myc-tagged full-length *ATXN7* (10/100Q)	Ataxin-7 colocalizes with full-length R85 (R85FL), an alternative splicing product of the gene SH3P12, a potential Cbl partner.	(Lebre et al., 2001)
PC12 (Rat Pheochromocytoma of adrenal medulla)	Tetracycline-regulated expression *ATXN7-GFP* (10/65Q)	Full-length and cleaved fragments of ATXN7 are differentially degraded. The ubiquitin–proteosome system (UPS) is essential for the degradation of full-length endogenous ATXN7 or transgenic full-length ATXN7 with a normal or expanded glutamine repeat	(Yu et al., 2012)
	Tetracycline-regulated expression *ATXN7-GFP* (10/65Q)	Increase in ROS levels and aggregation of *ATXN7* and later cellular toxicity.	(Ajayi et al., 2012)
	Tetracycline-regulated expression *ATXN7-GFP* (10/65Q)	p53 and mutant ATXN7 co-aggregated and transcriptional activity of p53 was reduced, resulting in a 50% decrease of key target proteins	(Ajayi et al., 2015)

Table 4. Summary Cell models of SCA7

2.Mouse Models

Different transgenic and knock-in mouse models have been generated during the past years with the majority expressing wild-type or expanded ATXN7 under the control of a heterologous promoter specific to the brain and/or retina. These models have provided important insights into the nature of SCA7 neurodegeneration.

a. Cerebellar pathology

Analyses of the PrP-SCA7-c92Q mouse model have highlighted the importance of cell-cell interactions in the cerebellar pathology (Garden et al., 2002). These mice develop motor defects and show dark degenerating Purkinje neurons. Interestingly, Purkinje cell pathology occurs despite the fact the MoPrP promoter drives the expression of mutant ATXN7 (mATXN7) in all cerebellar neurons, except for Purkinje cells, suggesting that they are affected via a non cell-autonomous mechanism. This same model displayed as well pathological signs in Bergman glial cells (Custer et al., 2006). Given that Bergmann glia are regulators of glutamate levels in the surrounding environment of Purkinje cells and that dark degeneration often results from excitotoxicity, new transgenic mice were generated to express mATXN7only in Bergmann glia cells to assess whether the pathology would affect Purkinje cells as well. Indeed, Gfa2-SCA7-92Q mice also show Purkinje cell degeneration and motor dysfunctions. However, compared to PrP-SCA7-c92Q mice, Gfa2-SCA7-92Q mice develop a late onset and milder ataxia, suggesting that other dysfunctional neurons may account for Purkinje cell degeneration in PrP-SCA7-c92Q mice.

The contribution of different cell types and their interaction to the cerebellar pathology was further addressed using a new set of engineered mice in which mATXN7 cDNA was flanked by loxP sites at the start site of translation in the murine PrP gene in a bacterial artificial chromosome (PrPfloxed-SCA7-92Q BAC) (Furrer et al., 2011). When crossed with mice expressing Cre recombinase under Bergmann glia promoter (Gfa2) or under promoter specific to Purkinje and inferior olive neurons (Pcp2), mATXN7 was deleted specifically in these cell types. Deletion of mATXN7 from Bergmann glia has mild beneficial effects and does not prevent Bergmann glia pathology. In contrast, deletion of mATXN7 from Purkinje and inferior olive neurons improves motor performance and histopathology as well as prevents Bergmann glia pathology. Finally, deletion of mATXN7 in the three cell types is more effective to prevent the pathology. Together, these results support a complex cell-cell interaction between Bergmann glia, Purkinje and inferior olive neurons in the development of SCA7 cerebellar dysfunction.

The expression profile of the cerebellum of Ataxin-7-Q52 transgenic mice, which also display motor dysfunction and Purkinje cell pathology, revealed gene deregulations affecting different pathways including synaptic transmission, axonal transport, glial functions and neuronal differentiation (Chou et al., 2010). Perhaps the most interesting finding is the down regulation of a set of myelin-associated proteins (CNP, MAG, MBP, MOG, MOBP and PLP1) and of their regulators, the transcription factor Olig1 and transferrin (Chou et al., 2010). This is consistent with the loose and poorly compacted myelin sheaths observed in the cerebellar white matter of these mice, and with the myelin pallor and loss of myelinated fibers reported in the cerebellar white matter of SCA7 patients (Rub et al., 2005).

Reminiscent to the loss of photoreceptor maturation in SCA7 mouse retina, mATXN7 toxicity might compromise genetic programs controlling oligodendrocyte maturation and myelin sheath integrity and function.

b. Retinopathy

In SCA7 models, the retina develops normally before showing a progressive reduction of electroretinograph activity, thinning of the retina and repression of photoreceptor-specific genes (La Spada et al., 2001; Yoo et al., 2003). Initially, these transcriptional alterations were attributed to the dysfunction of CRX (cone-rod homeobox protein), a key transcription factor of photoreceptor genes. This is because CRX was previously shown to require interaction with ATXN7 and SAGA for its transactivation activity on photoreceptor gene promoters, and because mATXN7 was shown to suppress the transactivation activity in SCA7 retina (Chen et al., 2004; La Spada et al., 2001). Later on, analysis of SCA7266Q/5Q KI and R7E mouse retina showed that transcriptional alterations were not restricted to CRX target genes (Abou-Sleymane et al., 2006; Yoo et al., 2003). In particular, the expression profile of R7E retina showed on the one hand the downregulation of the photoreceptors specific transcription factors CRX, NRL (neural retina leucine zipper protein), and Nr2E3 (Nuclear Receptor Subfamily 2, Group E, Member 3) as well as most of their target genes, and on the other hand the re-activation of OPTX2, STAT3 and HES5 that normally inhibit the differentiation of precursor neurons into mature photoreceptors during development (Abou-Sleymane et al., 2006).

SCA7 photoreceptors progressively lose their OS and cell polarity, and relapse to round cell shape (Yefimova et al., 2010). Thus, SCA7 retinopathy primarily results from the progressive regression of mature photoreceptor to an ill-defined state, which occurs long before cell death. The initial trigger leading to SCA7 photoreceptor degeneration remains to be determined. Degenerating photoreceptors in SCA7 retina ultimately die through a mechanism reminiscent

of dark neuronal cell death (Yefimova et al., 2010). Dark degeneration also occurs in SCA7 mouse cerebellum and was reported in several mouse models of polyQ disorders (Figiel et al., 2012). Different cellular responses may be triggered by different mATXN7 toxic species, since the relative amount of full-length mATXN7, proteolytic fragments, soluble and insoluble aggregates varies considerably from early to late disease stages and might influence the way individual photoreceptors respond to these different proteotoxic products.

3. Transcriptional alteration

Studies performed on cellular and mouse models of SCA7 have identified transcriptional alterations as an early pathogenic event associated with neuronal dysfunction (Abou-Sleymane et al., 2006; Chou et al., 2010; Helmlinger et al., 2006; La Spada et al., 2001; Yoo et al., 2003) This has also been reported in other polyQ disorders (Sugars and Rubinsztein, 2003).

Transcriptome analysis of SCA7 mouse retina revealed an early and progressive down-regulation of most photoreceptor-specific genes (Abou-Sleymane et al., 2006), while expression profile of SCA7 mouse cerebellum showed down-regulation of genes involved in the maintenance and function of neuronal dendrites and CNS myelin sheath (Chou et al., 2010).

Since the expanded form of ATXN7 has been shown to properly incorporate into SAGA, several studies have explored the possibility that transcriptional alterations in SCA7 could result from dysfunction of SAGA acetylation and deubiquitination activities (Helmlinger et al., 2004b; McMahon et al., 2005; Palhan et al., 2005). The outcome of these studies differs depending the model system investigated. In yeast and HEK2937 kidney cells, mATXN7-containing SAGA lacks critical subunits and leads to the reduction of GCN5 acetylation activity and gene transcription (McMahon et al., 2005; Palhan et al., 2005). In agreement with GCN5 dysfunction, promoters of photoreceptor-specific genes were shown to have histone H3 hypoacetylation, which would explain their decreased expression in SCA7 mouse retina (Prp SCA7-c92Q model) (Palhan et al., 2005). However, opposing with the above studies, mATXN7-containing SAGA purified from SCA7 mouse retina (R7E model) had normal incorporation of Gcn5, Taf12 and Spt3 and had normal acetylation activities (Helmlinger et al., 2006). In this study, promoters of photoreceptor-specific genes were found hyperacetylated, but the presence of RNA Pol II on promoters was strongly reduced, which would explain the low level of photoreceptor-specific mRNA transcripts (Helmlinger et al., 2006). The

discrepancy between these studies is yet unclear and might dependent on the use of two different SCA7 mouse models or on the analysis of different stages of retinal degeneration.

Interestingly, histone hyperacetylation in R7E mouse retina correlates massive chromatin decondensation of photoreceptor nuclei, which are enlarged compared to wild type (Helmlinger et al., 2006). It is thus possible that the overall perturbation of chromatin organization accounts for major changes in the expression of photoreceptor-specific genes. Besides hyperacetylation, chromatin decondensation in R7E retina might also result from an abnormal low expression of histone H1, which is involved in chromatin compaction (Kizilyaprak et al., 2011).

Studies linking other SAGA components in SCA7 pathogenesis have been performed. One allele inactivation of *GCN5* accelerates retina degeneration in SCA7 mice, but does not worsen the transcriptional repression of photoreceptor-specific genes, suggesting that *GCN5* might have non-transcriptional function in the retina. Furthermore, GCN5 appears to be necessary in Purkinje cells and total loss of *GCN5* leads to mild ataxia (Chen et al., 2012). This suggests that GCN5 could participate to some degree to SCA7 cerebellar ataxia. Potential dysfunction of DUB activity of SAGA has also been investigated in SCA7 cellular and mouse models. Monoubiquitination of H2B is globally increased in cultured cells expressing mATXN7 and in the cerebellum of SCA7 mice, but in the latter correlation with transcriptional alterations has not been established (Lan et al., 2015; McCullough et al., 2012; Yang et al., 2015). Two components of the DUB, ATXN7L3 and USP22, are sequestered in mATXN7 aggregates, which might lead to DUB dysfunction and hence an increased H2Bub. (Lan et al., 2015; Yang et al., 2015).

Interestingly, a recent study suggests that the increased expression of mATXN7 would be an indirect consequence of mATXN7-containing SAGA dysfunction (Tan et al., 2014). In fact, SAGA regulates the microRNA miR-124, which in turn controls the abundance of ATXN7 transcripts. Dysfunction of SAGA in SCA7 leads to post-transcriptional derepression of ATXN7 transcripts, due to the reduced level of miR-124. Given that miR-124 is highly expressed in the cerebellum and retina, posttranscriptional regulation of ATXN7 transcripts is thought to account for the tissue specificity of SCA7.

Besides SAGA dysfunction, other mechanisms are proposed to contribute to chromatin modifications and transcriptional alterations in SCA7. mATXN7 aggregates sequester CREB-binding protein (CBP) (Yvert et al., 2001), a histone acetyltransferase, and impair CBP-mediated and RORalpha1-mediated transcription in cultured neurons (Strom et al., 2005). Abnormal mitochondria were observed in SCA7 mouse retina (Yefimova et al., 2010), and

reduced electron transport chain activity and metabolic acidosis were reported in muscle biopsy of patients (Forsgren et al., 1996). Most interesting, a study in PC12 cells made a link between metabolic defect in SCA7 and transcriptional alterations. In PC12 cells expressing mATXN7, p53 is sequestered in aggregates and its transcriptional activity is reduced, leading to dysregulation of metabolic proteins, such as TIGAR, AIF and NOX1 (Ajayi et al., 2012). These alterations result in a reduced respiratory capacity, associated with an increased reliance on glycolysis for energy production and a subsequent reduction of ATP in SCA7 cells.

Investigation of these transcriptional and metabolic pathways in SCA7 mice is thus warranted, in particular because loss of AIF in mice results in primarily neurodegeneration of cerebellar and retinal neurons.

Multiple approaches have greatly provided insight to the possible pathomechanisms behind SCA7. And, even though the current data would support that SAGA dysfunction accounts for SCA7 transcriptional dysregulations, it remains to determine how the dysfunction of a general co-activator complex like SAGA, which is involved in the expression of all RNA Pol II-regulated genes, would only affect specific subsets of genes in SCA7 affected tissues. One can hypothesize that it could be relate to the nature physiological function of the protein.

SCA7 like other polyQ disorders have shown to be complex disorders and deciphering their selective nature and dysfunction has become a challenge. For many disease-involved proteins like ATXN7 there is no known physiological function. Combination of *in vitro* an *in vivo* models would be advantageous in order to perform this task.

Given that the retina is primarily affected in this disease one can hypothesize that ATXN7 might have an important function in the eye. However to test this hypothesis there is no knock out mouse model available. Interestingly, the increasingly developed approaches for genetic manipulation in the zebrafish makes it a good candidate model for understanding human disorders, such as SCA7.

IV. Zebrafish as an alternative model for SCA7

A thorough understanding of the development of the visual system forms the basis to understand ocular diseases. To achieve this goal several animal models have been important in the historical and recent advances in the field of retinal neurogenesis, including mouse, chick, *Xenopus* and zebrafish. Thanks to this, it has been shown that the retina is highly conserved among vertebrates, sharing almost identical anatomical and physiological characteristics.

This section will first focus on the current knowledge on the development of the zebrafish eye and the role of the morphogen *Shh* in this process. The second part will highlight the advantages of zebrafish as a model particularly for retinal diseases.

1. Development of the zebrafish eye

a. Optic vesicle and optic cup development.

Zebrafish eye development begins at late gastrula stage (10 hours post fertilization (hpf)) when the eye field is detectable as a consequence of overlapping expression of a number of transcription factors in discrete regions of the developing forebrain including *six3*, *pax6* and *rx3* (Figure 5A) (Chuang and Raymond, 2002). From 12 to 18 hpf the optic vesicle (OV) appears and undergoes through lateral evagination from the ventral forebrain towards the overlying surface ectoderm. Simultaneously the formation of the dorsal-ventral (D-V) and proximal-distal (P-D) patterns take place (Figure 5B-C and Figure 6A-B). The optic primordia (OP) remains attached to the forebrain at the anterior end by the optic stalks, a transient structure that eventually will be filled by RGC axons and form the optic nerve. Lens induction is initiated around 16 hpf as the OV comes in close contact with the surface ectoderm (Vihtelic, 2008). Around 19 hpf the OV invaginates symmetrically forming the optic cup (OC) (Figure 5D). The OC consists of two layers: the RPE and the neural retina. The prospective neural retina is derived from the distal ventral OV (Figure 5B-C). Moreover, the invagination process from the dorso-distal (D-D) of the OV makes contact along the forming retina and optic stalk, resulting in the formation of a transient opening along the ventral optic known as choroid fissure, that allows entry of blood vessels and exit of retinal axons from the eye (Figure 5D-E and Figure 6C). By 24 hpf the zebrafish bi-layered OC and the now detached lens are well formed. At 48-60 hpf the ventro-nasal and ventro-temporal lips of the choroid fissure in the retina fuse together and forms a continuous retina confined within the OC (Chow and Lang,

2001; Schmitt and Dowling, 1994). The development of the zebrafish retina is extraordinarily rapid facilitating numerous studies addressing retinal development and its genetic control (Table 5).

Eye developmental stage	**Human (gestation days)**	**Mouse (days)**	**Zebrafish (Hours post fertilization)**
Eye field specification	<22	E8.0	10
OV Evagination	22	E8.5	12-18
Lens Placode formation	28	E9.5	16
OV invagination	32	E10	19
OC neurogenesis initiation	33	E11.5	28

Table 5 Comparison of key developmental stages in vertebrate eye development. (adapted from (Zagozewski et al., 2014)).

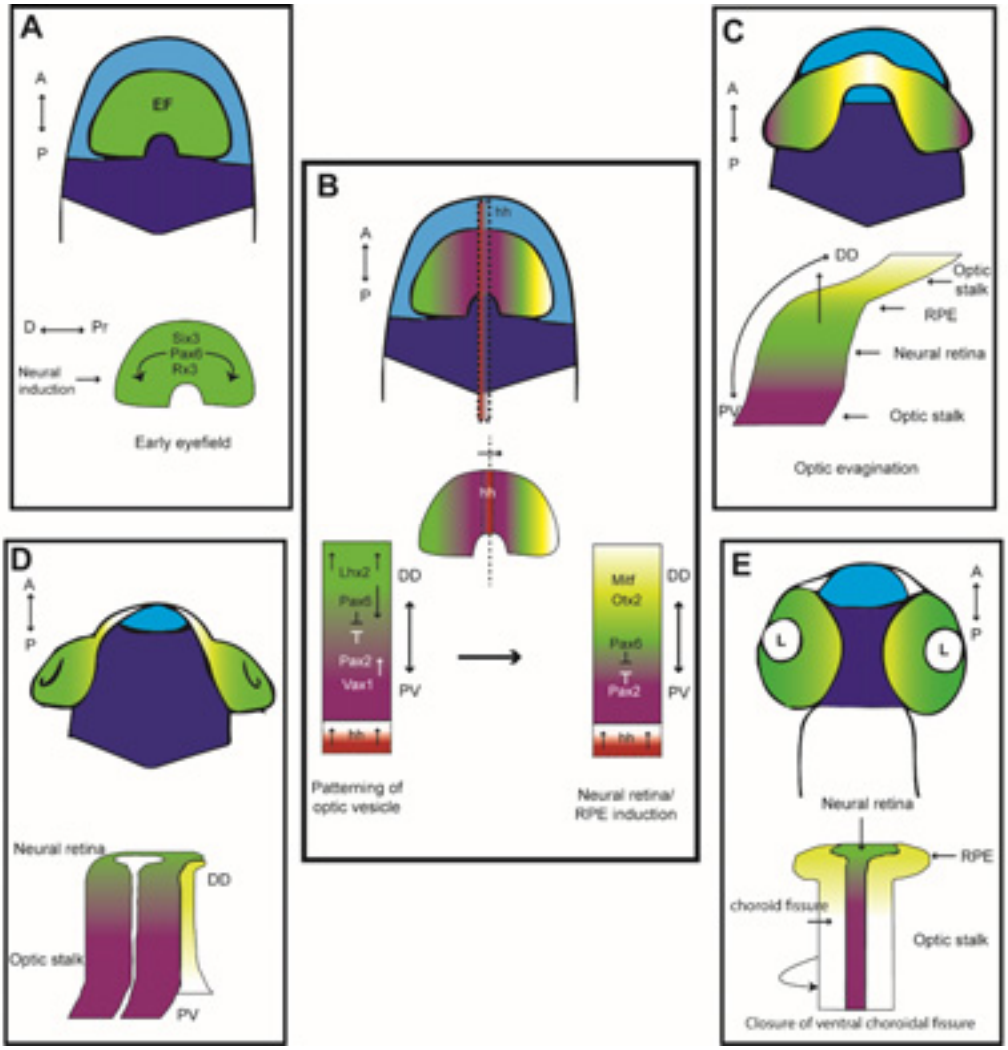

Figure 5 Schematic overview of eye development.

The figure represent a ventral view of different stages of eye morphogenesis (**A**) Formation of the eye field. (**B**) Early events for the definition of the dorso ventral patterning of the optic vesicle (left). Induction of the neural retina and RPE (right). (**C**) Optic evagination is the first morphological event that alters the shape of the presumptive eye tissues and dorso ventral patterning of the neural retina. (**D**) Optic vesicle invagination and subsequent formation of the optic cup, presumptive RPE folds back over the presumptive neural retina. (**E**) Ventral fissure closure occurs as the laterally extending edges of the neural retina and RPE, sweep in a ventral movement and eventually fuse. This process is completed in approximately 14 hours. Based on (Chow and Lang, 2001).

Abbreviations: A: Anterior; P: Posterior; EF: Eye Field; D: Distal; Pr: Proximal; DD: Dorso-distal; PV: Proximo-Ventral; hh: Hedgehog signaling; RPE: Retinal Pigmented Epithelium; L: Lens.

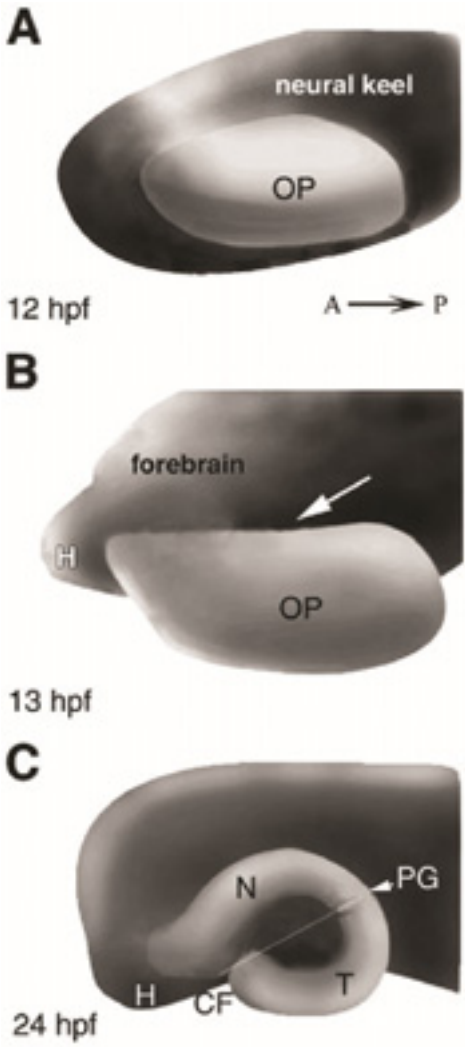

Figure 6 Schematic overview of the morphogenesis of the optic primordia in zebrafish.

The figure represents the lateral view of a zebrafish embryo in 3D.

(**A**) The optic primordia (OP) arise at 12 hpf. (**B**) At 13 hpf, the optic primordia begin to evaginate (*white arrow*), leaving the primordium attached by the optic stalk at the anterior end. (**C**) By 24 hpf, invagination of the lateral surface creates the optic cup. After ventral rotation, the optic stalks are located on the ventral side of the forebrain. The choroid fissure (CF) is positioned near the anterior of the optic cup, opposite the posterior groove (PG). The line between the choroid fissure and posterior groove subdivides the retina into nasal (N) and temporal (T) parts.

Abbreviations H, hypothalamic primordium; A, anterior; P, Posterior

Image from (Hitchcock and Raymond, 2004).

b.Retina development

Similar to other vertebrates, the zebrafish retina is also arranged into three nuclear layers and two plexiform layers. Unlike mammals, the zebrafish retina displays continual neurogenesis throughout life and has the ability to regenerate any type of retinal neuron in response to injury (Wan and Goldman, 2016).

Retinal neurogenesis during zebrafish development require a precise spatiotemporal control. This spatiotemporal pattern has several components including cell-specific timing of cell cycle exit, tissue polarity and neuronal migration. Moreover, this process has been shown is present in a wave-like manner that starts at the ventro nasal center of the retina and then spirals out ending in the ventro temporal periphery. Several transcription factor families are required to specify and promote the differentiation of each retina cell. (Almeida et al., 2014; Hu and Easter, 1999).

At 24 hpf the zebrafish neural retina still consists of a single sheet of pseudostratified neuroepithelium. The first postmitotic cells appear between 27 and 28 hpf in the ventro nasal retina. By 32 hpf these cells differentiate into RGCs (Burrill and Easter, 1995; Schmitt and Dowling, 1996). Cells of the INL are generated next, starting at 36 hpf. Cone photoreceptor cells are born later, around 48 hpf. The genesis of rod photoreceptors in the teleost retina is delayed. Retinal lamination and cell differentiation are completed around 96 hpf (Stenkamp, 2007).

Functionally, the zebrafish eye detects light surprisingly early, the first visual response can be detected by electroretinogram (ERG) as early as 72 hpf, however, full-fledged ERGs can only be measured at slightly later stages (Branchek, 1984; Saszik et al., 1999).

In total the retina is comprised of six neural and one glial type, arising from a common pool of multipotent progenitor cells, organized into a trilaminar structure.

c. Photoreceptor development

Due to the relevance of the photoreceptors in the SCA7 disease, is important to review in more detail the development of this structure.

Photoreceptor cells include two different populations rod and cone photoreceptors cells. The differentiation of zebrafish photoreceptors, starting from the exit of the cell cycle up to the formation of OS and synaptic ribbons, occurs in a short period of less than 20 hours. Starting between 43 and 48 hpf when the zebrafish photoreceptors first exit the cell cycle, by 48 hpf

they develop their characteristic elongated form and at 54 hpf rudiments of photoreceptor OS appear. Finally the synaptic ribbons are apparent in the ventral area by 62 hpf and are well differentiated throughout the retina by 72 hpf. (Hu and Easter, 1999; Schmitt and Dowling, 1999).

Functionally, the expression of the rod opsin becomes detectable around 50 hpf followed by the rest of the opsins shortly after. In total zebrafish express six opsins: blue, red, rod, ultraviolet and two types of green (Raymond et al., 1995; Vihtelic et al., 1999).

2.Molecular pathways involved

The developmental events that take part in the formation of the eye are highly regulated by different secreted signaling molecules, including the Wnt,Transforming Growth Factor Beta (TGF-β), Fibroblast Growth Factor (FGF) and Hedgehog (Hh) families (Adler and Canto-Soler, 2007; Bazin-Lopez et al., 2015; Fuhrmann, 2010; Zagozewski et al., 2014). The latter being one of the most extensively studied.

a.Hh signaling

More than two decades ago Hh was first identified (Nusslein-Volhard and Wieschaus, 1980). Since then many studies have shown the relevance of Hh signaling not just in the development of neural tissues, limb buds, bones, cartilage, and germ cells; but novel biological insights have implicated Hh signaling with congenital diseases, and several cancers as well (Briscoe and Therond, 2013).

Unlike drosophila that presents a single *Hh* gene, or mammals that present three Hh family members including Sonic hedgehog (*SHH*), Indian hedgehog (*IHH*) and Desert Hedgehog (*DHH*); zebrafish has five Hh genes *shha*, *shhb* (also known as tiggy- winkle hedgehog, *twhh*), *ihha*, *ihhb* and *dhh* (Currie and Ingham, 1996; Ekker et al., 1995; Krauss et al., 1993).

b. Shh involvement in the Optic Vesicle formation and patterning

Zebrafish Hh members regulate several aspects of OV formation, patterning and morphogenesis (Amato et al., 2004). Hh signaling from the ventral midline plays a critical role in optic field separation by directing the separation of the eye field into two bilateral OVs (Figure 4B and Figure 4). This phenomenon has also been documented in both mice and human embryos (Chiang et al., 1996; Roessler et al., 1996). Moreover, Hh signaling plays a role in

the P-D and D-V patterning of the OV (Ekker et al., 1995; Hernandez-Bejarano et al., 2015; Macdonald et al., 1997).

Hh expression is first crucial for the separation of the OP. Loss of *Shh* function in both, human and mice, have been reported to cause severe developmental defects, particularly with the presence of cyclopia due to a failure in the eye field separation (Chiang et al., 1996; Roessler et al., 1996). Interestingly, *shh* mutations in the zebrafish embryo, do not lead to cyclopia, likely due to redundancy present with *twhh* (Karlstrom et al., 1999; Schauerte et al., 1998).

The second fundamental role in the OV is the determination of the P-D axis. The Shh signals emanating from the ventral midline define distinct ocular tissue identities by regulating expression of key transcription factors. In response to Shh, paired box gene 2 (*pax2)* and ventral anterior homeobox (*vax)* genes are expressed in adjacent regions to the midline and specify the optic stalk, choroid fissure and ventral retinal fates respectively, whereas paired box gene 6 (*pax6)* and retinal homeobox (*rx)* are expressed in regions further distal to the midline and defines the optic cup and RPE respectively (Figure 5B and Figure 7) (Macdonald et al., 1995; Stenkamp and Frey, 2003; Take-uchi et al., 2003). While *pax2* expression is critical for the specification of the optic stalk and the proper formation of the optic nerve, the correct expression of *pax6* in the optic vesicle, is required for proper retinal neurogenesis, RPE and lens formation (Baumer et al., 2003; Oron-Karni et al., 2008; Torres et al., 1996).

Shh overexpression promotes the expression of *pax2* in more distal OV territories where it is normally absent. Furthermore, there is a corresponding retraction of the *pax6* expression in the OV area (Ekker et al., 1995; Lee et al., 2008; Macdonald et al., 1995; Pillai-Kastoori et al., 2014; Wen et al., 2015). Conversely loss of midline Hh expression leads to a reduction or no expression of pax2, resulting in failure in optic primordium separation (Ekker et al., 1995). The distinctive expression of *pax2* and *pax6* is due to a reciprocal regulation. They both repress each other's transcription and thereby form a precise boundary between the optic stalk and retina (Schwarz et al., 2000) (Figure 7).

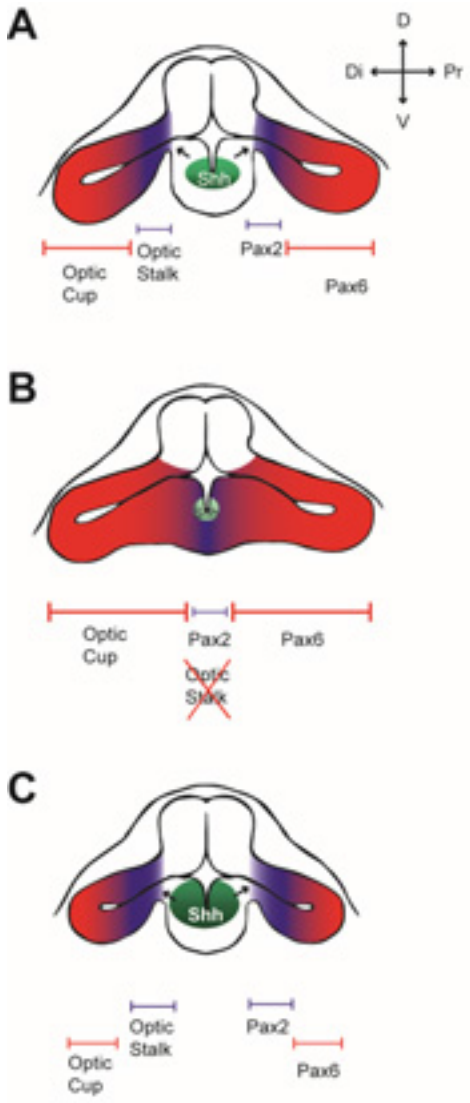

Figure 7 Overview of cell fate changes in the Optic Vesicle depending on Shh signaling.

Schematic representations of frontal views of the zebrafish CNS. **(A)** In the wild-type embryo, Pax6 (blue) is present in the pigment epithelial and neural layers of the retina and Pax2 (red) is present in the optic stalks and a small region of the ventral anterior retina. The Pax6-expressing region of the optic primordium later invaginates with more distal cells forming neural retina and more proximal cells forming the pigment epithelium. **(B)** In low shh expression levels Pax6 protein is present in cells across the rostral midline of the forebrain, Pax2 is almost absent and most if not all cells differentiate as retina (example: Cyclops). **(C)** In shh-overexpression embryos, Pax6 protein is absent from most cells in the optic primordia whereas Pax2 expression is expanded. Optic stalk-like tissue is hypertrophied and the retina is greatly reduced. Based on (Macdonald et al., 1995)

Abbreviations: Di: Distal; Pr: Proximal; D: Dorsal; V: Ventral.

c.Shh involvement in the retinal differentiation

Additional to its role in the OV formation and patterning, Hh signaling appears to be also involved in the retina and RPE cell differentiation (Choy and Cheng, 2012; Neumann and Nuesslein-Volhard, 2000; Perron et al., 2003).

The first postmitotic cells appear between 27 and 28 hpf in the ventro nasal retina in proximity to the optic stalk. These cells differentiate into ganglion cell and present two waves of gene expression: a wave of *ath5* and a wave of *shh* (Masai et al., 2000). *Ath5* expression is required for the differentiation of RGCs, as the zebrafish *lakritz* mutant that harbors a mutation in the *ath5* locus exhibits a complete loss of RGCs (Kay et al., 2001). Interestingly midline-derived Shh signaling prior to retinal neurogenesis is required for the timing of *ath5* expression and RGC differentiation (Kay et al., 2005). Moreover, the midline Hh activity is also required for the RGC axon pathfinding and confines the growth cone of the optic nerve during optic chiasm formation (Trousse et al., 2001). Additionally experiments in *shh* mutant *sonic-you (syu)* have shown that the expression of *shh* is required for its own spread through the retina. Interestingly the Hh signaling is required for the spread, but not the induction of the first Hh-expressing neurons. Despite the disruption in the *shh* gene, *syu* mutant presented retinal neurogenesis. This has been attributed to the expression of *twhh* in the ganglion cell layer. Treatment of embryos with cyclopmaine (inhibit signaling of Hh family members (Incardona et al., 1998)) during neurogenesis, blocked both the spread and the wave of neurogenesis (Neumann and Nuesslein-Volhard, 2000).

Soon after the initial expression in the ganglion cell layer, a second independent wave of *shh* expression is initiated in the differentiating amacrine cells in the INL of the zebrafish retina. Experiments with *shh* mutant shown that, *shh* activity in the INL is required for the differentiation of amacrine cells, bipolar cells and Müller glia. Shh acts as a short-range signal in the neural retina to direct the differentiation of these cell types, as well as the formation of plexiform layers (Shkumatava et al., 2004).

The RPE is a thin monolayer of cells that underlies the retina and maintains the function and development of the photoreceptors (Sheedlo et al., 1998; Strauss, 2005). Around 45 hpf *shh* and *twhh* expression is detected in a discrete ventral patch of the zebrafish RPE. This expression occurs immediately prior to the first morphological manifestation of photoreceptor differentiation, and it is proposed that Hh genes may play a role in the propagation of the photoreceptor differentiation wave across the developing eye (Stenkamp et al., 2000).

Several studies in zebrafish strains known to have mutations in the Hh signaling pathway genes exhibit retardation in the differentiation as well as reduction in the number of photoreceptors. Moreover, abnormalities in the retinal lamination were observed in these mutants (Stenkamp and Frey, 2003; Stenkamp et al., 2000). It is worth to mention that no such abnormalities were found in the expression of *neuroD*, *crx* and *rx2*. All of these genes are implicated in the photoreceptor differentiation. However, reduced expression of *rx1*, a photoreceptor progenitor gene, is observed in the *smu* mutant (mutation of smoothened), suggesting that rx1 might be regulated by Hh signaling activity (Stenkamp et al., 2002).

d. Otx2 and Crx involvement in the photoreceptor morphogenesis.

Photoreceptor specification has been attributed mainly to two homeobox transcription factors, orthodenticle homeobox 2 (*Otx2)* and *Crx*. These two control the earliest stages of photoreceptor development. *Otx2* is a transcriptional factor that is also required to specify the forebrain and the RPE. *Otx2* mutants have shown a loss of RPE pigmentation, photoreceptor cells and an increase in amacrine cell numbers (Lane and Lister, 2012; Nishida et al., 2003). *Crx*, a downstream target of *Otx2,* is required for development and maintenance of the photoreceptors (Furukawa et al., 1999). *Crx* deficient animals form photoreceptors but they express dramatically reduced amounts of visual pigments as well as other components of the phototransduction cascade. Moreover, photoreceptors fail to form and eventually degenerate. (Furukawa et al., 1999). In zebrafish it has been demonstrated that *crx* has earlier and broader roles in retinal development compared to mice, including retinal specification and a delayed retinal differentiation including but not limited to photoreceptors (Shen and Raymond, 2004),

Different mutations in *CRX* lead to human cone-rod dystrophies or retinitis pigmentosa, suggesting that human *CRX* is also essential for the maintenance of photoreceptors (Sohocki et al., 1998). Together, *otx2* and *crx* play a role in the photoreceptor cell fate and differentiation, rod or cone cell fate is dependent on the expression of other three transcription factors, *TRβ2* (also known as *NR1A2*), *Nrl* and *Nr2e3* (also known as *PNR*).

3.Retinal disease models in zebrafish

Zebrafish (*Danio rerio*) is a small freshwater fish species original from the rivers of India that since the 1970's has become an attractive model for study as its embryogenesis is similar to higher vertebrates, including humans. Moreover, it offers advantages such as large numbers of offspring, external and rapid development that makes it an attractive model for study.

Furthermore, its characteristic optical transparency during embryonic morphogenesis can take advantage of microscopy techniques.

Zebrafish have 25 chromosomes and its genome is well curated by multiple databases. This has allowed the identification of zebrafish orthologs of most human genes. Approximately 72% of human genes have at least one ortholog in the zebrafish genome, with 84% of known human disease-causing genes having a zebrafish counterpart (Howe et al., 2013). This combined to the number of techniques that have been successfully adapted to the zebrafish has enable relatively straightforward reverse genetic manipulation of genes of interest (Hruscha et al., 2013; Huang et al., 2012) .

Taking together these advantages, the zebrafish has emerged as an outstanding model for understanding the development of multiple organs including the eye. Zebrafish are visually responsive by 72 hpf by which time the retina resembles adult retinal morphology that is anatomically and functionally similar to humans (Chhetri et al., 2014). Additionally the zebrafish is remarkable for its diurnal color vision, the cone rich zebrafish retina resembles the human macula, making it a good candidate to complement studies from the nocturnal rod-dominated mouse retina, a relevant system for mammalian genetics and retinal biology but insufficient in cones.

Large scale genetic screens have allowed the identification of candidate genes related to ocular defects (Muto et al., 2005). Currently more than 50 human ocular disorders affecting a particular retinal layer or eye morphogenesis have been associated with a zebrafish homologue (Figure 8).

Of particular interest for us is the modeling of Cone-Rod dystrophies (CRDs) which are most frequently non syndromic, but they may also be part of several syndromes, such as Bardet Biedl syndrome and Spinocerebellar Ataxia Type 7 (SCA7). Zebrafish is being used to model cone–rod dystrophies by studying mutants of human gene orthologs or by expression of validated disease associated human genes (Link and Collery, 2015; Richardson et al., 2017).

There has been remarkable progress in the effort to better understand the molecular mechanisms underlying the vertebrate eye development. As a result, it has been possible the identification of a large number of genes expressed at different points of the developing eye. Additionally different signaling molecules and intrinsic transcription factors have shown a relation to human ocular disorders when mutated. However we are just beginning to understand how these molecules interact with one another to regulate different aspects of eye morphogenesis, maintenance and function. Understanding the role of these genetic

interactions in vertebrate eye will be essential to better understand human inherited eye diseases and eventually develop novel therapies. Even though the general principles in retinal synaptic organization and function are conserved among vertebrate, there are species-specific variations in these principles. Adaptation to the environment plays an important role. For example diurnal vertebrates who have to distinguish color in their environment need more cones in comparison with animals whose environment is depleted of light or those who are primarily nocturnal.

The zebrafish, as a diurnal animal, appears as an attractive model because of its relative simplicity, rapid development and accessibility to genetic analysis. Moreover, the remarkable evolutionary conservation of the vertebrate eye provides the basis for the use of the zebrafish retina as a model of human inherited eye defects

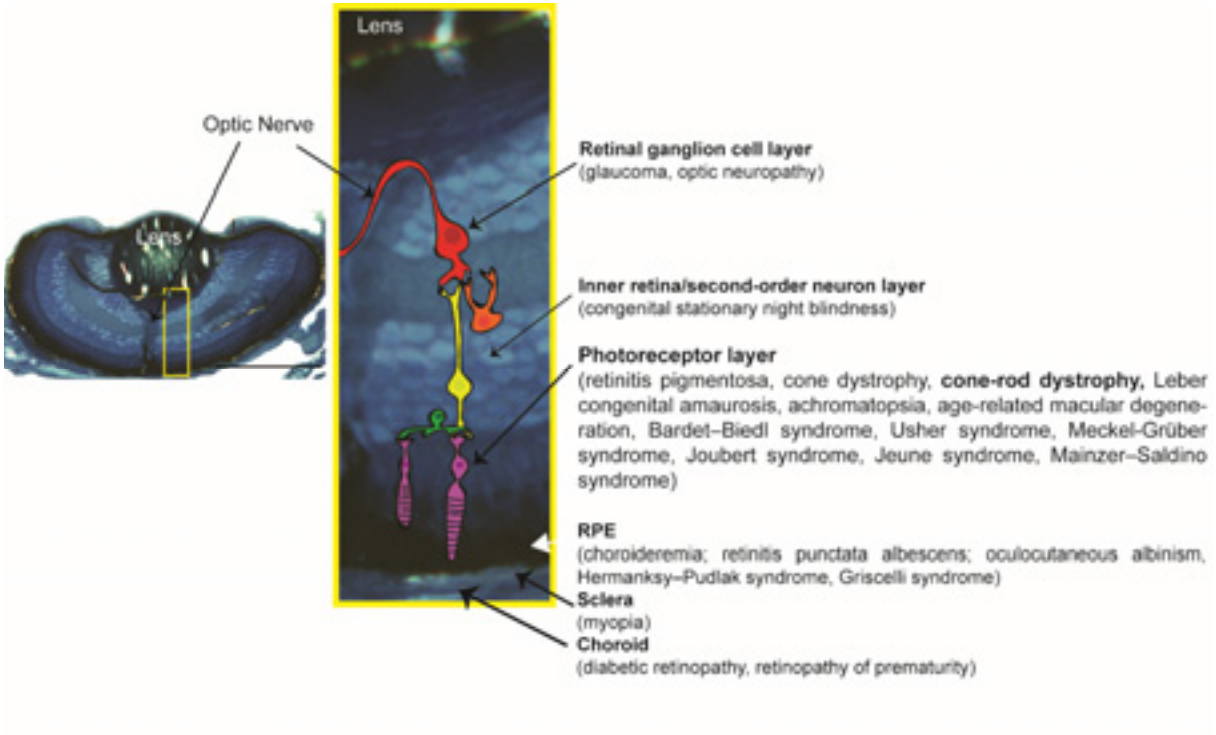

Figure 8 Toluidine blue-stained zebrafish retinal coronal section of 5 dfp larvae.

Schematic representation of the cell layers of the eye. Diseases modeled in zebrafish are listed next to each layer. Based on (Link and Collery, 2015).

Abbreviation: RPE, retinal pigment epithelium.

Objective, hypothesis and experimental approaches

The objective of this thesis was to determine the physiological role of ATXN7 in vertebrate. Given that loss of function mechanism is thought to account for polyQ pathogenesis and that SCA7 primarily affects specific CNS tissues (e.g. cerebellum and retina) and selective neuronal cell types (e.g. Purkinje cells and photoreceptors) despite the ubiquitous expression of ATXN7 protein, we hypothesized that ATXN7 has very important functions specifically in these disease-targeted tissues and neurons. The sensitivity of these tissues/neurons to ATXN7 dysfunction would make them more susceptible to degeneration in SCA7. We also wished that this study would reveal new molecular and cellular pathways in which ATXN7 would play a role. We anticipated that the characterization of the physiological function of ATXN7 would provide insight into the pathogenic mechanisms underlying neuronal specific dysfunction and loss in SCA7.

To determine the physiological role of ATXN7 and to test our hypothesis, we have used zebrafish as a model system. Our choice was motivated by several criteria. There is current no knock-out mouse model for Atxn7 gene. The International Mouse Phenotyping Consortium has very recently regenerated embryonic stem cells with a cre/lox cassette to inactivate the mouse Atxn7 gene, however, the KO mice has not been yet generated despite several attempts. As we mentioned above, the zebrafish offers several advantages to characterize the function of a gene, including the large numbers of offspring, the external and rapid development and its characteristic optical transparency during embryonic morphogenesis. Additionally, zebrafish is remarkable for its diurnal color vision, which makes zebrafish retina more alike the human macula, and a better model than nocturnal mouse on this respect.

The approach of the present work was to inactivate the atxn7 ortholog gene in zebrafish using morpholino antisense oligonucleotides and CRISPR/Cas9 technology. Given that eye anomalies appeared to be the most prominent phenotypes, we conducted a careful characterization of these phenotypes at the morphological, cellular and molecular levels.

MATERIALS AND METHODS

Chapter 2

Materials and Methods

RT-PCR analysis.

RNA extraction

Total RNA was extracted from 50 embryos at required stage by TRIzol Reagent (Invitrogen) adapting recommended volumes from the user guide manual for zebrafish embryos. Resulting protocol:

1. Dechorionate embryos if needed with Dumont Tweezers #5, transfer to 1.5 mL Eppendorf tubes removing as much liquid as possible and freeze in liquid nitrogen.
    a. For embryos younger than 24 hpf dechorionation was performed on a petri dish coated with agarose 2% to avoid breaking.
2. Add 200µL of TRIzol Reagent (Invitrogen cat. no. 15596-018) and homogenize sample with Disposable Polypropylene, RNase-Free Pellet Pestles.
3. Centrifuge 12,000 rpm for 10 min at 4°.
4. Remove and discard the fatty layer and transfer the remains to a new 1.5 mL Eppendorf tube.
5. Incubate for 5 min at room temperature (RT) and add 40 µl of chloroform. Mix by manual inversion 15 seconds.
6. Incubate for 3 min at RT and centrifuge samples at 12,000 rpm for 15 min at 4°.
7. Remove aqueous phase and place into a new 1.5 mL Eppendorf tube and add 100 µL of 100% isopropanol.
8. Incubate at RT for 10 min.

9. Quick vortex.
10. Centrifuge at 12,000 rpm for 10 min at 4°. Remove and discard supernatant.
11. Wash the remaining pellet with 200 µL of 75% ethanol.
12. Quick vortex.
13. Centrifuge 7,500 rpm for 5 min at 4°. Remove and discard the ethanol and air dry the remaining pellet.
14. Add 30 µL of water
15. Measure the concentration using NanoDrop

Produced RNA was kept at -80°.

Reverse transcription

RNA was reverse transcribed into cDNA with random primers and the SuperScript II Reverse Transcriptase (Invitrogen cat. No. 18064-014) according to the manufacturer's instructions (user manual p.2). All experiments performed in this study were performed with the corresponding –RT (without reverse transcriptase) control.

PCR

The resulting cDNA was amplified with Taq polymerase and the following mix:

Component	**Volume**
cDNA	2 µL
Mix 5X *	4 µL
Primers 10µM	1 µL
Taq	0.1 µL
H_2O	12.9 µL
FINAL VOLUME	20 µL

Table 6 PCR mix.

* PCR Sigma 10X buffer without MgCl2 (cat. No. P2317) added MgCL 1.5mM final

Cycling parameters for β-actin, atxn7 (MO2) *atxn7L2a* and *atxn7L3.*

1: 95°C 3 min; 2: 94°C 30 sec; 3: 61.5°C 20 sec; 4: 72°C 30 sec; 5: Go to 2, 30 times; 6: 72°C 7 min; 9: 15°C forever.

Cycling parameters for *atxn7*, *atxn7L1and atxn7L2b.*

1: 95°C 3 min; 2: 94°C 30 sec; 3: 64°C 20 sec; 4: 72°C 30 sec; 5: Go to 2, 30 times; 6: 72°C 7 min; 7: 15°C forever.

The RT-PCR products were then electrophoresed on a 2% agarose gel.

	Fwd	**Rv**	**Expected band size**
atxn7	5'-CCCTGCCTAGTCCCGAAATA-3'	5'-GACGATTGGTGGCCTTTCC-3'	694 bp
atxn7 Mo2	5'-GCCTTCCAAGCACATTAC-3'	5'-TTGTCTTGGGACGATTGGTG-3'	471 WT 590 Mo2
atxn7L1	5'-GTCTACCCACCCAAAGGAGC-3'	5'-TCCAGAGGAGCCGAGAGAAA-3'	1178 bp
atxn7 L2a	5'-AGAGGAACCAAGACGCACAA-3'	5'-AAAGTGAAGACACCGTGACC-3'	548 bp
atxn7L2b	5'-GCACGCGCTAAAACGGTAAT-3'	5'-TCTCGTGGTTGACAGACCCT-3'	889 bp
atxn7L3	5'-TCAGAGTCTTCCTCCTTGGG-3'	5'-GCCTGCTATTCTGTCTCGCT-3'	275 bp
β-actin	5'-CGAGCAGGAGATGGGAACC-3'	5'-CAACGGAAACGCTCATTGC-3'	102 bp

Table 7 Expected band size and primers.

mRNA Human N10 generation.

Capped human mRNA for microinjection was prepared with mMESSAGE mMACHINE SP6 kit (Ambion Ref no. AM1340). pCS2+ vector containing the full-length coding sequences for the human wild-type ATXN7a with 10Q (N10) was linearize with PvuII. Phenol-chloroform purification and 100% ethanol precipitation was performed. Capped RNA transcription was performed following the manufacturer's instructions (User Guide p.11). Followed by a verification of the mRNA integrity on a 1% agarose gel.

Produced RNA was kept at -80°.

Morpholino and mRNA injections.

Translation blocker, splicing and control MOs were designed and obtained from Gene Tools.

- Morpholino MOs and mRNA were diluted in nuclease free water .
- Mo1 was injected at the concentration of 3 ng (dose response included 1.5 ng, 2 ng, 3 ng, 6 ng and 9 ng).
- Control morpholino was injected at the concentration of 6 ng.
- Mo2 was injected at the concentration of 1.5 ng (dose response included 1 ng, 1.5 ng and 2 ng).
- mRNA was injected at 150 ng (different concentrations 50, 100, 200 and 300 ng to assess the toxicity).

CRISPR sgRNA and Cas9mRNA synthesis, injection and efficiency.

gRNA design

Atxn7 target sites were identified and the corresponding sgRNA oligos were designed using the Chop-Chop online software (Labun et al., 2016).

Target	gRNA exon1 (19+1)	Primer FW	Primer RV
5'-GGCCGATGATGACGTCAGG-3'	*5'-TAATACGACTCACTATAGGCCGATGATGACGTCAGGGTTTTAGAGCTAGAAATAGCAAGTTAAAATAAGGCTAGTCCGTTATCAACTTGAAAAAGTGGCACCTGAGTCGGTGCTTTT-3'*	*5'-TAATACGACTCACTATAGGGCCGATGATGACGTCAGG-3'*	*5'-TTCTAGCTCTAAAACCCTGACGTCATCATCGGCC-3'*

Table 8_ATXN7 gRNA and specific primers

gRNA generation

Oligos were mixed with the Master mix and tracer fragment T7 included in the GeneArt Precision gRNA Synthesis kit (Invitrogen Ref. Num. A29377) for generation of the gRNA template, following the manufacturer's instructions (User Guide p.12). Cycling parameters PCR amplification 1: 98°C 10 sec; 2: 98°C 5 sec; 3: 55°C 15 sec; 4. 72°C 30 sec; 5 Go to 2 32 times; 6: 72°C 5 min; 7. 15°C forever. Product was verified in an agarose 2% gel (120 bp). In vitro transcription of the template was conducted with the same kit according to manufacturer's instructions (User Guide p.14).

Injection

A mix containing .2 µg/µL Cas9 protein from *Streptococcus pyogenes* (PnaBIO Ref Num. CP 01-50), .1 µg/µL of gRNA was injected into embryos at the one cell stage using a Nanoject II micro-injector (Drummond scientific). Injection was performed directly in the cell.

Validation

To determine the efficiency of the gRNA, genomic DNA of 24hpf embryos was obtained individually by alkaline lysis with 100 µL NaOH 50mM for 10 min at 95° then placed the tubes on ice and neutralized with 10 µL TRIS 1M. Amplification of the fragment surrounding the target site was performed with *atxn7* specific primers (fw-5'CCTCAGAAATTCGCGCACAC 3') (rv-5' ATTTCGGGACTAGGCAGGGA 3'). Cycling parameters PCR amplification 1: 95°C 3 min; 2: 94°C 15 sec; 3: 65°C 20 sec4. 72°C 30 sec; 5 Go to 2 35 times; 6: 72°C 5 min; 7 15°C

forever. For the Heteroduplex mobility assay (HMA), 2μL Gel loading Blue Dye added 7 μL PCR product. Denaturation parameters: 1. 95° 2 min; 2. Go to 85° (2°/sec); 3. Go to 25° (-0.1°/sec); 4. 16° forever and loaded product on 15% polyacrylamide gels. For sequence analysis PCR products were sublconed with PCR Cloning Kit Vector pJet1.2 (Thermo scientific) according to manufacturer's instructions (User guide p.5) and send to sequence to GATC Biotech Company.

In Situ Hybridization.

In situ hybridization on whole-mount embryos was performed principally as described previously (Thisse and Thisse, 2008). However, some modifications were done. Here is the final protocol used in this study.

Probe synthesis

Linearization of the DNA plasmid containing individual probes was performed with the appropriate enzyme.

Probe	Enzyme	RNA Polymerase
atxn7	EcoR1	T7
crx	EcoR1	T7
pax2a	BamH1	SP6
pax6	AatII	SP6
shh	Hind III	T7
twhh	Bam H1	T7
vax2	Not1	SP6

Table 9 Probes with the corresponding linearizing enzyme

Transcription of all probes was perform at 37°C for 2 hours using the mix:

For SP6 polymerase	For T7 polymerase	
2 µL	4 µL	Buffer Transcription (5x or 10X)
2 µL	2 µL	Roche Mix (DIG RNA REF 11277073910)
0.5µL	0.5µL	RNAsine 400 u/µL
-	2 µL	DTT 0.5mM
2 µL	2 µL	DNA (linearized)
2 µL	2 µL	Corresponding RNA polymerase (as indicated in previous Table)
11.5µL	7.5µL	H2O

Table 10 Probe generation mix

Verification of the transcript integrity was performed on a 1% agarose gel. Followed by a LiCl and ethanol precipitation. Finally dissolved in Hybridization Mix 1 (Anex 1) and stored at -20°C

Staining

Embryo Preparation

Embryos were kept at 28.5°C in water until reached the desired stage according to previous reports (Kimmel et al., 1995). Embryos were dechorionated manually with Dumont Tweezers #5, alternative to the suggested pronase treatment. For embryos younger than 24 hpf removal of the chorion was performed on a petri dish coated with agarose 2% due to the fragility of the embryos. Embryos were then transferred to 1.5 mL Eppendorf Tubes and fixed in 4% paraformaldehyde (PFA: 4% in PBS) over night at 4° C.

It is worth to mention that embryos intended for in situ hybridization were always kept in water without PTU. For older embryos (after 28 hpf) removal of pigmentation was performed by hydrogen peroxide treatment. Fixed embryos were rinsed in phosphate-buffer saline (PBS) and incubated at room temperature in a 3% H2O2/0.5% KOH medium until pigmentation completely disappeared. The time depended on the stage of the embryos. Depigmented embryos were rinsed with PBS.

Staining Day 1

Embryos rinsed in PBS were permeabilized with 500µL of proteinase K (10µg/mL) at room temperature for different time according to the stage (1-4 hpf: 30 sec; 18hpf: 5 min; 24-28 hpf: 12 min; 42: 16 min; 48hpf: 18 min; 54hpf: 20 min; 72hpf: 30 min). The reaction was stopped by replacing the proteinase K by PFA 4% for 20 min at room temperature, followed by series of rinses with PBS (5x5 min at room temperature). Pre hybridization was performed with 500µL of Hybridization Mix 1 (Anex 1) for 3 hours at 70°C in a water bath. Then replaced with the appropriate probe (2µL of probe/200µL hybridization buffer) and incubated the embryos overnight at 70°C in water bath.

Staining Day 2

Gradual substitution of the Hybridization Mix 2 (Anex 1) to 2X saline-sodium citrate (SSC) buffer was performed through a series of 10 min at 70°C in water bath. Wash once in each of the following: 75% MH-25% 2X SSC, 50% MH-50% 2X SSC, 25% MH-75% 2X SSC followed by two additional washes in 100% 0.2X SSC for 30 min. Gradual substitution of the 0.2X SSC to Maleic Acid Buffer containing Tween 20 (MABT) (alternative to the suggested PBS) solution was performed through a series of 10 min at room temperature. Wash once in each of the following: 25% MABT -25% 0.2X SSC; 50% MABT-50% 0.2X SSC; 75% MABT-25% 0.2X SSC; 100% MABT for 10 min. Followed by incubation in blocking reagent 1X (Anex 1) for 3 hours at room temperature with gentle rocking. Then replaced with anti-DIG (Roche Ref. Num. 11093274910), dilution 1:4000 in blocking reagent 1X overnight at 4°C with gentle rocking.

Staining Day 3

The anti-DIG was replaced with 500µL of PBST. Followed by 6 washes with PBST of 15 min each at room temperature. After the last wash embryos were transferred to a 24-well plate and washed 3 times with 500µL of revelation solution (Anex 1) for 5 min at room temperature. Following the last wash the revelation solution is replaced with staining solution (Anex 1). The time in the staining solution is variable depending on the probe. During this phase embryos were regularly checked. To stop the reaction series of PBST washes were performed and a final 20 min fixation in PFA 4% was performed. Embryos were either prepared for imaging or stored at 4°. Embryos were imaged in 100% glycerol Leica M420 Macroscope with COOLSNAP coupled camera.

For eye dissection of stained embryos, chemically etched tungsten needles were used to preserve the integrity of the structure.

RESULTS

Chapter 3

Results

The results of my thesis will be presented in the format of a manuscript including: Abstract, Introduction, Materials and Methods, Results, References and Figures. The discussion for the manuscript is included as part of the general Thesis discussion contained in Chapter 4.

ABSTRACT

Spinocerebellar ataxia type 7 (SCA7) is an autosomal dominant neurodegenerative disorder caused by a toxic polyglutamine (polyQ) expansion in Ataxin-7 which leads to degeneration of cone and rod photoreceptors and cerebellar Purkinje and granule cells. The selective nature of degeneration remains unclear since Ataxin-7 is ubiquitously expressed. Ataxin-7 is a subunit of the multiprotein complex SAGA, a co-regulator of transcription, but its physiological function is unknown.

Here, we have explored the function of the Ataxin-7 ortholog in zebrafish. We show that *atxn7* is expressed throughout the zebrafish embryogenesis and has a highly dynamic tissue-expression pattern, with particular high level in the eye. Inactivation of *atxn7* in zebrafish – through antisense oligonucleotides or CRISPR/Cas9 approaches- primarily resulted in a coloboma defect, a structural malformation of the eye caused by failure of the choroid fissure to close during morphogenesis of the eye. *atxn7* morphants displayed altered proximo-distal patterning of the optic vesicle, including expanded *pax2a* expression from the area of the optic stalk with a corresponding retraction of the *pax6* expression in the area of the optic vesicle. We further show that the abnormal ocular morphogenesis observed in atxn7-deficient zebrafish is caused by elevated Hedgehog (Hh) signaling.

Careful examination of the photoreceptors reveals a defect in the morphogenesis of the outer segments. Consistent with this, *atxn7* morphants displayed strong decreased expression of *crx*, a key transcription factor involved in photoreceptor terminal differentiation.

Taken together our results indicate that atxn7 plays an essential role in vertebrate eye morphogenesis and assembly of photoreceptor outer segments. The eye sensitivity to variations in atxn7 function could account for SCA7 physiopathology. Our study also suggests that *atxn7* loss of function may contribute to the development of human coloboma.

Key words: Spinocerebellar Ataxia type 7, retina, photoreceptor, coloboma, zebrafish

INTRODUCTION

Spinocerebellar ataxia type 7 (SCA7) is an autosomal dominant, neurodegenerative disorder characterized by progressive neuronal loss in the cerebellum and associated structures, leading to cerebellar ataxia, dysarthria and dysphagia (David et al., 1998; Martin, 2012; Michalik et al., 2004). SCA7 is pathomechanistically related to the group of CAG/polyglutamine (polyQ) expansion disorders, which includes other SCAs (1-3, 6 and 17), Huntington's disease (HD), spinobulbar muscular atrophy (SBMA) and dentatorubral-pallidoluysian atrophy (DRPLA); where a translated CAG repeat expansion in the different causative genes leads to the expansion of a polyQ tract in the corresponding mutant proteins. The precise repeat threshold to pathogenesis varies within the disease (David et al., 1997; Zoghbi and Orr, 2000). Cumulative evidence indicates that toxic gain of function of mutant proteins and loss of normal protein function account for polyQ pathogenesis (Cattaneo et al., 2005; Lim et al., 2008; Zoghbi and Orr, 2000). Consequently, determining the normal function of the polyQ related proteins can contribute to a better understanding of the pathogenesis behind these disorders.

SCA7 is caused by the expansion beyond the normal range of the polyQ tract (4-35 repeats) located at the N-terminus of the ATAXIN-7 protein (ATXN7), an evolutionary conserved 892 amino acids protein (Michalik et al., 2004). ATXN7 is a highly conserved member of the multiprotein Spt-Ada-Gcn5 Acetyltransferase (SAGA) complex (also known in human as the TBP-free TAF-containing complex (TFTC) and the SPT3-TAF9–GCN5 complex (STAGA). SAGA regulates transcription through GCN5-dependent histone H3 acetylation and USP22-dependent H2B deubiquitination activities fundamental to normal cell function (Helmlinger et al., 2006; Kohler et al., 2008; Zhao et al., 2008). Two distinctive characteristics of SCA7 are the strong anticipation by which earlier onset and more severe symptoms are observed in successive generations of affected families, and the loss of visual acuity caused by cone-rod photoreceptor degeneration found in 83% of patients (Benton et al., 1998; David et al., 1998; Hoche et al., 2008; Stevanin et al., 1998).

The retinal disease begins with an initial deterioration of the central vision affecting first cone photoreceptors, manifested by the loss of blue/yellow color discrimination (dyschromatopsia) and of visual acuity (due to loss of cone function); and then progresses toward a cone-rod dystrophy, this is manifested by the loss of peripheral visual fields (due to loss of rod function). This progressively spreads out to the whole retina, declining toward complete blindness. (Enevoldson et al., 1994; Gouw et al., 1994; Thurtell et al., 2009).

Over the past 17 years, multiple studies have been performed in transgenic and knock-in mouse models of SCA7 to characterize in particular the degeneration of the retina.

Retinal dystrophy present in SCA7 is characterized by accumulation/aggregation of mutant ATXN7 (mATXN7) in retinal neuron nuclei and progressive reduction of electroretinograph activity primarily due to photoreceptor dysfunction, which precedes cell death (Helmlinger et al., 2004a; La Spada et al., 2001; Yoo et al., 2003). In the SCA7 R7E transgenic mouse, which specifically expresses mATXN7 in rods (Yvert et al., 2000), the expression of photoreceptor specific genes is progressively lowered and photoreceptors undergo extensive morphological remodeling characterized by the disappearance of outer segments (Yefimova et al., 2010). SCA7 photoreceptor thus shows an atypical scheme of degeneration, reminiscent of loss of the terminal differentiation status (Marc and Jones, 2003; Yefimova et al., 2010).

While biochemical approaches and the characterization of cellular and animal models of SCA7 have greatly advanced our understanding of disease pathogenesis in SCA7, much more needs to be learned before we get a solid comprehension of the pathogenic mechanisms underlying neuronal specific dysfunction and loss.

Yet there is no knock-out mouse model available and zebrafish then emerges as an alternative model, having an *atxn7* ortholog gene that shares 51.74% of identity with the human *ATXN7*. Zebrafish is a popular model for the study of vertebrate development and genetics, this is mainly due to its transparent embryos that develop ex-utero, making the visualization of developmental events possible (Ota and Kawahara, 2014). Furthermore, the zebrafish is

remarkable for its diurnal color vision, the cone rich zebrafish retina resembles the human macula, making it a good candidate to complement studies from the nocturnal rod-dominated mouse retina (Chhetri et al., 2014).

In this study, we examined the function of *atxn7* in zebrafish ocular development. We show that *atxn7* is required for choroid fissure closure and proper proximo-distal patterning of the optic vesicle. Furthermore, we show that the ocular phenotype of *atxn7*-deficient zebrafish is caused by an alteration in the Hh signaling pathway.

MATERIALS AND METHODS

Zebrafish. Zebrafish were maintained as described previously at 28° in a standard zebrafish facility (Westerfield, 2000). Embryos were kept at 28.5°C in water with or without 0.003% 1-phenyl-2-thiourea (PTU, Sigma Aldrich) to prevent pigment formation. Embryos were staged according to hours (hpf) or days (dpf) post-fertilization as previously described (Kimmel et al., 1995). Wild-type embryos were from the *AB* strain and transgenic SoFa1 strain was kindly provided by Dr. William A Harris (Almeida et al., 2014).

RT-PCR analysis. Total RNA was extracted from 50 embryos at required stage by TRIzol Reagent (Invitrogen) and reverse transcribed into cDNA using the SuperScript II Reverse Transcriptase (Invitrogen) according to the manufacturer's instructions. cDNA fragment (694 bp) encompassing the *atxn7* exon 1 to 5 was amplified using the *atxn7* specific primers (fw 5'-CCCTGCCTAGTCCCGAAATA-3') (rev 5'-GACGATTGGTGGCCTTTCC-3'.). Expression of β-actin (fw 5'-CGAGCAGGAGATGGGAACC-3') (rev 5'-CAACGGAAACGCTCATTGC-3') was used as an internal control. To determine the efficiency of the *atxn7* MO2 cDNA fragments (471 WT and 590 Mo2) encompassing exon 3 and exon 5 were amplified using *atxn7* specific primers (fw 5'- GGCCTTCCAAGCACATTAC-3') and (rev 5'-TTGTCTTGGGACGATTGGTG-3'). PCR products were cloned with PCR Cloning Kit Vector pJet1.2 (Thermo scientific) according to manufacturer's instructions and sequenced. Paralogs expression was analyzed using the corresponding primers: *atxn7L1* (fw 5'-GTCTACCCACCCAAAGGAGC-3') (rv 5'-TCCAGAGGAGCCGAGAGAAA-3'); *atxn7L2a* (fw 5'-AGAGGAACCAAGACGCACAA-3') (rv 5'-AAAGTGAAGACACCGTGACC-3'); *atxn7L2b* (fw 5'-GCACGCGCTAAAACGGTAAT-3') (rv 5'-TCTCGTGGTTGACAGACCCT-3') and *atxn7L3* (fw 5'-TCAGAGTCTTCCTCCTTGGG-3') (rv 5'- GCCTGCTATTCTGTCTCGCT-3').

Morpholino (MO) – mediated knockdown of Zebrafish atxn7. MO1 blocking the translation of *atxn7* [AUG; 5'-CGTCATCATCGGCCCTTTCCGACAT-3'], MO2 blocking the splice site [SPL; 5'-CAAGCGGAAGGTGGTCTTACCGTAA-3'] and a standard Control MO [ctrl: 5′-CCTCTTACCTCAGTTACAATTTATA -3'] were obtained from Gene Tools (Oregon, USA).

Embryos at one or two cell stages were injected at indicated MO concentrations using a Nanoject II micro-injector (Drummond scientific).

Phenotypic Rescue. Capped human mRNA for microinjection was prepared with SP6 mMESSAGE mMACHINE SP6 kit (Ambion) using linearized pCS2+ vector containing the full-length coding sequences for the human wild-type ATXN7a with 10Q (N10). For rescue experiments, a mix containing MO1 (3ng) and human *atxn7* N10 mRNA (150ng), was injected into embryos at the one to two-cell stage using a Nanoject II micro-injector (Drummond scientific), and the phenotypes were analyzed at the indicated stage.

CRISPR sgRNA and Cas9mRNA synthesis and injection. *Atxn7* target sites were identified and the corresponding sgRNA oligos were designed using the Chop-Chop online software (Labun et al., 2016). Oligos were mixed with the Master mix and tracer fragment T7 included in the GeneArt Precision gRNA Synthesis kit (Invitrogen) for generation of the gRNA template, followed by a PCR amplification (120 bp). In vitro transcription of the template was conducted with the same kit according to manufacturer's instructions. A mix containing 2 µg/µL Cas9 protein from *Streptococcus pyogenes* (PnaBIO), 1 µg/µL of gRNA was injected into embryos at the one cell stage using a Nanoject II micro-injector (Drummond scientific). To determine the efficiency of the gRNA, genomic DNA of 24hpf embryos was obtained by alkaline lysis and amplified with *atxn7* specific primers (fw-5'CCTCAGAAATTCGCGCACAC 3') (rv-5' ATTTCGGGACTAGGCAGGGA 3'). For the Heteroduplex mobility assay (HMA), PCR products were analyzed by electrophoresis on 15% polyacrylamide gels. For sequence analysis PCR products were sublconed with PCR Cloning Kit Vector pJet1.2 (Thermo scientific) according to manufacturer's instructions and sequenced. Sequence analysis was performed using Serial Cloner 2.6. For generation of the figure, alignment was performed with using Clustal Omega (McWilliam et al., 2013) figure generated with Jalview 2.10.1 (Waterhouse et al., 2009).

Phenotype analysis. Different retina phenotypes were analyzed between 24 hpf to 5 dpf according to the desired experiment. Embryos were anesthetized with 0.02% Tricaine (Sigma-

Aldrich) and mounted in 3% methylcellulose. Bright field images were captured using Leica M420 Macroscope with COOLSNAP coupled camera.

Angle measurement and body length. Images captured using Leica M420 Macroscope with COOLSNAP coupled camera were analyzed using *ImageJ* software (Schneider et al., 2012). Corresponding statistical analysis and figures were performed using *GraphPad Prism* version 6.00 for Windows.

In situ hybridization. Anti-sense RNA probe were generated by in vitro transcription of the corresponding plasmid containing a portion of the coding sequence of the gene of interest, using SP6, T7 or T3 polymerase and digoxigenin (DIG) (Roche Applied Science, Indianapolis, IN). The *atxn7* was generated by cloning PCR products into the pJET1.2/blunt Cloning Vector (Thermo scientific) according to manufacturer's instructions and sequenced. Subsequently transcribed using the T7 polymerase. s*hh*, *twhh* and *pax6* were kindly provided by Dr. Julien Vermot. The plasmids for *pax2.a* and *Vax2* were kindly provided by Dr. Stephen Willson. The plasmid for *crx* was kindly provided by Dr. Pamela Raymond. Embryos were fixed in 4% PFA at 4°C for 4 h to overnight and *In situ* hybridization on whole-mount embryos was performed principally as described previously (Thisse and Thisse, 2008). Images were captured using Leica M420 Macroscope with COOLSNAP coupled camera.

Axon Pathfinding Analysis. SoFa1 injected embryos were kept at 28.5°C in water with 0.003% 1-phenyl-2-thiourea (PTU, Sigma Aldrich) to prevent pigment formation. Embryos were anesthetized with 0.02% Tricaine (Sigma-Aldrich). For general optic nerve visualization, embryos were mounted in 3% methylcellulose in a depression slide and oriented for imaging. Images were captured using Leica DM 400B with COOLSNAP coupled camera using the 10X objective. For eye 3D models SoFa1 embryos were staged, anaesthetized with 0.02% Tricaine (Sigma-Aldrich) and mounted in 0.5% low melting-point agarose (Sigma Aldrich). Confocal imaging was performed on a Leica SP8 confocal microscope. Images were acquired with a low-magnification water immersion objective.

Cryosections. SoFa1 injected embryos were fixed with PFA 4% 4°C for 4 h to overnight. Cryosections were performed adapted from previous report (Fadool, 2003). Embryos were rinsed in phosphate-buffer saline (PBS) and cryoprotected in 30% sucrose solution. Embryos were mounted in HistoMolds (Leica, 2x15mm) with Shandon Cryomatrix embedding resin (Thermo scientific) and frozen on dry ice. Sections, 8 µm in thickness, were adhered to pre cleaned microscope slides (Thermo scientific) and stored at −80°C. Previous to imaging cryosections were counterstained with DAPI. Images were captured using Leica DM 400B with COOLSNAP coupled camera using the 20X objective.

Sections and Electron Microscopy. 5 dpf larvae were fixed in 2.5% glutaraldehyde, 2.5% formaldehyde in cacodylate buffer (0.1 M, pH 7.4), post fixed in 2% osmium tetroxide in 0.1 M cacodylate for 1 h at 4°C and dehydrated through graded ethanol (50, 70, 90, 100%) and propylene oxide for 30 min each. Samples were oriented and embedded in Epon 812. Semi-thin (2µm) sagittal sections were cut with an ultramicrotome (Leica Ultracut UCT) and stained with toluidine blue Images were captured using Leica DM 400B with COOLSNAP coupled camera using the 20X objective. Selected sections were histologically analyzed by light microscopy. Images were captured with Mega View II (Soft Imaging system) and contrast was adjusted for display purposes.

Paralogs sequence analysis Human ATXN7 and paralog sequences were used to identify orthologue sequences in zebrafish using ENSEMBL database similarity searches (http://www.ensembl.org/). Human ATXN7 (ENST00000295900.10), ATXN7L1 (ENST00000419735.7), ATXN7L2 (ENST00000419735.7), ATXN7L3 (ENST00000454077.6). Zebrafish Atxn7 (ENSDART00000110499.3), Atxn7L1 (ENSDART00000122605.2), Atxn7L2a (ENSDART00000090520.4), Atxn7L2b (ENSDART00000143922.1) and Atxn7L3 (ENSDART0000010418.3). Conserved domains in Atxn7 and paralogs were based in previous report (Helmlinger et al., 2004b) alignment was performed with using Clustal Omega (McWilliam et al., 2013), figure generated with Jalview 2.10.1(Waterhouse et al., 2009).

RESULTS

Expression pattern of *atxn7* transcript in zebrafish embryo development.

BLAST search with the Ensembl zebrafish (Zv9) database identified a single orthologue of human *ATXN7* gene in the zebrafish. This gene referred to hereafter as *atxn7* (ENSDARG00000074804) is localized in the chromosome 11 and comprises 14 exons, 12 of which encode a single protein of 866 amino acids (referred hereafter as Atxn7, ENSDART00000110499.3) that shares 51.74% identity with its human orthologue. Sequence comparison revealed domain conservation. The expandable polyQ stretch is present and localized in the N-terminal portion of both orthologues followed by a C2H2 zinc-finger domain (Zfn Domain), an atypical Cys-X9–10–Cys-X5–Cys-X2-His motif, known as SCA7 domain and a conserved C-terminal domain (Figure 1A).

Using reverse-transcription PCR (RT-PCR), it was possible to determine the temporal expression profile of the zebrafish *atxn7* mRNA. a*txn7* was expressed at constant levels throughout the development (Figure 1B). *atxn7* expression was detected from the cleavage period as early as 1 hour post fertilization (hpf), also known as 4 cell stage, and maintained expression during the blastula period represented by the sphere stage, showing that the transcript for *atxn7* is maternally provided. The expression continued from early to late segmentation period (12 and 24 hpf, respectively), and throughout the hatching period (48-72 hpf), up until the early larval stage of 5 days post fertilization (dpf).

To determine the spatial expression of *atxn7,* whole-mount *in situ* hybridization (WISH) was performed on selected stages ranging from 1 hpf to 3 dpf with a DIG-labeled antisense RNA probe specific for *atxn7* (Figure 1C-F' and Supplementary Figure S1). The spatial expression of *atxn7* was dynamic during embryonic development. Consistent with the RT-PCR observations, a*txn7* was expressed during zygotic period as early as 4 cell stage, and was

ubiquitously distributed as in the blastula period, represented by the sphere stage (Supplementary Figure S1A-B). During early segmentation period, at 18 hpf, zygotic *atxn7* mRNA was shown to be ubiquitously expressed and enriched in the developing brain and eyes (Figure 1C-C' and Supplementary Figure S1C). This pattern was maintained at 24 hpf where *atxn7* expression was found without any restrictions (Figure 1D-D' and Supplementary Figure S1D). By 48 hpf the expression becomes predominantly anterior, in the brain and eyes, but excluding the lens and in the fin buds (Figure 1E-E' and Supplementary Figure S1E). Finally by 72 hpf (3 dpf) expression continues to be restricted predominantly to the anterior portion of the larvae (Supplementary Figure S1F). Moreover, expression was observed in dissected eyes with particular interest in the area of the photoreceptor, where expression was found in the outer nuclear layer (ONL) (Figure 1F-F'). WISH with a DIG-labeled sense RNA probe specific for *atxn7* (*s.atxn7*) was used as a staining control (Figure Supplementary Figure S1G).

These results demonstrate that *atxn7* is both maternally and zygotically expressed during zebrafish embryogenesis, has a highly dynamic expressing pattern and may play a role in the eye development.

Alteration in the expression of *atxn7* causes ocular coloboma.

Knockdown of *atxn7* causes coloboma.

Previous studies have suggested that in addition to brain defects, alteration in the levels of expression of *atxn7* can result in eye abnormalities (Mohan et al., 2014; Yanicostas et al., 2012). In order to address this point in a developmental context, translation blocking morpholino targeting the 5'-UTR at translation start site of the corresponding mRNA was designed to knock down *atxn7* expression in zebrafish embryos (Figure 2A). BLAST search

with the Ensembl zebrafish database (Zv9) for the proposed morpholino confirms that there is no presence of similar sequence elsewhere in the genome that could be a potential off-target.

Since there is no known existing mutant to phenocopy, concentration-effect experiments were carried out to establish a working concentration with minimal toxicity level. One to 2 cell stage-embryos injected with 2 and 3 ng of morpholino displayed easily visible morphological anomalies of the eye with high frequency at 72 hpf (60.9% and 89.1 %, respectively; see Supplementary Figure 2B). With 6 and 9 ng, the frequency of eye phenotype reached 100%. However, with these high amounts of morpholino, embryos showed mortality superior to 10% already at 24 hpf (Supplementary Figure 2A), and the survivors often displayed severe body anomalies with gnarled tails or abnormal shortening of the body axis at 72 hpf (Supplementary Figure 2E & F). In contrast, embryos injected with 3 ng or less always had straight anteroposterior body axis, as in non-injected embryos or in embryos injected with Control morpholino (6ng) (Supplementary Figure 2C & D and data not shown), and their mortality was low. For the rest of the studies here presented, wild-type zebrafish embryos of the strain AB, were injected with 3 ng of translation blocking morpholino per embryo, hereafter referred as Mo1 morphants or Mo1, and analyzed for eye phenotype.

The formation of the eye cup involves key morphogenetic events. In particular, in the ventral area of the developing eye, the two edges of neuroectodermal layers meet at 24 hpf to form a narrow choroid fissure. Later, the choroid fissure closes to circumscribe the retina and the RPE in the eye cup (Illustrated Figure Supplementary 2H) (Chow and Lang, 2001; Sinn and Wittbrodt, 2013). Compared to the Control morphants at 24 hpf, Mo1 morphant eyes presented larger opening of the choroid fissure (Figure Supplementary 2G-G'). The extent of opening varied in severity, and was sometime accompanied by neuroectodermal lip bent backwards. To ensure this was not a developmental delay, embryos were followed throughout the development. By 48 hpf, the ocular defects in Mo1 morphant were more pronounced, with the choroid fissure that clearly failed to close, a morphological anomaly called coloboma (compare Figure 2 C-C' and E-E' for control and Mo1 morphant, respectively).

In addition to coloboma, when the Mo1 morphants were visualized laterally, they lacked pigmentation in the ventral area surrounding the choroid fissure. The pigmentation of the eye comes from the melanosomes of the underlying retinal pigmented epithelium (RPE). These defects persist throughout the development. At 5 dpf, Mo1 morphants displayed a striking difference in the coloration through the lens, in the area corresponding to the RPE in the posterior retina; compared to the Control that presented a uniform black coloration through the lens, the Mo1 that had no coloration (Figure 2D-D' and F-F' respectively). Notably, when the same Mo1 morphants were visualized dorsally, the posterior eye cup had irregular edge, incomplete pigmentation and extrusion of non-pigmented tissues toward the forebrain (Figure 2 F"), which might explain the apparent lack of pigmentation when visualized laterally. (Figure 2 F").

To perform quantitative analysis of the variably-penetrant coloboma and associated pigmentation phenotypes, four point grading scale was defined at 72 hpf, "No Phenotype", "Mild", "Unilateral", and "Bilateral" (see Figure legend 2B for definition). Non injected and Control fish behaved identically with 96.9% "No Phenotype" (Figure 2B). In contrast, 89.3% of Mo1 morphant showed eye phenotype, with 67.8% of "Bilateral" phenotype, 14.2 % of "Unilateral" and 7.1% "Mild". When this point grading scale was used to score embryos in the concentration-effect curves, the penetrance and severity of the phenotype increased in a concentration dependent manner (Supplementary Figure 2B).

Although bioinformatic analysis didn't reveal a possible off-target effect, a second experiment was performed using a non-overlapping *atxn7* morpholino in order to confirm the specificity of the Mo1 morphant coloboma phenotype. This second morpholino (Mo2) was designed to target a splice site of the *atxn7* intron4 (Figure 2A and Supplementary Figure 3A). BLAST search in the Ensembl zebrafish database (Zv9) using the sequence of the Mo2 splice-blocker morpholino confirmed that there is no presence of similar sequence elsewhere in the genome that could be a potential off-target site. Wild-type zebrafish embryos of the strain AB, injected at 1 to 2 cell stage with Mo2 morpholino were scored for ocular phenotypes at 24, 48, 72 hpf

and 5 dpf by light microscopy in the same conditions as the Mo1. As shown in Figure 2G-H", Mo2 (1 ng) injected embryos presented similar alterations of choroid fissure closure and eye pigmentation, with similar progression as the ones found with the translational morpholino (Mo1). The phenotype present in Mo2 was as in Mo1, concentration dependent (not shown).

Inhibition of intron4 splicing by Mo2 splice-blocker should lead to retention of intron4 in the *atxn7* mRNA, hence the creation of a premature stop codon. To confirm the efficacy of Mo2 to block intron4 splicing, RT-PCR experiment was performed with specific oligos encompassing *atxn7* exons 3 to 5, using 24 hpf-embryos injected with an increasing amount of Mo2 morpholino (Figure Supplementary 3C). The efficacy of Mo2 was demonstrated by the dose-dependent decreased intensity of the band corresponding to the spliced intron4 PCR product (471 bp without intron4) and increased intensity of the non-spliced intron4 product (590 bp with intron4). Furthermore, sequence analysis of the 590 bp PCR product confirmed the specificity and efficiency of the Mo2 splice-blocker as this sequence showed the retention of intron4 and the introduction of a premature stop codon (Figure Supplementary 3B-D).

RT-PCR analysis also revealed an additional 302 bp product in Mo2-treated samples (Supplementary Figure S3B-D). Sequence analysis indicated that it results from the use of a cryptic 5' donor splice site located in the exon4. This aberrant splicing creates a shift in the reading frame and a premature stop codon. It is noteworthy that this 302 bp band was never present in any of the RT-PCR experiments performed at the different time points through the development in Control embryos, suggesting that its appearance is a direct consequence of the Mo2 morpholino injection.

Altogether, the consistent eye phenotype produced by the two morpholinos and the proven efficiency of the splice-blocker Mo2 supports the specificity of the coloboma phenotype resulting from the downregulation of *atxn7*.

To further support that the coloboma phenotype observed in morphants was caused by the downregulation of zebrafish *atxn7*, rescue experiments were performed by the expression of

ectopic *ATXN7* mRNA into Mo1 morphants. Human mRNA expressing ATXN7 with ten glutamines (*N10*) was injected into Mo1 morphants and the four points grading scale was used to quantify its effect on the variably- penetrant coloboma phenotype. As shown in Figure 3A, injection of *ATXN7 N10* mRNA (Mo1-N10) significantly reduced the frequency or the severity of the coloboma phenotype, as compared to embryos injected with Mo1 alone (Chi square $P<0.0001$). There was a striking 2.5 fold increase in the proportion of larvae with "No Phenotype" when embryos were coinjected with N10 (Mo1-N10), and an important 2 fold decrease of larvae that displayed the most severe phenotype ("Bilateral" phenotype) (Figure 3B-E). These data suggested that human ATXN7 can compensate for the loss of zebrafish atxn7 and that the developmental role of *atxn7* in the eye formation is conserved between zebrafish and humans. Additionally, these results further support that the coloboma of *atxn7* morphants was due to reduced expression of *atxn7*.

Analysis of *atxn7*gRNA + Cas9 injected P0 founder embryos revealed coloboma defect.

In order to recapitulate the coloboma defect found in the *atxn7* morphants the CRISPR-Cas9 system was utilized as previously reported (Hruscha et al., 2013; Hwang et al., 2013; Jao et al., 2013). A single guide RNA (sgRNA) was designed to target the coding region in the first exon of *atxn7* gene to increase the likelihood of altering the protein reading frame (Figure 4A). The gRNA was co-injected with Cas9 protein from *Streptococcus pyogenes* into fertilized one-cell stage embryos. Injected embryos were analyzed at 24 hpf for genome modifications of the target locus or at 24 and 48 hpf for phenotypic analysis. Three controls were used for analysis: Non-injected, injected with sgRNA but not Cas9 and injected with Cas9 alone.

PCR amplification of the target region (357 bp) was performed on genomic DNA of individual embryos using flanking primers and the products were analyzed by electrophoresis on 15% polyacrylamide gels to determine the presence of indel mutations. 68.62% (35/51) of embryos injected with sgRNA and Cas9 presented indels, as reflected by the presence of multiple

heteroduplex bands (Figure 4B). None of the control embryos (n= 5 out of 20 from each of the three control conditions) showed similar multiple band pattern.

For 3 randomly selected embryos, the PCR products were subcloned and multiple clones were sequenced. All the 53 sequences of *atxn7*gRNA + Cas9 injected embryos had altered sequences generating 19 different types of mutation, which include deletion, insertion or deletion plus insertion of various numbers of nucleotide. Importantly, 100% of sequences analyzed in embryo #1 (21 sequences), embryo #2 (15 sequences) and embryo #3 (17 sequences) bear mutation (Figure 4C-E). Bioinformatic translation tool available on Jalview, was used in order to translate the nucleic acid sequence to the corresponding peptide sequences. All but one sequences translated revealed a premature stop codon, with that one sequence remaining in frame but missing an Aspartic Acid. Sequence analysis of the control samples didn't show any mutation. These results indicate that the sgRNA in our CRISPR/Cas9 system introduced DNA double-strand breaks at the target genomic sequence in the *atxn7* gene and thereby induced indels via error-prone non homologous end joining repair with high efficiency.

Once the efficiency of CRISPR/Cas9 system was established, injection for phenotype analysis was perform in embryos of the strain AB. Embryos were scored for ocular phenotypes at 24 and 48 hpf by light microscopy. At 24 hpf, sgRNA injected embryos presented first signs of eye defect. At 48 hpf, 24.48 % (12/49) of the sgRNA injected embryos displayed a clear coloboma defect. None of the control larvaes showed the appearance of eye phenotype (Figure 4F).

Taken together, the consistent phenotype observed in *atxn7*gRNA + Cas9 injected embryos and in Mo1 and Mo2 morphants strongly supports that alteration of *atxn7* expression during zebrafish development leads to coloboma.

Down regulation of *atxn7* causes coloboma but not Microphtalmia.

Coloboma is part of a spectrum of ocular malformations that also includes microphthalmia and anophthalmia (MAC), which can be present in a unilateral or bilateral manner; and may occur in any combination when bilateral (Skalicky et al., 2013). Microphthalmia is defined as the presence of a small eye within the orbit. A microphthalmic eye in human is defined as an eye with a total axial length that is at least two standard deviations below the mean of wild type for a selected age (Weiss et al., 1989).

To assess whether *atxn7* morphants may have microphthalmic eye in addition to coloboma, larvaes were transiently anesthetized with tricaine (0.02%) and imaged, at 3 different days in order to follow the same larvaes through development. Eye axial length and anteroposterior body length were measured on images of Mo1 morphants and Control morpholino- and non-injected embryos (Supplementary Figure S4A). At 48 hpf, the length of nasal to temporal ocular axis of Mo1 morphant eyes was significantly shorter, as compared to control eyes (ANOVA with post-hoc Dunnett test $p<0.0001$, n=30 embryos/condition). This reduced axial length of Mo1 morphant eye was maintained at 72 hpf and at 5 dpf (Supplementary Figure S4B) and was more than two standard deviations below the means of Control eyes in all the three selected stages (-2.68 at 2 dpf, -2.67 at 3 dpf and -2.55 at 5dpf Mo1 morphant compared to non-injected; similar results were present in comparison to Control morphants). While these results indicate the possible presence of microphthalmia combined with coloboma in Mo1 morphants, further analysis of the images indicated that the body length at the anteroposterior axis of Mo1 morphant larvaes was also significantly shorter compared to Controls (Figure Supplementary 4B). As a normalization of eye measurement, a ratio between the eye and body lengths was calculated. The eye/body ratio was strikingly similar in the Mo1 morphants and in the Controls at all stages, indicating that there is no clear presence of microphthalmia in the Mo1 morphants.

Ocular coloboma in Mo1 morphant is caused by an alteration of the Hh pathway.

Downregulation of *atxn7* causes proximo-distal patterning alterations.

Multiple studies have shown that genetic perturbations of developmentally important genes and signaling pathways results in the failure of the optic fissure closure in vertebrate eye (Azuma et al., 2003; Eccles and Schimmenti, 1999; London et al., 2009; Schimmenti et al., 2003; Vissers et al., 2004; Wang et al., 2008; Wyatt et al., 2008). Some of these genes are proposed to form a network of transcriptional factors and signaling molecules that regulate the developmental events for correct formation of the eye in a precise manner (Gregory-Evans et al., 2013).

Central in this network is Sonic Hedgehog (*shh*), that acts as a key regulator of other genes associated with the optic vesicle formation, patterning and morphogenesis (Amato et al., 2004). Notably, the Hh signal is required at several developmental stages following its expression from the ventral midline where it first regulates the separation of the eye field into two bilateral optic vesicles. Subsequently, Hh signaling controls proximo-distal patterning of the optic vesicle into optic stalk domains in a concentration dependent manner, particularly controlling the expression pattern of two genes, the proximal *pax2a,* which is expressed in the optic stalk, and the distal *pax6,* expressed in the optic vesicle. (Ekker et al., 1995; Macdonald et al., 1995). Moreover, studies have shown that there is a reciprocal transcriptional repression between *pax2* and *pax6* to form a boundary between the optic stalk and vesicle (Schwarz et al., 2000).

Taking this in account, we hypothesized that a possible alteration in the Hh signaling pathway could be responsible for the coloboma phenotype here described. To test this hypothesis, WISH was performed by the time the optic vesicle has fully evaginated at 18 hpf using the probes *shh, pax2a* and *pax6* in Control and Mo1 morphants. Compared to the Control, the *shh* signal in Mo1 morphant appeared to be properly localized at the ventral portion of the

diencephalon in the intermediate region flanked by the optic vesicles. However, the signal was more intense in the Mo1 morphants (Figure 5A-C). This was consistently visualized in multiple Mo1 injections and WISH experiments. Interestingly, the region of expression of *pax2a* was expanded into the area of the optic vesicle in the Mo1 morphants compared to the Control where the signal was restrained to the presumptive optic stalk (Figure 5D-E). Furthermore, there was a corresponding retraction of the *pax6* expression in the area of the optic vesicle in Mo1 morphants (Figure 5F-G). The increase expression of *shh* in the ventral portion of the diencephalon and the altered expression of *pax2* and *pax6* in the optic vesicle were also observed on the lateral view (Figure 5A'-G').

These results suggest an alteration in the proximo-distal patterning of the developing eye in the Mo1 morphants. An important point to consider is that this same altered pattern of expression of pax2a and pax6 has been reported in other mutants and morphants with coloboma phenotype as a result of alteration in the expression of genes related to the Hh pathway (Lee et al., 2008; Sehgal et al., 2008; Wen et al., 2015). The expansion of *pax2a* signal in Mo1 morphant persisted later on in development. At 28 hpf, it was still visualized in an expanded form, ruling out the possibility of being an effect due to a developmental delay (Supplementary Figure S5A-B).

To further support the increase of the Hh signaling, the expression of *vax2* was tested by WISH. The expression of vax2 in the optic stalk positively correlates with the expression level of *shh*, but is independent of pax2a expression (Take-uchi et al., 2003). 28 hpf-Mo1 morphants presented an increased signal of *vax2* in the optic stalk and an expansion of this signal into the dorsal retina compared to the Control, consistent with the increased *shh* signaling (Supplementary Figure S5C-D).

In addition to *shh* another member of the Hh family that is expressed in the zebrafish ventral midline is tiggy-winkle hedgehog (*twhh*), which has also been associated with the development of the retina (Ekker et al., 1995). WISH was performed to determine if variations could be observed in the expression of this gene. Similar to *shh*, *twhh* appeared to be properly localized

in the Mo1 morphants, and as for *shh*, *twhh* expression was more intense compared to the control (Supplementary Figure S5E-F).

Angles in Mo1 somite are more obtuse.

Multiple studies have well characterized the developmental consequences of perturbing the *shh* signaling pathway, particularly in the somite formation. These perturbations were studied either in mutants (Koudijs et al., 2008; Koudijs et al., 2005; van Eeden et al., 1996) or by chemical alteration on the levels of *shh* signaling (Rost et al., 2014), and revealed an acute dosage sensitivity.

To determine if the alteration of *shh* expression level in Mo1 morphants could have other morphological impact, the formation of the somites, shape and angle of somites were analyzed at 72 hpf. On light microscopy, somites of Mo1 morphants displayed a subtle but consistent phenotype when compared to the Controls. Indeed, the usual chevron-shape of somites was maintained in Mo1 morphant embryos at 72 hpf, however, their angle was slightly different (Figure 6B). To quantify this difference, the angle of 5 somites anterior to the end of the ventral fin was measured (Figure 6C). Statistical analysis showed that the mean somite angle in the Mo1 larvae was significantly more obtuse (117.3° +/- 12.1°) compared to the non-injected and Control embryos (91.7° +/- 4.4°) (ANOVA with post-hoc Dunnett test $p<0.0001$). However, this subtle change in somite angle of Mo1 morphant didn't result in a flatten phenotype, as reported in zebrafish when *shh* is overexpressed (Hammerschmidt et al., 1996). This is likely because in the latter overexpression experiment the Hh signaling is much higher than that in Mo1 morphant. WISH demonstrates that the expression of *shh* is slightly increased in the area of the neural tube and notochord, of Mo1 morphant compared to Control, consistent with the observed somite phenotype (Supplementary Figure S5G-H)

Together, these results show that *atxn7* downregulation leads to an increased Hh signaling, as reflected by the increased level of *shh and twhh* by WISH and by characteristic phenotypic consequences such as coloboma and increased angle of somites in Mo1 morphant embryos.

Knockdown of *atxn7* doesn't alter retinal differentiation but affects the optic nerve formation.

After its role in the formation of the optic cup, Hh signalings play additional roles in the development of the eye, specifically in the regulation of the retinal neurogenesis by controlling the proliferation and differentiation of progenitor cells (Marti and Bovolenta, 2002; Stenkamp et al., 2000).

Retinal sections of 5 dpf larvae were obtained to examine if Mo1 morphants presented alterations beyond the coloboma defect. Lens formation was unaffected. Overall, the retinal lamination was normal, as both Mo1 and Control morphants present the characteristic 3 nuclear layers separated by two plexiform layers (Figure 7 A-B). Mild defects were found in some part of Mo1 ganglion cell layer (Figure Supplementary 6B). Interestingly, on retinal section, it was possible to visualize the tissue previously described as extruding into the area of the brain (yellow arrows in Figure 2F'' and H"), which is composed of neural retina with preserved lamination even in the extruding area. The formation of the RPE was normal in the anterior part, but was disrupted in the posterior part, where the neural retina extrudes into the brain (Figure 7 A' B'). This likely explains the lack of pigmentation at the posterior part of morphant eyes and the hole, as visualized at macroscopic level (Figure 2E and H"). Additionally, sections allowed for imaging of the different degrees of the phenotype severity that also correlated with the macroscopic observations (Figure Supplementary 6 A-B").

For better visualization of the area surrounding the lack of pigmentation, electron microscopy (EM) images were obtained. EM confirms a proper layering of the retina, with only mild

disorganization in the outer plexiform layer (OPL) of Mo1 morphants. Moreover, compared to the Control, Mo1 morphant photoreceptors were properly polarized with mitochondria in the apical side of the inner segment. However, the photoreceptor outer segments (OS) were smaller in Mo1 morphant than in Control (Figure 7 C-D).

The transgenic line Spectrum of Fates (SoFa1) allows to analyze at the cell type level the retinal lamination as well as neuronal differentiation (Almeida et al., 2014). This particular line combines several transgenes to generate a color code for each class of retinal neurons, allowing a synchronized visualization of the main retinal cell types. This gives the advantage of visualizing the retinal ganglion cells (RGC) in the RFP spectrum, amacrine (AC) and horizontal cells (HC) in the GFP spectrum and bipolar and photoreceptors in the CFP spectrum.

Mo1 was injected in the SoFa1 line and visualized at 5 dpf. In this genetic background, the lamination and differentiation of AC, HC and RGC were also overall normal (Figure 7 E-F). Interestingly, the Mo1 SoFa1 morphant retina revealed the coloboma defect at cellular level, showing the nasal and temporal lobes of the retina not fused and separated by a gap (Figure 7 E'-F'). Given that Hh signaling has been related with the differentiation of RGC (Zhang and Yang, 2001), this neuronal cell type was examined more carefully in Mo1 SoFa1 morphants. The RGC axon properly converged at the posterior part of the retina in Control and Mo1 morphants in order to form the optic nerve (Figure 7 E-F). However, compared to the Control that form a single bundle of axons, axons in Mo1 morphants fail to merge properly, resulting in the axons forming two bundles that exit through the colobomatous retina. (Figure 7 G-H).

Additionally, there has been evidence that the Hh cascade is also involved in the regulation of the axon pathfinding. Experiments in chick embryos revealed that the overexpression of *shh* in the chiasm misrouted the retinal axons in a concentration dependent manner in an ipsilateral fashion (Trousse et al., 2001). Moreover, analysis of fish mutant related to the Hh pathway revealed anomalies in pathfinding (Macdonald et al., 1997). Analysis of Mo1 SoFa1 morphants revealed mild changes in the axon pathfinding. The axons of morphants properly crossed the

ventral midline of the diencephalon to form the optic chiasma, and ultimately to innervate the contralateral tectal lobe (Figure Supplementary 6C-D"). However, 30.76% (n=4/13) of Mo1 morphant embryos presented axons that aberrantly extended toward the anterior commissure, suggesting a more relaxed axon bundle (Figure Supplementary 6D'). Furthermore, the Mo1 morphants present a minor alteration in the pathfinding. This might be a consequence of the retinal tissue extruding into the area of the brain, changing the morphology of the ventral diencephalon (Figure Supplementary 6 E-F').

These results show that *atxn7* downregulation doesn't have a strong effect in the retina layering and differentiation of AC, HC and RGC. However, the RGC axon pathfinding and the optic nerve bundling are affected, which is consistent with RGC alterations upon increased expression of *shh* previous reported.

The RPE is a source for secreted factors, including shh, for photoreceptor differentiation, alterations present in the photoreceptors could only be related to areas depleted of RPE, however here we have shown areas with RPE that also presented alterations suggesting that the interruption of RPE and a possible consequent lack of *shh* appear not to affect the differentiation of the photoreceptors and doesn't appear to explain the decreased size of the OS present in the Mo1 morphants.

Photoreceptor terminal differentiation is altered in Mo1 morphant.

The interaction between photoreceptors and RPE is essential for a proper visual function (Strauss, 2005). Moreover, during development of the retina, the RPE is a source for secreted factors, including shh, towards the photoreceptors for their differentiation (Raymond and Jackson, 1995; Sheedlo et al., 1998). Surprisingly, as shown in Figure 7D, the morphology of Mo1 morphant photoreceptors was almost normal in area lacking RPE, except for the OS which were smaller.

To assess whether these smaller OS in the RPE disrupted region was a simple consequence of anomalies in the architecture of the extruding retina, photoreceptor OS were further analyzed in region where RPE was not disrupted and the retina not extruded. This analysis reveals that the formation of photoreceptor OS was strongly altered in Mo1 morphant, but at variable degree along the retina. Some regions had polarized photoreceptors with small OS, as the ones encountered in the area lacking RPE (compare Figure 8B and 8C). In other retinal region, photoreceptors were also polarized with normal inner segment (IS), but completely lacking OS (Figure 8D). Finally, there were regions where photoreceptors lack OS, and present disorganized IS where the distinctive ellipsoid morphology was lacking the characteristic mitochondria in the most apical area (Figure 8E). Importantly, no obvious sign of cell death was visualized in these different retinal regions of Mo1 morphant. Together, these observations suggest that the terminal differentiation of photoreceptors with the formation of OS is compromised in Mo1 morphant, independent of the presence or the absence of RPE.

Therefore, we hypothesized that intrinsic factors in the photoreceptors, rather than the signaling coming from the RPE, might be altering the photoreceptor differentiation in Mo1 morphants. In order to test this hypothesis, WISH was performed with *crx* probe at 48 hpf in Control and Mo1 morphants. Selection of this gene was based on three key aspects: first, its expression is important for proper differentiation of zebrafish photoreceptors (Shen and Raymond, 2004); second, mouse crx is required for terminal differentiation of photoreceptors with the formation of OS; and third, previous studies have reported an interaction between ATXN7 and CRX in mammalian cells (Chen et al., 2004; La Spada et al., 2001)

Compared to the Control, Mo1 morphant presented a significant difference in the intensity and localization of the *crx* signal. Notably, Mo1 morphants presented areas with complete lack of signal and areas of decreased signal, which could explain the different level of photoreceptor differentiation in Mo1 morphant (Figure 8F-G). To determine if this was due to a delay in the Mo1 development, WISH was performed in Control embryos at 42 hpf. Compared to the 48 hpf Mo1 morphants, 42 hpf Control embryos presented homogenous and widespread

expression of *crx*, except for very few areas lacking the signal, which did not match the abnormal *crx* expression pattern seen in 48 hpf Mo1 morphant retinas (compare Figure 8G and 8H). Furthermore, compared to Mo1 morphants at 48 hpf, older Mo1 morphants at 54 hpf presented an improvement in the *crx* signal, however, some regions were still lacking *crx* expression (compare Figure 8G and 8I). These regions lacking crx expression in 54 hpf morphant appeared as important as, if not larger than the ones seen in Control embryos at 42 hpf (i.e. 12 hpf difference) (compare Figure 8H and 8I).

Together, these results indicate that the downregulation of *atxn7* leads to alteration in the expression of *crx*, and compromise the terminal differentiation of the photoreceptors.

Interestingly, it has been reported that the expression of *crx* is independent of variations in the expression of *shh* (Stenkamp et al., 2002), suggesting that there could be more than one signaling pathway affected in the Mo1 morphants.

ATXN7 paralogs and its expression in the developing zebrafish

Previous reports identified four paralogs in vertebrates that share a distinctive conserved domain known as SCA7. This signature is specific to this family of genes (Helmlinger et al., 2004b). BLAST search with the Ensembl zebrafish (Zv9) database identified single orthologues for human *ATXN7*, *ATXN7L1* and *ATXN7L3* genes (*atxn7, atxn7l1, atxn7l3* respectively), and duplicated orthologues for *ATXN7L2* in the zebrafish genome (*atxn7l2a* and *atxn7l2b*) (Supplementary Figure S7A).

Sequence comparison analysis was performed to determine if the previously described conserved blocks were present in the zebrafish orthologues. The first N-terminal domain (Block I) contains a Cys-X_2-Cys-X_{11}-His-X_{3-4}-Cys/His motif. Deletion of this domain was shown to cause the dissociation of the DUB module from the SAGA complex (Kohler et al., 2008). All zebrafish paralogs presented this conserved domain with the exception of *atxn7l1*, suggesting

that at least this paralog might not share a redundant function with *atxn7* in zebrafish (Supplementary Figure S7C). The atypical Cys-X_{9-10}–Cys-X_5–Cys-X_2-His motif, known as SCA7 domain (IPR013243) was conserved in all paralogs (Block II) (Supplementary Figure 7D). Finally, a conserved C-terminal domain, whose function remains unknown was conserved in all the paralogs with the exception of *atxn7l3*, as expected. (Block III) (Supplementary Figure 7E). The localization of these blocks is summarized in the Supplementary Figure 7A. Interestingly, *atxn7* is the only paralog that presents a PolyQ stretch.

RT-PCR was performed to determine the temporal expression profile of the zebrafish *atxn7* paralogs. *atxn7L2a, atxn7L2b* and *atxn7L3* were expressed at 24 hpf and 48 hpf. Interestingly, *atxn7L1* is not expressed during late segmentation period (24 hpf), and begins expression during early hatching period (48 hpf) suggesting that *atxn7L1* might not be essential during the first stages of development (Supplementary Figure 7B).

Furthermore, to determine if there was an increase in the expression of any of the paralogs that could suggest a compensation when *atxn7* was downregulated, RT-PCR was performed in the Mo1 morphant context. None of the paralogs presented a significant altered expression compared to the Control Morphant (Supplementary Figure 7B).

Together, these results show for the first time that all the ATXN7 paralogs have a corresponding orthologue in the zebrafish (Atxn7L1 was not previously described). Additionally sequence analysis revealed the presence of the conserved SCA7 domain. Nonetheless, RT-PCR didn't reveal a possible compensation effect, which could mask *atxn7* function.

FIGURES

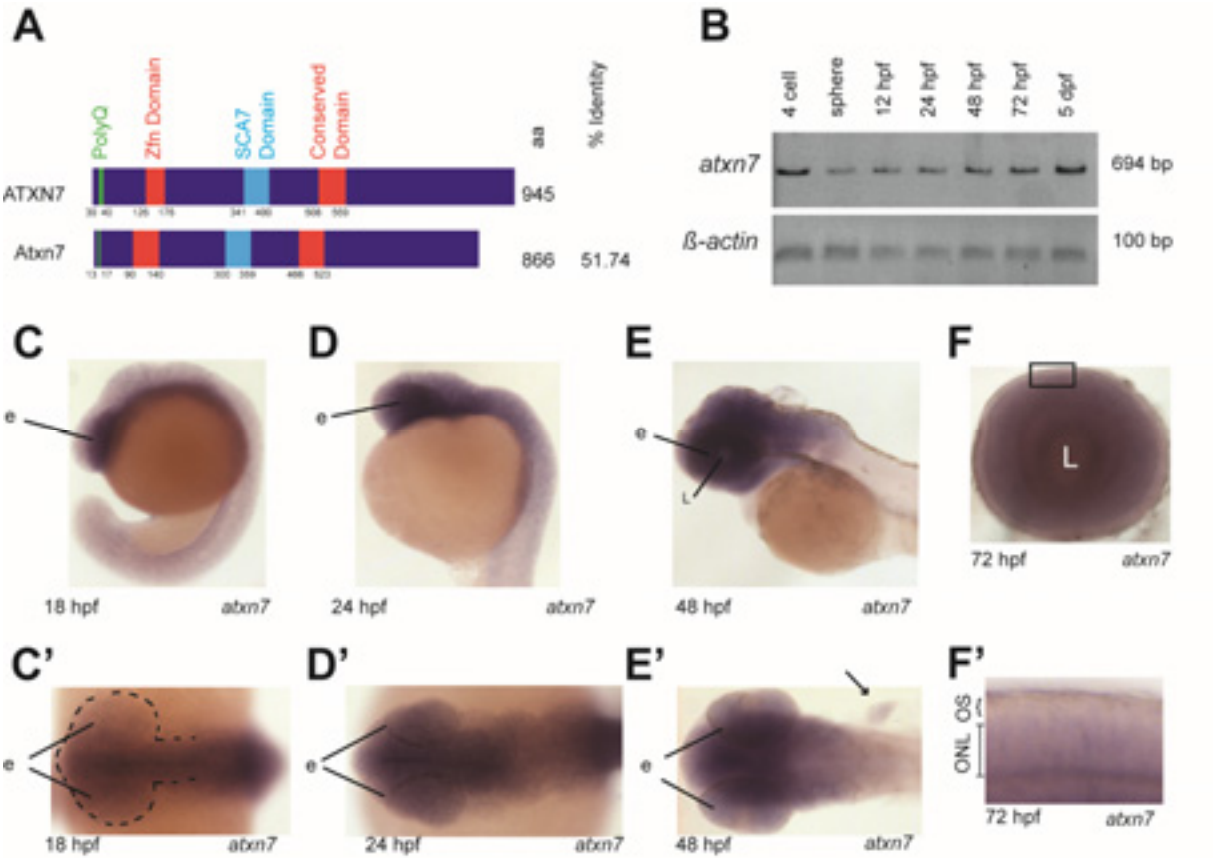

Figure 1 Expression pattern of *atxn7* transcript in zebrafish embryo development.

Figure 1

Expression pattern of *atxn7* transcript in zebrafish embryo development.

(**A**) Modular structure of human and zebrafish ATXN7 proteins contains a polyQ stretch, a C2H2 zinc-finger domain (Zfn Domain), an atypicalCys-X9–10–Cys-X5–Cys-X2-His motif, known as SCA7 domain and a conserved domain, sharing an identity of 51.74%. The polyQ stretch is composed of 5 residues in zebrafish and is polymorphic from residues 4 to 35 in human.

(**B**) mRNA expression in developing zebrafish. Total RNA was reverse transcribed into cDNA and analyzed by semi-quantitative PCR using *atxn7*-specific primers. *ß-actin* expression is shown as reference control. The maternal origin of *atxn7* transcript is supported by its presence at 4 cell and sphere stages. From early somitogenesis stage, 12 hpf, up to 5 dpf, atxn7 expression is maintained.

(**C-E'**) *atxn7* mRNA expression pattern in wild-type embryos by whole-mount *in situ* hybridization of embryos with *atxn7* specific antisense probe. Typical lateral view of embryos at 18 hpf (**C**), 24 hpf (**D**) and 48 hpf (**E**) are presented and the corresponding dorsal views of the head region (**C'-E'**). During early somitogenesis stage (**C, C'**) the *atxn7* transcript is detected ubiquitously in the embryo with higher intensity in the eye area. This expression is maintained through the development as seen at 24 hpf (**D, D'**) and 48 hpf, arrow indicates fin bud (**E, E'**).

(**F-F'**) Dissected eye from a 72 hpf embryo (**F'**) with enlarged lateral view of photoreceptor layer. Expression in the photoreceptors is supported by the presence of signal in the ONL.

Abbreviations: e, eye; L, lens; ONL, Outer Nuclear Layer; OS, Outer Segments.

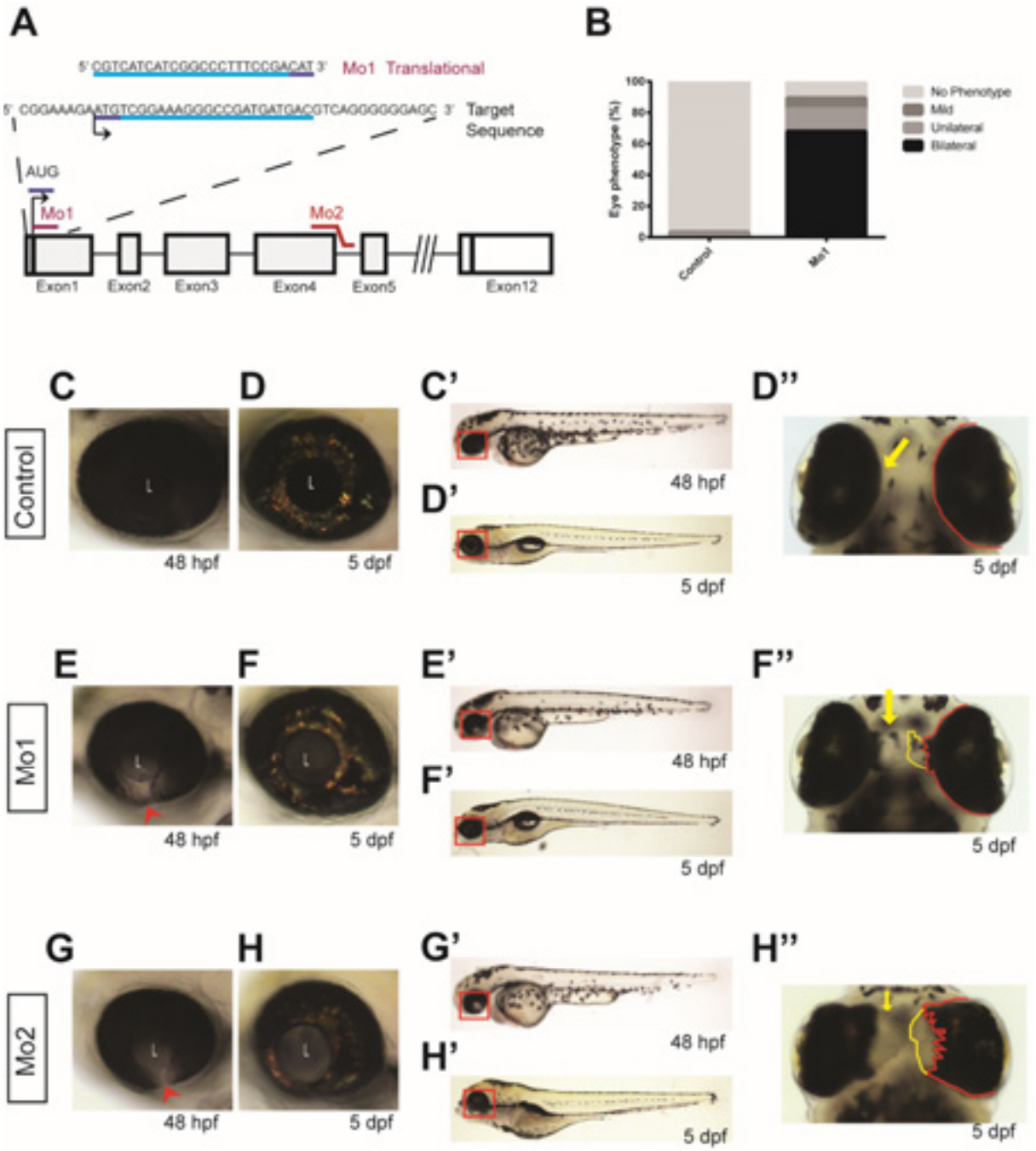

Figure 2 Knock down of *atxn7* causes coloboma.

Figure 2

Knock down of *atxn7* causes coloboma.

(**A**) Schematic representation of the *atxn7* gene showing coding exons 1 to 5 and 12 (empty boxes) and untranslated intronic sequences (single lines). Antisense morpholino corresponding to the sequence at the translational start site in exon 1 was designed to inhibit translation (Mo1), and morpholino located at the exon 4 intron 5 boundary was designed to inhibit splicing and create premature stop codon (Mo2).

(**B**) Histogram showing the frequency of eye anomalies induced by *atxn7* gene knockdown. Embryos were injected with 3 ng of Mo1 (n=112 embryos) or 6 ng of Control morpholino (n=133) The severity of eye phenotype was estimated at 72 hpf, according to the following classification: “No Phenotype” being the normal eye where the two edges of the choroid fissure fused normally and the posterior eye cup shows no tissue extruded into the brain area; categories “Mild”, when there was minimal but present defect; “Unilateral”, when there was presence of strong phenotype in one eye and Bilateral when there was presence of severe anomaly in both eyes. Defining severe anomaly as the presence of combined hole and visible extrusion, while mild was the possible range between normal and severe defect.

(**C-H’’**) Representative light microscopic images of Control embryos (**C-D”**), Mo1 (**E-F”**) and Mo2 (**G-H”**) morphants. Respectively: 48 hpf eye lateral view (**C, E, G**) and the corresponding whole lateral view of the same embryos (**C’, E’, G’**); 5 dpf eye lateral view (**D, F, H**) and the corresponding dorsal view (**D”, F”, H”**) and whole lateral view (**D’, F’, H’**) of the same larvae. Several pigmentation defects are visible on lateral and dorsal views of morphant eyes. On 48 hpf-eye lateral view, red arrowhead indicates the lack of pigmentation in the area of choroid fissure and developing lens (L) in Mo1 and Mo2 (**E** and **G**, respectively) compared to the Control (**C**). On 5 dpf- eye lateral view, a pale coloration through the lens in Mo1 and Mo2 (**F** and **H** respectively) compared to the black coloration in Control (**D**). On the corresponding 5 dpf- eye dorsal view, Mo1 and Mo2 (**F”** and **H”** respectively) have irregular eye edge (red line) and non-pigmented tissue extruding into the area of the forebrain (yellow line and arrow) in comparison with the Control (**D”**). Abbreviation: L, lens.

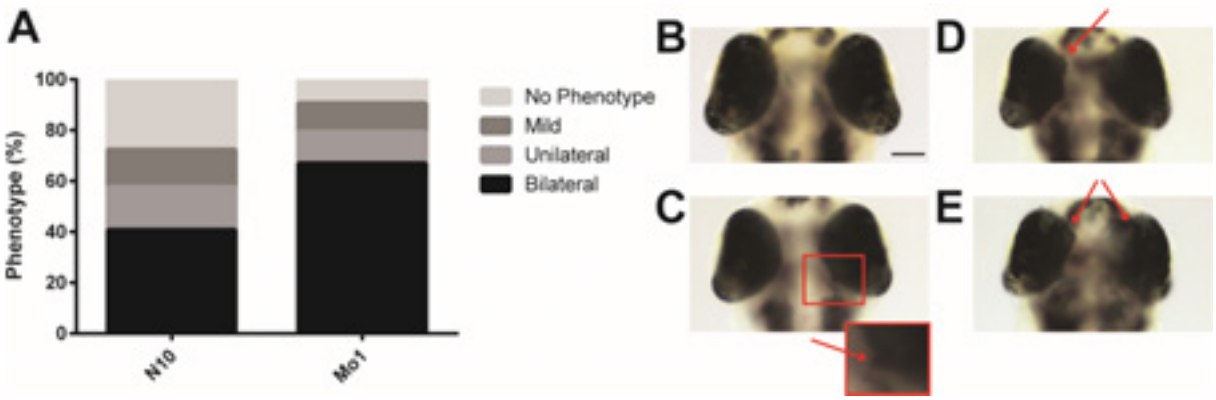

Figure 3 Human *ATXN7* can partially compensate the loss of zebrafish *atxn7.*

(**A**) Histogram of the four point grading scale used to quantify the variably penetrant coloboma phenotype induced by *atxn7* knockdown (Mo1) compared to Mo1 morphants that also received 150 µg human *ATXN7* mRNA (N10). With expression of N10, there were significantly fewer 72 hpf larvae with a "Bilateral" phenotype and more larvae with "No Phenotype". N=100/condition (Chi square P<0.0001).

(**B-E**) Representative images in dorsal view of the phenotypes found at 72 hpf in Mo1 morphants and in Mo1 + N10. "No Phenotype" being the control phenotype where no tissue extruded into the brain area. Categories "Mild", "Unilateral", and "Bilateral" indicate increasing severity of eye phenotype with, respectively, little but present defect (**C**), severe defect but just in one eye (**D**) or both eyes with severe phenotype respectively (**E**). Red arrow indicate affected areas.

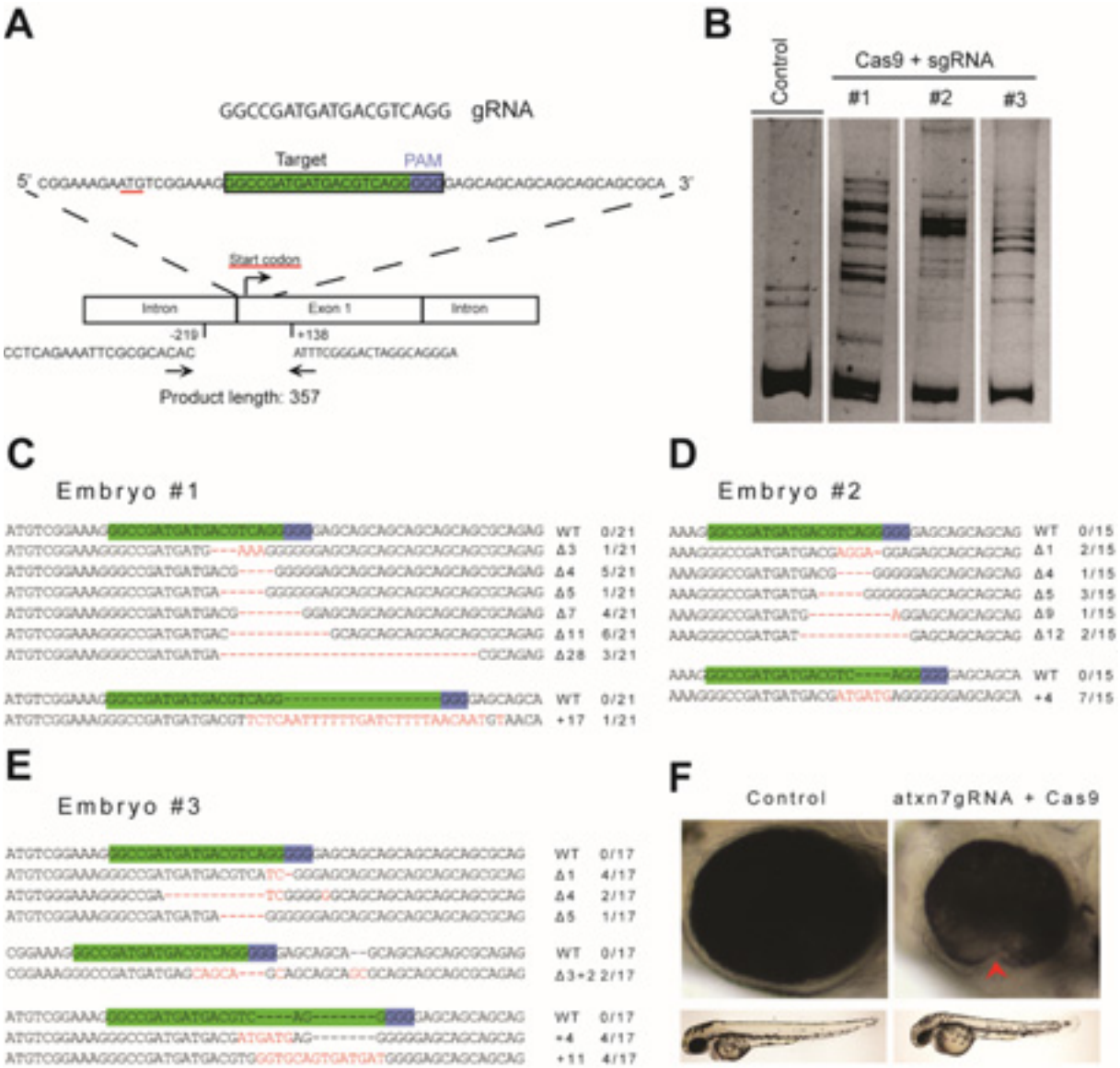

Figure 4 Mutation analysis of *atxn7*gRNA + Cas9 injected P0 founder embryos.

Figure 4

Mutation analysis of *atxn7*gRNA + Cas9 injected P0 founder embryos.

(**A**) Schematic representation of the genomic structure of the *atxn7* gene exon1. The 19-bp target sequence of sgRNA is indicated in green box, adjacent to GGG motif (PAM) sequence in light blue box. Bottom primers indicate the amplified region for sequence analysis.

(**B**) Heteroduplex mobility assay (HMA) in embryos injected with ~2-nl of a solution containing .2 µg/µL Cas9 protein and .1 µg/µL of sgRNA. Multiple heteroduplex bands were observed in PCR products from sgRNA+Cas9 injected embryo (#1–#3), whereas a three band pattern was observed from each control embryo without injection.

(**C-E**) Sequence analysis from subcloned PCR products from injected embryos. Red dashes and letters indicate the identified mutations. The sgRNA targeting sequence and PAM indicate in green and light blue boxes, respectively. The size of deletions and insertions are shown to the right of each mutated sequence (Δ, deletions; +, insertions). Numbers on the right edge indicate the numbers of mutated clones identified from all analyzed clones from each embryo.

(**F**) Representative images of eye and body lateral views of the same larvaes at 48 hpf. Red arrow head indicates the persistence of choroid fissure in 24.48 % (12/49) of the *atxn7*gRNA+Cas9 embryos, which displayed a coloboma defect. None of the control embryos (n= 5 out of 20 from each of the three control conditions) presented coloboma.

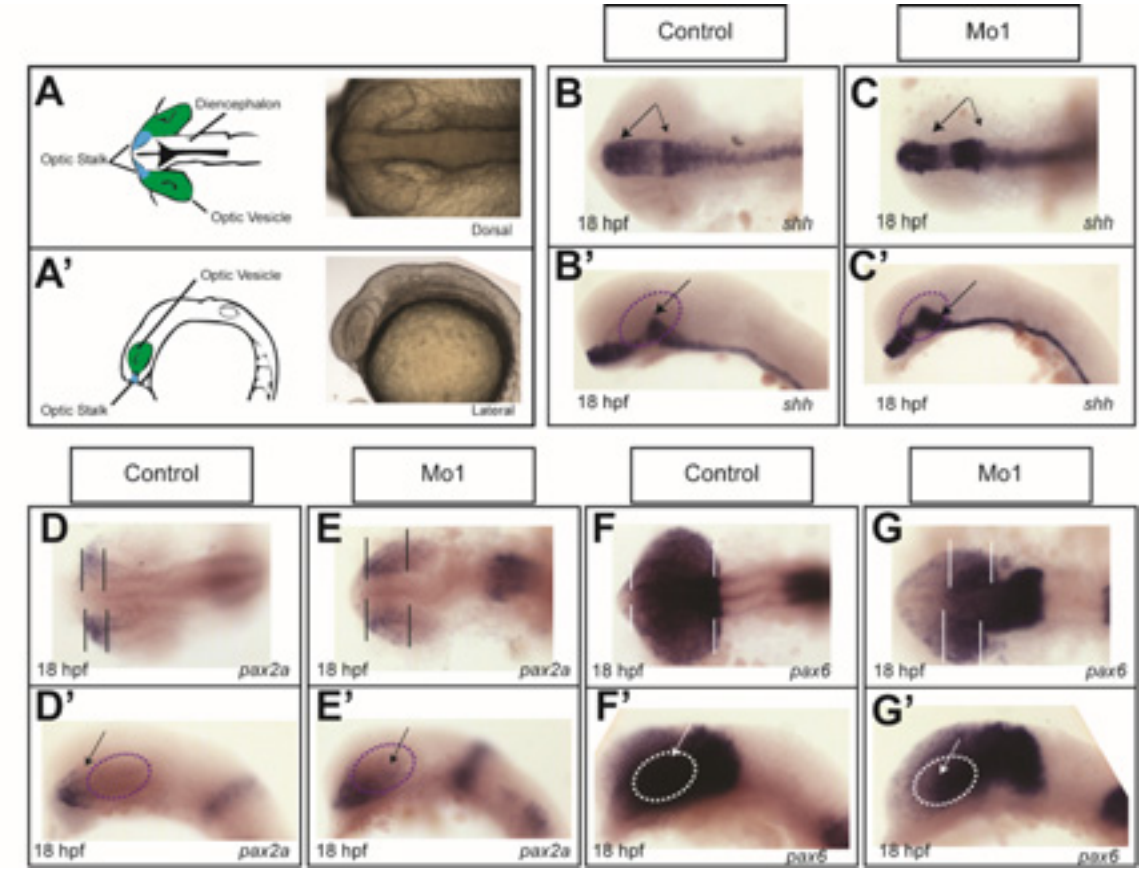

Figure 5 Knock down of *atxn7* alters the expression of *shh* and proximo-distal axis gene markers**.**

Figure 5

Knock down of *atxn7* alters the expression of *shh* and proximo-distal axis gene markers.

(**A-A'**) Schematic diagram with the corresponding bright field image of larvae at 18 hpf stage in dorsal and lateral positions respectively, highlighting areas of interest - blue optic stalk and green optic vesicle. Whole-mount in situ hybridization was conducted to study the expression dynamics of *shh*, *pax2a* and *pax6*. Representative images of control and Mo1 morphants at 18 hpf dorsal view (**B-G**) and lateral view (**B'-G'**) of stained embryos. 30 embryos were treated per condition and at least 5 imaged. Yolks were removed for better visualization.

(**B-C'**) The *shh* probe labels the areas of forebrain and floor plate in Control and Mo1 morphants at 18 hpf. (**B-C'**), however, an increased expression of *shh* is found in the Mo1 compared to the Controls (arrows).

(**D-E'**) The *pax2a* probe labels the proximal optic stalk in control and Mo1 morphants at 18 hpf. The region of *pax2a* expression is abnormally extended within the optic vesicle in Mo1 region. Horizontal black lines represent the boundaries of expression in dorsal view while arrow show in lateral view.

(**F-G'**) Conversely, the *pax6* probe labels the distal optic vesicle at 18hpf. The *pax6* expression is substantially contracted within distal optic vesicle of Mo1 morphants. Horizontal white lines represent the boundaries of expression in dorsal view while arrow show in lateral view.

Dotted circle indicates area where the optic vesicle is localized in lateral views.

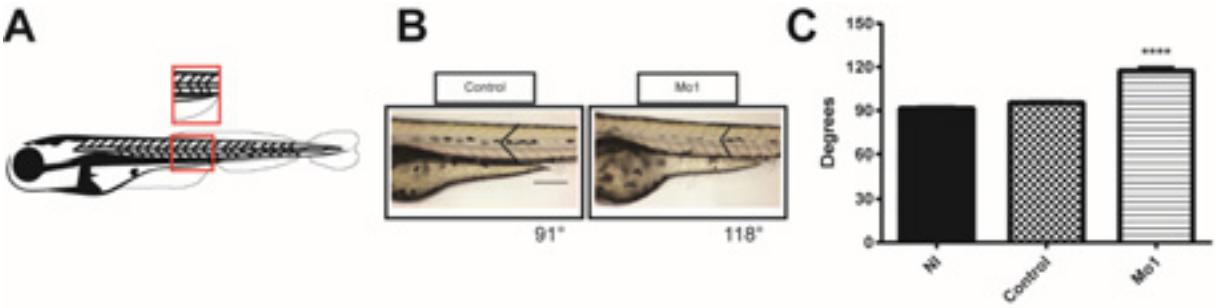

Figure 6 Knock down of *atxn7* have an impact in the somite angle, making them more obtuse.

(**A**) Schematic diagram of a larval zebrafish indicating the area where somite shape and angle were studied. Average of the 5 somites anterior to the end of the ventral fin were measured.

(**B**) Representative image of Control and Mo1 morphants taken at 72 hpf. Both control and Mo1 morphant show the typical chevron shape of somites. However, the mean angle are different: 118° for the Mo1 larvae compared to 91° for the Control.

(**C**) Histogram of angle measurements from non injected (NI), Control and Mo1 morphants. The error bars show the SEM. N=25. One-way ANOVA with post-hoc Dunnett test $p<0.0001$.

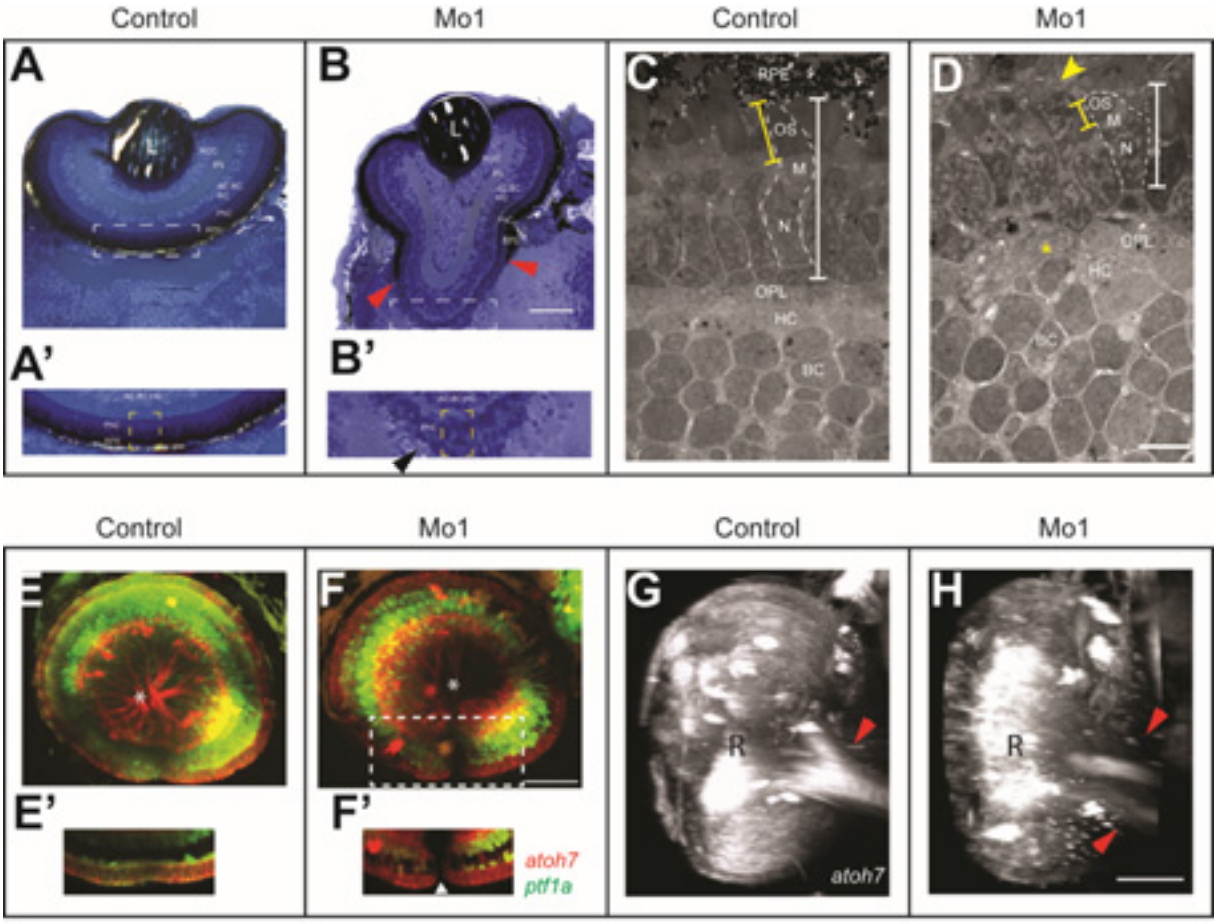

Figure 7 Retinal differentiation in *atxn7* morphants.

Figure 7

Retinal differentiation in *atxn7* morphants.

(**A,B**) Toluidine blue-stained retinal coronal sections of 5dpf Control (**A**) and Mo1 morphant (**B**) larvae. Dorsal histological section of Mo1 retina showing ectopic retinal tissue extruded into the brain area, red arrow heads indicate interruption of the RPE; Dotted box indicates area amplified in (**A'-B'**). Scale bar: 50 µm.

(**C,D**) Transmission electron microscopy of retinal coronal sections of 5dpf larvae from the area in dotted yellow box from **A'** and **B'**, respectively. In the Control (**C**), photoreceptor OS were elongated and melanin-filled granules were clearly visible in the RPE. In the Mo1 morphant (**D**), photoreceptor OS were present but smaller in the region devoided of pigmented RPE (yellow arrowhead). Photoreceptors in both cases were polarized with mitochondria in the apical side of the inner segment, directly below the outer segment. Mild disorganization in the OPL area was also visualized (yellow asterisk). Scale bar: 10 µm.

(**E,F**) Confocal 3D lateral view of 5 dpf SoFa1 Control (**E**) and Mo1 morphant (**F**) retina. Atoh7:gapRFP RGC layer (red), Ptf1a:Gal4/UAS:gapGFP AC and HC (green). In SoFa1 Control and Mo1 morphant, the layering and differentiation of AC, HC and RGC were completed and overall normal. Mo1 morphant retina revealed the presence of coloboma defect (**F'**), as nasal and temporal lobes of the retina are not fused and separated by a gap (white arrowhead). The RGC axon (white asterisk) converged at the posterior part of the retina in Control (**E**) and Mo1 morphants (**F**).

(**G,H**) Confocal 3D frontal view of 5 dpf SoFa1 Control (**E**) and Mo1 morphant (**F**) retina (**R**) in the red spectrum (Atoh7:gapRFP RGC). Compared to the Control, Mo1 morphant axon fails to bundle and is split in two portions. Scale bar: 50 µm.

Abbreviations: L, lens; RGC, Retinal Ganglion Cells; IPL, Inner Plexus Layer; AC, Amacrine Cells; BC, Bipolar Cells; HC, Horizontal Cells; PhC, Photoreceptor Cells; OS, Outer Segment; M, Mitochondria; N, Nucleus; OPL, Outer Plexus Layer; RPE Retinal Pigmented Epithelium; R, Retina.

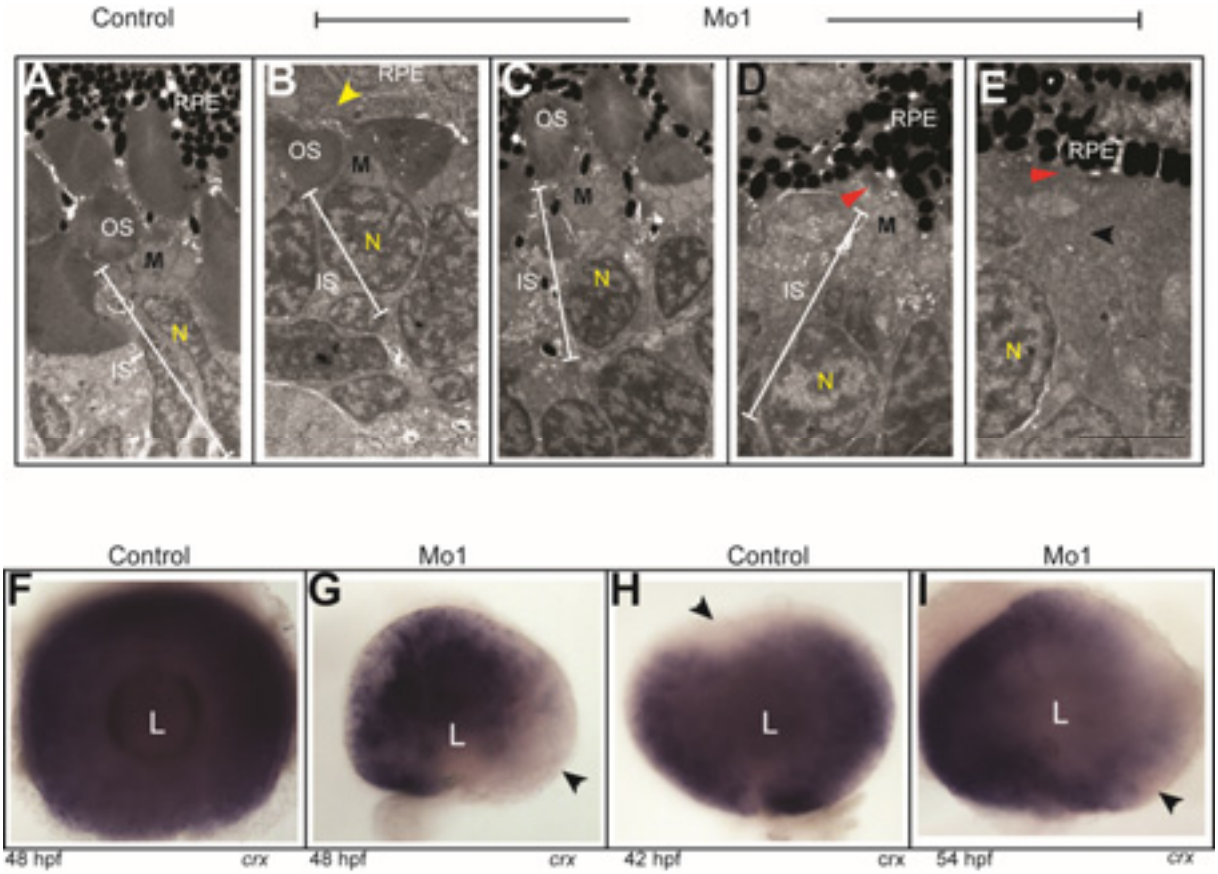

Figure 8 Photoreceptor morphology in Mo1 morphants.

Figure 8

Photoreceptor morphology in Mo1 morphants.

(**A-E**) Transmission electron microscopy of 5dpf larvae retinal sections. (**A**) In Control, RPE shows melanin-filled granules, while photoreceptors presents elongated OS and distinctive IS ellipsoid with the characteristic mitochondria in the most apical area just below the OS.

(**B**) In regions where pigmented RPE is lacking in Mo1 retina, photoreceptors have smaller OS (yellow arrowhead). (**C,D**) In some regions where pigmented RPE is present, Mo1 photoreceptors have smaller OS (**C**) or no OS at all (red arrow) (**D**). (**E**) In other regions, Mo1 photoreceptors do not have OS (red arrow), but also lack the distinctive IS ellipsoid with apical mitochondria. Scale bar: 10 µm.

(**F-I**) Whole-mount in situ hybridization comparing the expression of crx in Control and Mo1 morphant at different hours post fertilization. Representative images of dissected eyes from 48 hpf Control and Mo1 morphants (**F-G**), Control morphant at 42 hpf (**H**) and Mo1 morphant at 52 hpf (**I**). 30 embryos were treated per condition and at least 5 imaged.

Abbreviations: RPE Retinal Pigmented Epithelium; OS, Outer Segment; IS, Inner Segment; M, Mitochondria; N, Nucleus; L, Lens.

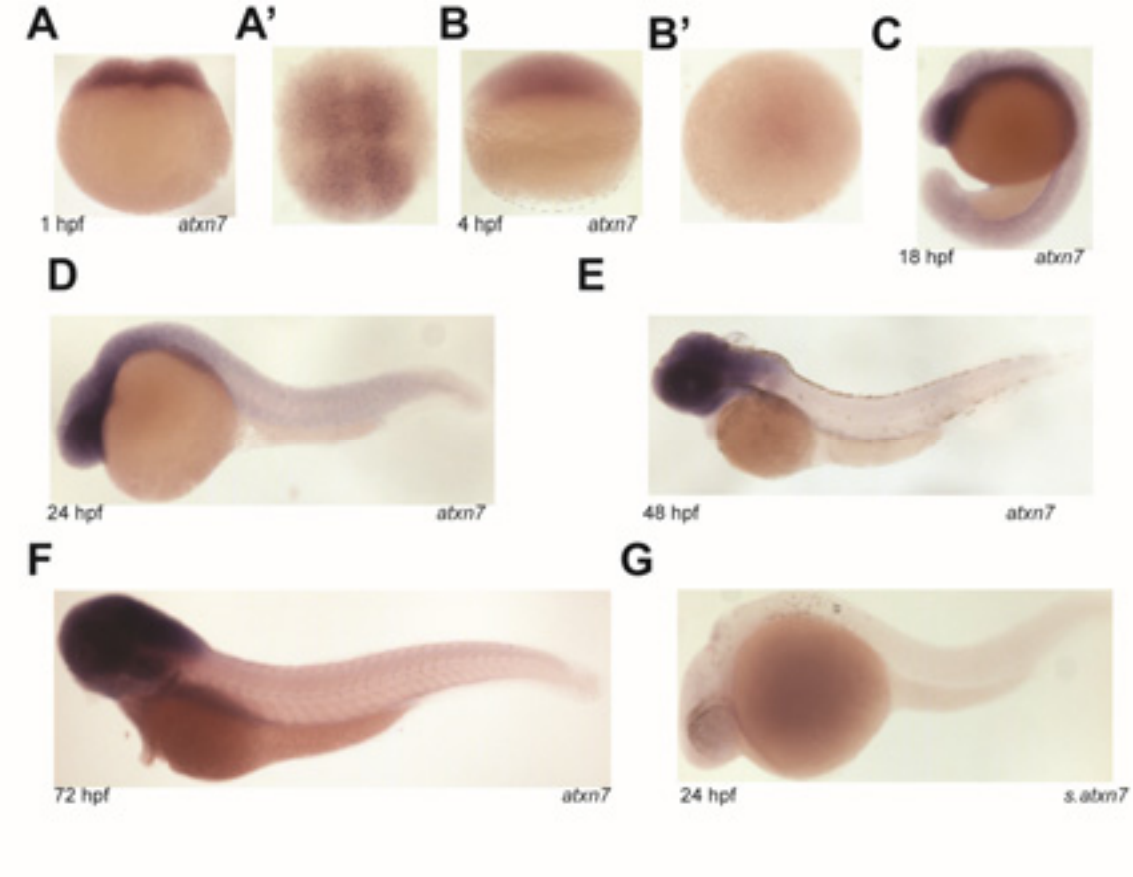

Supplementary Figure S1 Expression of *atxn7* by whole-mount *in situ* hybridization at different stages during zebrafish development.

Embryos at (**A**) 1 hpf (4 cell stage) lateral and (**A')** dorsal; (**B**) 4 hpf, (sphere stage) lateral and (**B'**) dorsal; (**C**) 18 hpf (18 somites); (**D**) 24 hpf; (**E**) 48 hpf; (**F**) 72 hpf were examined by whole-mount *in situ* hybridization with an antisense *atxn7*–specific probe (*atxn7*). (**G**) 24 hpf embryo with the *atxn7* sense probe (*s.atxn7*). The maternal origin of *atxn7* transcript is supported by its presence at 4 cells and sphere stages at the animal pole (**A, B**). During early somitogenesis stage (**C**) the *atxn7* transcript is detectable ubiquitously in the embryo. At the end of somitogenesis, the hybridization signal is still ubiquitous but more intense in structures of the developing central nervous system and eye (**D**). Later on, at 48 (**E**) and 72 hpf (**F**), the expression is preferentially maintained in the anterior part of the larvae.

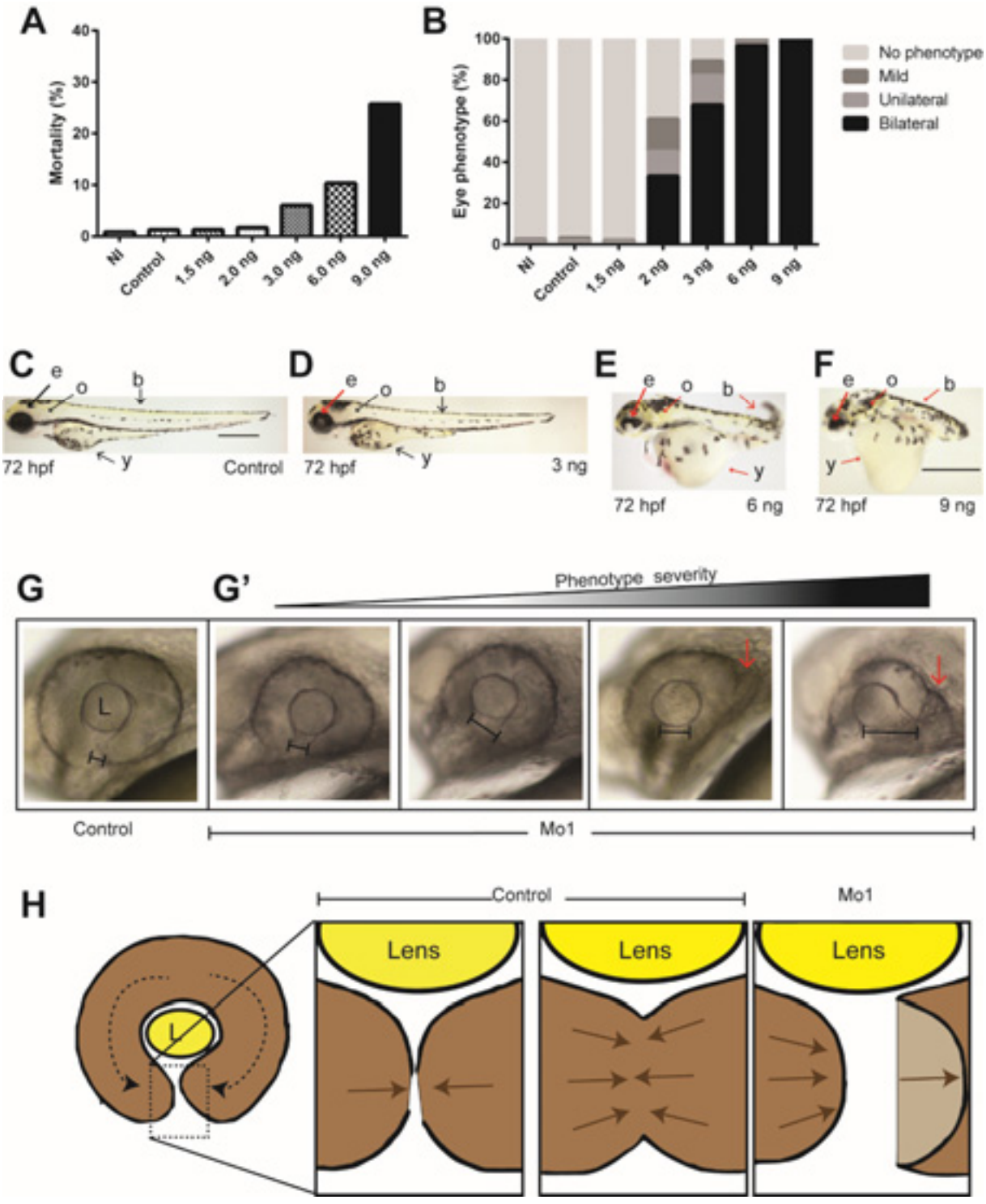

Supplementary Figure S2 Concentration dependent effects of *atxn7* morpholino on mortality and phenotypes.

Supplementary Figure S2

Concentration dependent effects of *atxn7* morpholino on mortality and phenotypes.

(**A**) Histogram showing the mortality induced by injection of translation blocking morpholino (Mo1) (ranging from 1.5 to 9.0 ng/embryo), by Control morpholino (6 ng) or not injected (NI). n=118 to 138 embryos injected/condition. Mortality was analyzed at 24 hpf.

(**B**) Histogram showing the frequency of eye anomalies induced by *atxn7* gene knockdown. Embryos were injected with translation blocking morpholino (Mo1) (ranging from 1.5 to 9.0 ng/embryo), Control morpholino (6 ng) or not injected (NI) (n=71 to 151 embryos injected/condition). Severity of the eye phenotype was scored at 72 hpf. Defining severe anomaly as the presence of combined hole and visible extrusion, while mild was the possible range between normal and severe defect. The severe defect could be present unilaterally or bilaterally.

(**C-F**) Representative images of control and Mo1 morphants (injected at 3, 6 and 9 ng respectively) at 72 hpf. Arrows indicate different structures of the embryo (black show non affected, red show affected). Scale bar equals 500 μM.

(**G-G'**) Representative light microscopic images of Control and Mo1 morphant eyes at 24 hpf. Mo1 morphants display large opening of the choroid fissure with different degree of severity. Line shows the gap between the two edges of the neuroectoderm. Red arrow shows areas where one of the neuroectodermal lip of the eye is bent backwards.

(**H**) Diagram representing closure of the choroid fissure. Dotted square highlights the ventral area of the developing eye, where the two edges of neuroectodermal layers must get in touch and fuse in order to circumscribe the retina and the RPE in the eye cup, as shown in the Control panels. Failure of choroid fissure closure results in a coloboma as shown in the Mo1 panel.

Abbreviation: e, eye; o, otholit; b, body; y, yolk; L, lens.

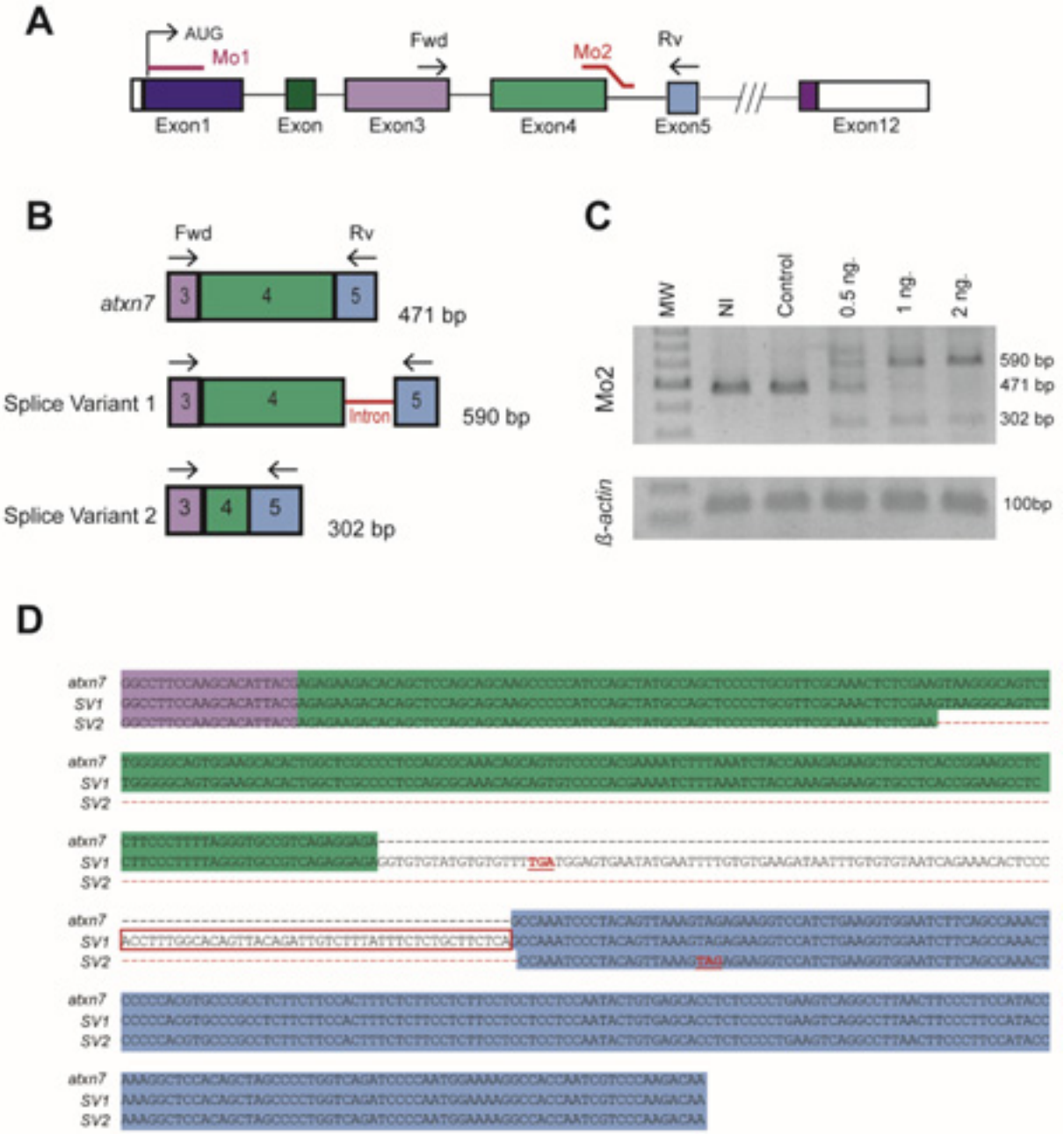

Supplementary Figure S3 Non overlapping morpholino analysis (Mo2).

Supplementary Figure S3

Non overlapping morpholino analysis (Mo2).

(**A**) Schematic representation of the *atxn7* gene showing exons 1 to 5 and 12 (colored boxes), untranslated intronic and exonic regions are depicted as single lines and empty boxes respectively. Antisense morpholino corresponding to the sequence around the translational start site in exon 1 was designed to inhibit translation (Mo1), morpholino located at the exon 4 intron 5 boundary was designed to inhibit splicing (Mo2). Top arrows indicate the localization of the primers used for RT-PCR and sequence analysis. (fw 5'- GGCCTTCCAAGCACATTAC-3') (rev 5'-TTGTCTTGGGACGATTGGTG-3').

(**B**) Schematic representation of the *atxn7* cDNA and two spliced variants resulting from Mo2 injection. Numbers and colored boxes correspond to each exon, red single line in Splice Variant 1 represents the inserted intron4 as a result of the splicing morpholino. Numbers on the right edge indicate the size of the product represented.

(**C**) Total RNA was reverse transcribed into cDNA and analyzed by PCR using *atxn7* splice - specific primers (Fwd and Rv) in non-injected (NI), control embryos and morphant embryos that had received increasing concentrations of Mo2 (0.5, 1 and 2 ng). *ß-actin* is shown as a reference control.

(**D**) Sequence analysis from subcloned PCR products from 1 ng injected embryos. Colors correspond to the representations in figures A and B; intron included in spliced variant 1 (SV1) represented in the red box; red dashes represent deleted sequence in SV2. Red underlined triplets indicate the stop codon for SV1 and SV2.

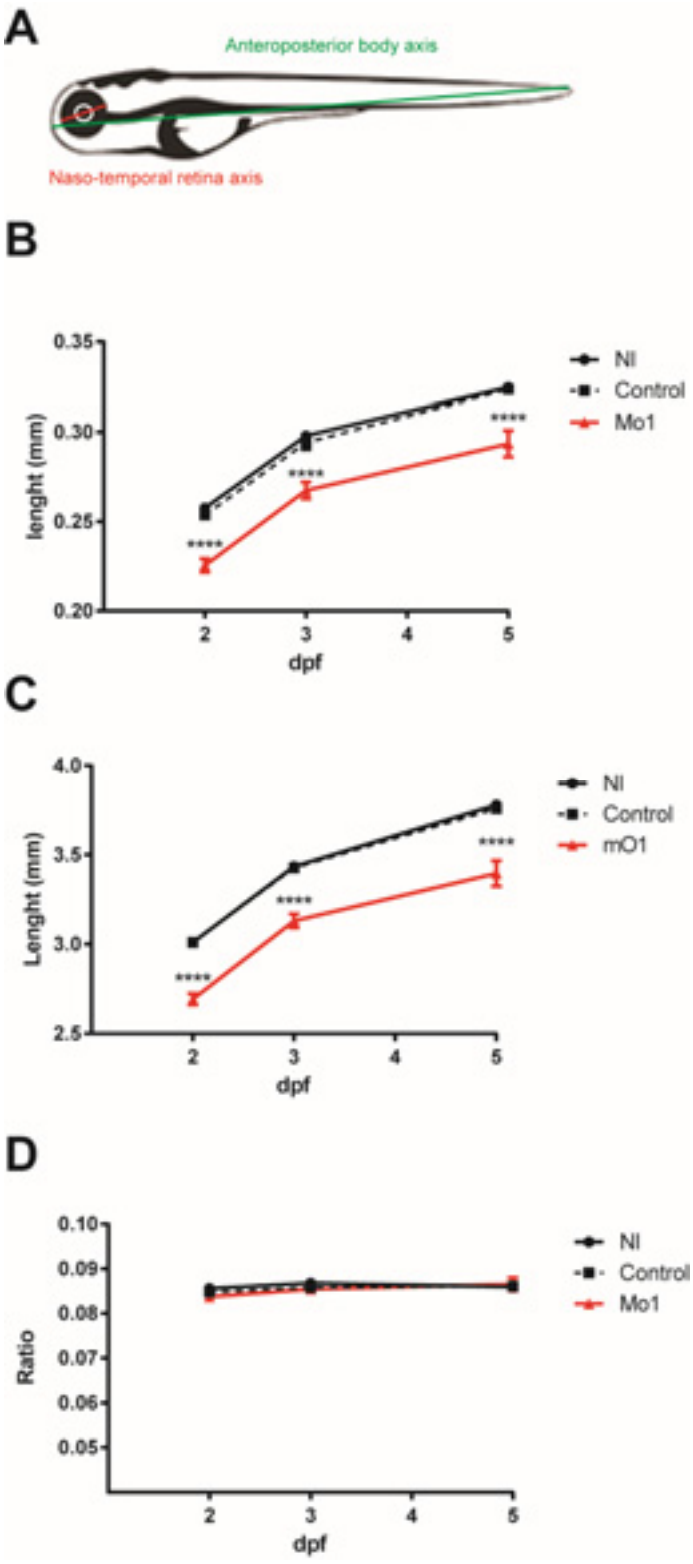

Supplementary Figure S4 Knock down of *atxn7* affects eye and body lengths similarly.

Supplementary Figure S4

Knock down of *atxn7* affects eye and body lengths similarly.

(**A**) Schematic diagram of zebrafish larvae depicting the two measurements taken into account to quantify the eye (red line) and body (green line) lengths of Mo1 morphants.

(**B-C**) Plot of average lengths of the naso-temporal eye axis (**B**) or the anteroposterior body axis (**C**) of non injected (NI), Control and Mo1 morphant larvae at 2, 3 and 5 dpf. The error bars show the SEM. N=30 embryos per condition.

(**D**) Plot of the average of eye/body length ratios of non injected (NI), Control and Mo1 morphant larvae at 2–5 dpf. The error bars show the SEM. N=30. One-way ANOVA with post-hoc Dunnett test $p<0.0001$. .

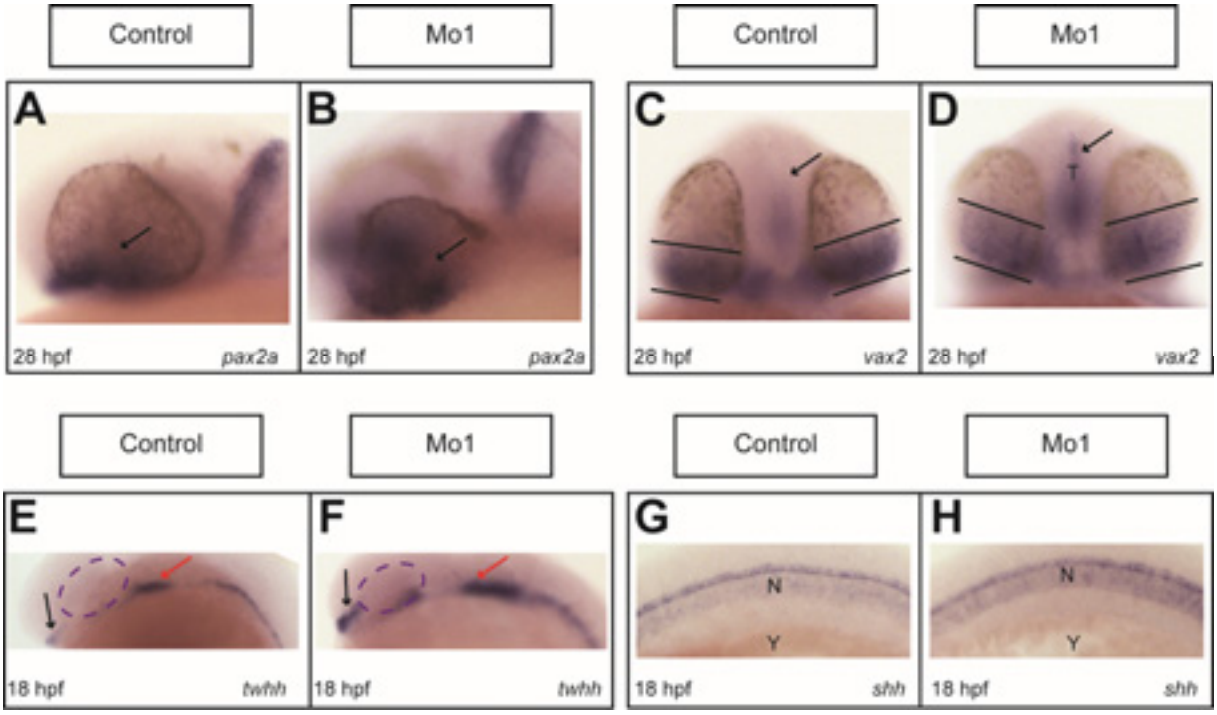

Supplementary Figure S5 Knock down of atxn7 alters expression of Hh signaling genes.

Supplementary Figure S5

Knock down of atxn7 alters expression of Hh signaling genes.

Whole-mount in situ hybridization was conducted to study the expression dynamics of *pax2a, vax2* at 28 hpf and *twhh* and *shh* at 18 hpf. 30 embryos were treated per condition and at least 5 imaged.

(**A-B**) Head portion lateral view where the *pax2a* probe labels the proximal optic stalk (arrow) in control and Mo1 morphants at 28 hpf. Expression in Mo1 is observed in a broader domain in comparison with the controls.

(**C-D**) Head portion frontal view where *vax2* marks the ventral optic cup at 28hpf, expression is substantially expanded into the dorsal optic cup in the Mo1 compared to Control. Horizontal lines represent the boundaries of expression in frontal view while arrow show expression in the telencephalon.

(**E-F**) Head portion lateral view where *twhh* marks the ventral forebrain (black arrow) and the floor plate (red arrow) in embryos staged 18 hpf. Compared to the controls; Mo1 morphants present an increased intensity of the staining in both areas.

(**G-H**) Portion of the trunk in a lateral view where *shh* mark the notochord and the floor plate in embryos staged 18 hpf. Compared to the controls, Mo1 morphants displayed an increase intense of the staining in the notochord area.

Dotted circle indicates area where the optic vesicle is localized in lateral views.

Abbreviations: T, telencephalon ; Y, yolk; N, notochord.

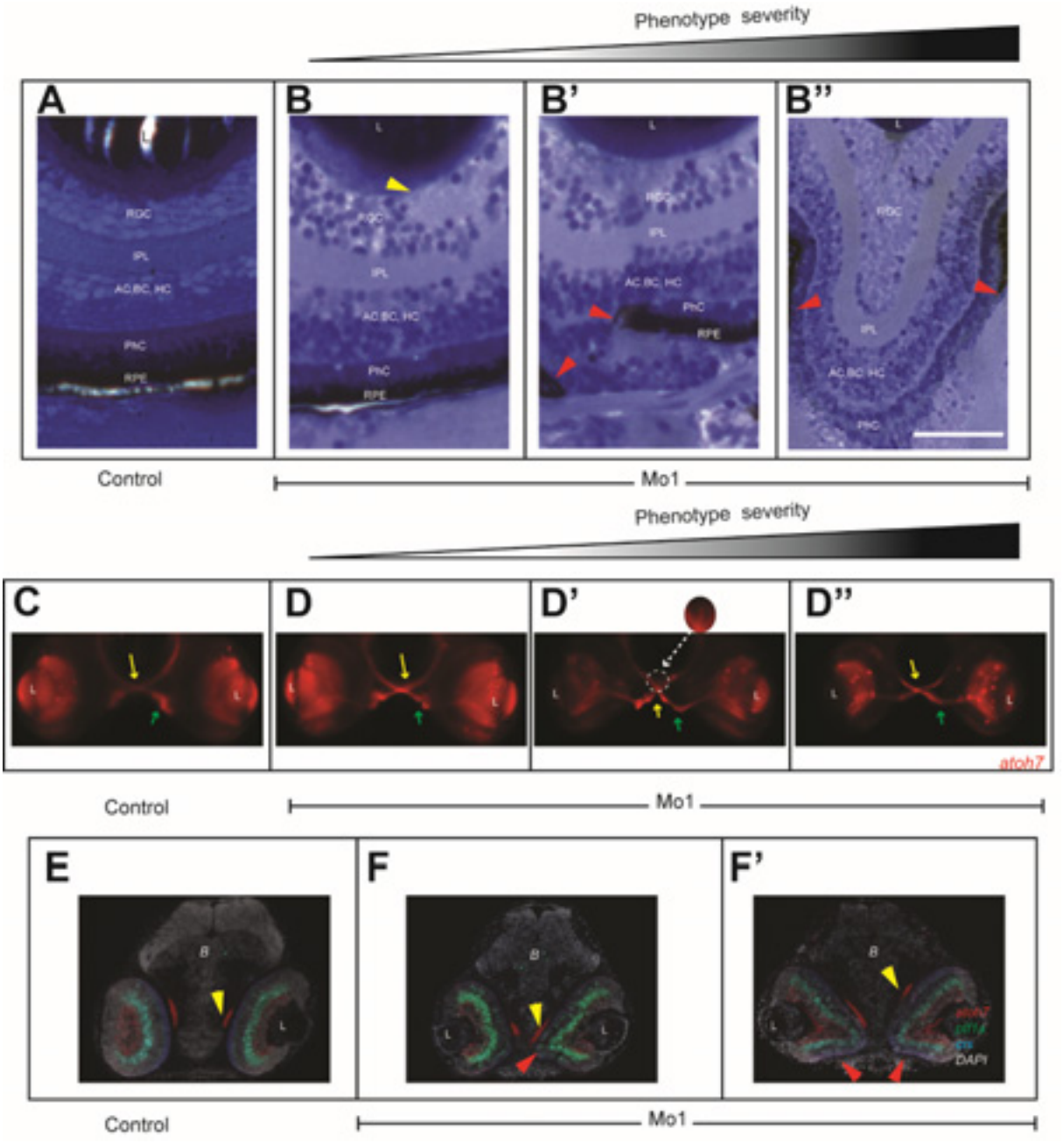

Supplementary Figure S6 Retinal differentiation in atxn7 morphants.

Supplementary Figure S6

Retinal differentiation in atxn7 morphants.

(**A-B''**) Toluidine blue-stained zebrafish retinal coronal sections of 5 dpf Control (**A**) and Mo1 morphant larvae with different phenotype severity (**B-B"**). Yellow arrow head indicates altered area in the RGC layer. Red arrows indicate interruption of the RPE. Scale bar: 50 µm.

(**C-D''**) Epifluorescent images of 5dpf SoFa1 embryos frontal view. Atoh7:gapRFP allowed visualization of RGCs and their axon in Control (**C**) and Mo1 morphant (**D-D"**). Optic nerve with increasing phenotype penetrance in Mo1 morphants (green arrow in **D-D"**). Proper formation of the optic chiasma in Control and Mo1 morphants (yellow arrow in **C-D"** respectively). Occasionally Mo1 morphant presented axons that aberrantly extended toward the anterior commissure (doted white circle and amplified circle in **D'**). Scale bar: 10 µm.

(**E-F'**) Transversal cryosections of 5dpf SoFa1 Control (**E**) and Mo1 morphants (**F-F"**). Atoh7:gapRFP RGC layer, Ptf1a:Gal4/UAS:gapGFP AC and HC and Crx:gapCFP photoreceptors and BC. Yellow arrow points the optic nerve. Red arrow indicates the area of extruding retina in the Mo1 morphant brain. Scale bar: 50 µm.

Abbreviations: L, lens; RGC, Retinal Ganglion Cells; IPL, Inner Plexus Layer; AC, Amacrine Cells; BC, Bipolar Cells; HC, Horizontal Cells; PhC, Photoreceptor Cells; RPE Retinal Pigmented Epithelium; B, Brain.

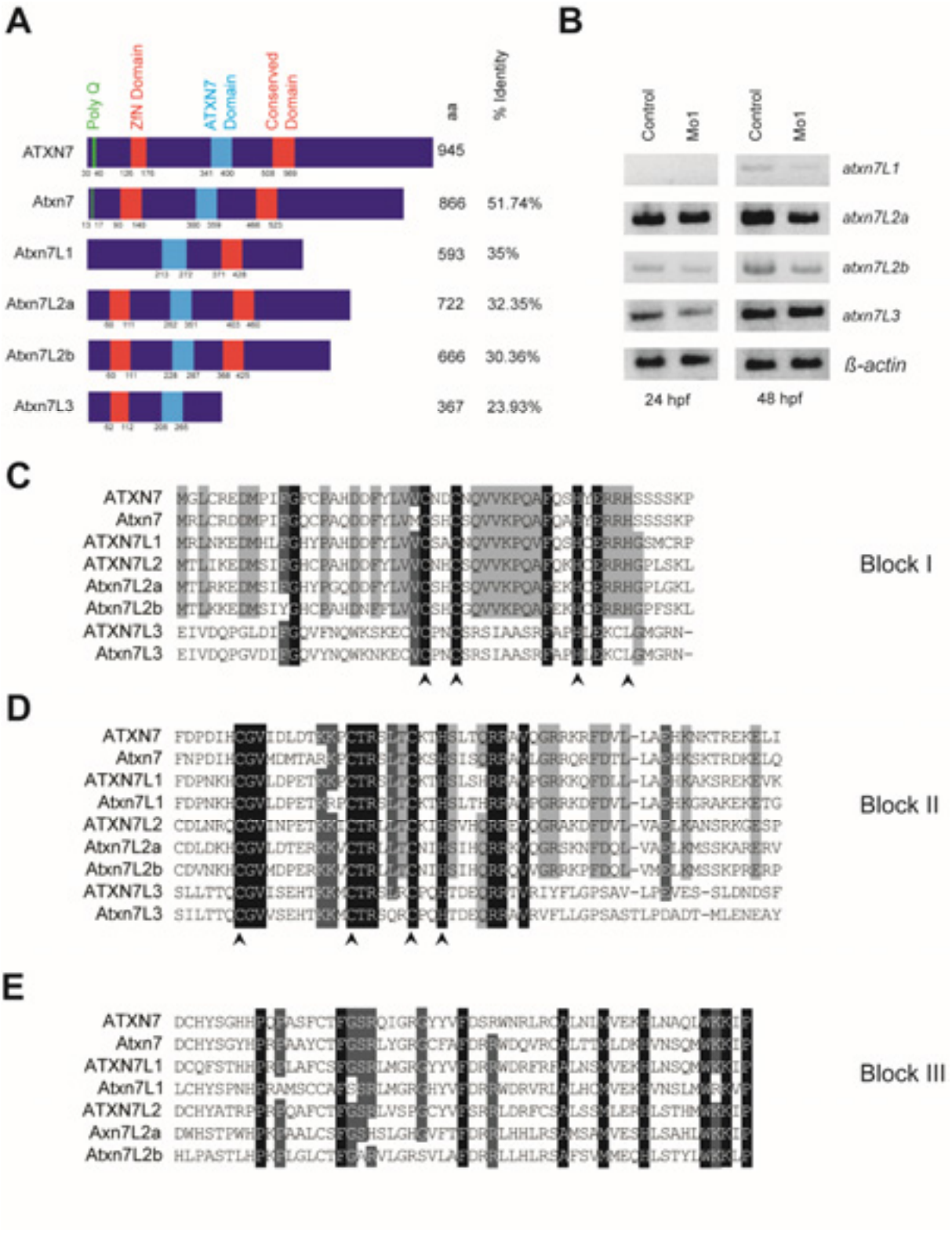

Supplementary Figure S7 Atxn7 Paralogs.

Supplementary Figure S7

Atxn7 Paralogs.

(**A**) Modular structure of human and zebrafish *ATXN7* orthologs and paralogs. A polyglutamine stretch (PolyQ) (green) is present in the N terminal portion of *ATXN7* human and zebrafish orthologs, but it is absent in *atxn7* zebrafish paralogs. A C2H2 zinc-finger domain (Zfn Domain) is shared in all zebrafish paralogs but *atxn7L1*. An atypical Cys-X9–10–Cys-X5–Cys-X2-His motif, known as SCA7 domain is conserved in all zebrafish paralogs. A C-terminal domain is conserved in all zebrafish paralogs but *atxn7L3*. Numbers on the right edge indicate the percentage of identity with the human *ATXN7* (%).

(**B**) mRNA expression at two different stages during the zebrafish development. Total RNA from Control and Mo1 morphants was reverse transcribed into cDNA and analyzed by semi-quantitative PCR using specific primers for each paralog. *ß-actin* expression is shown as a reference control. No significant change was found in the Mo1 context for all the paralogs at different time points.

(**C-E**) Sequence alignment of ATXN7 conserved blocks. Block I (**C**) (residues 126 to 176, according to the numbering of the human sequence), block II (**D**) (residues 341-400) and block III (**E**) (residues 508-565). Conserved areas without change (100% identity) are indicated with black shading, conserved areas with one residue difference (<80% identity) are indicated with dark gray shading and areas with two residues difference (>80 % identity) are indicated in light gray. Black arrow heads indicate conserved His and Cys residues.

REFERENCES

Almeida, A.D., Boije, H., Chow, R.W., He, J., Tham, J., Suzuki, S.C., Harris, W.A., 2014. Spectrum of Fates: a new approach to the study of the developing zebrafish retina. Development 141, 1971-1980.

Amato, M.A., Boy, S., Perron, M., 2004. Hedgehog signaling in vertebrate eye development: a growing puzzle. Cell Mol Life Sci 61, 899-910.

Azuma, N., Yamaguchi, Y., Handa, H., Tadokoro, K., Asaka, A., Kawase, E., Yamada, M., 2003. Mutations of the PAX6 gene detected in patients with a variety of optic-nerve malformations. Am J Hum Genet 72, 1565-1570.

Benton, C.S., de Silva, R., Rutledge, S.L., Bohlega, S., Ashizawa, T., Zoghbi, H.Y., 1998. Molecular and clinical studies in SCA-7 define a broad clinical spectrum and the infantile phenotype. Neurology 51, 1081-1086.

Cattaneo, E., Zuccato, C., Tartari, M., 2005. Normal huntingtin function: an alternative approach to Huntington's disease. Nat Rev Neurosci 6, 919-930.

Chen, S., Peng, G.H., Wang, X., Smith, A.C., Grote, S.K., Sopher, B.L., La Spada, A.R., 2004. Interference of Crx-dependent transcription by ataxin-7 involves interaction between the glutamine regions and requires the ataxin-7 carboxy-terminal region for nuclear localization. Hum Mol Genet 13, 53-67.

Chhetri, J., Jacobson, G., Gueven, N., 2014. Zebrafish--on the move towards ophthalmological research. Eye (Lond) 28, 367-380.

Chow, R.L., Lang, R.A., 2001. Early eye development in vertebrates. Annu Rev Cell Dev Biol 17, 255-296.

David, G., Abbas, N., Stevanin, G., Durr, A., Yvert, G., Cancel, G., Weber, C., Imbert, G., Saudou, F., Antoniou, E., Drabkin, H., Gemmill, R., Giunti, P., Benomar, A., Wood, N., Ruberg, M., Agid, Y., Mandel, J.L., Brice, A., 1997. Cloning of the SCA7 gene reveals a highly unstable CAG repeat expansion. Nature genetics 17, 65-70.

David, G., Durr, A., Stevanin, G., Cancel, G., Abbas, N., Benomar, A., Belal, S., Lebre, A.S., Abada-Bendib, M., Grid, D., Holmberg, M., Yahyaoui, M., Hentati, F., Chkili, T., Agid, Y., Brice, A., 1998. Molecular and clinical correlations in autosomal dominant cerebellar ataxia with progressive macular dystrophy (SCA7). Hum Mol Genet 7, 165-170.

Eccles, M.R., Schimmenti, L.A., 1999. Renal-coloboma syndrome: a multi-system developmental disorder caused by PAX2 mutations. Clin Genet 56, 1-9.

Ekker, S.C., Ungar, A.R., Greenstein, P., von Kessler, D.P., Porter, J.A., Moon, R.T., Beachy, P.A., 1995. Patterning activities of vertebrate hedgehog proteins in the developing eye and brain. Curr Biol 5, 944-955.

Enevoldson, T.P., Sanders, M.D., Harding, A.E., 1994. Autosomal dominant cerebellar ataxia with pigmentary macular dystrophy. A clinical and genetic study of eight families. Brain 117 (Pt 3), 445-460.

Fadool, J.M., 2003. Development of a rod photoreceptor mosaic revealed in transgenic zebrafish. Dev Biol 258, 277-290.

Gouw, L.G., Digre, K.B., Harris, C.P., Haines, J.H., Ptacek, L.J., 1994. Autosomal dominant cerebellar ataxia with retinal degeneration: clinical, neuropathologic, and genetic analysis of a large kindred. Neurology 44, 1441-1447.

Gregory-Evans, C.Y., Wallace, V.A., Gregory-Evans, K., 2013. Gene networks: dissecting pathways in retinal development and disease. Prog Retin Eye Res 33, 40-66.

Hammerschmidt, M., Bitgood, M.J., McMahon, A.P., 1996. Protein kinase A is a common negative regulator of Hedgehog signaling in the vertebrate embryo. Genes Dev 10, 647-658.

Helmlinger, D., Abou-Sleymane, G., Yvert, G., Rousseau, S., Weber, C., Trottier, Y., Mandel, J.L., Devys, D., 2004a. Disease progression despite early loss of polyglutamine protein expression in SCA7 mouse model. The Journal of neuroscience : the official journal of the Society for Neuroscience 24, 1881-1887.

Helmlinger, D., Hardy, S., Abou-Sleymane, G., Eberlin, A., Bowman, A.B., Gansmuller, A., Picaud, S., Zoghbi, H.Y., Trottier, Y., Tora, L., Devys, D., 2006. Glutamine-expanded ataxin-7

alters TFTC/STAGA recruitment and chromatin structure leading to photoreceptor dysfunction. PLoS Biol 4, e67.
Helmlinger, D., Hardy, S., Sasorith, S., Klein, F., Robert, F., Weber, C., Miguet, L., Potier, N., Van-Dorsselaer, A., Wurtz, J.M., Mandel, J.L., Tora, L., Devys, D., 2004b. Ataxin-7 is a subunit of GCN5 histone acetyltransferase-containing complexes. Hum Mol Genet 13, 1257-1265.
Hoche, F., Seidel, K., Brunt, E.R., Auburger, G., Schols, L., Burk, K., de Vos, R.A., den Dunnen, W., Bechmann, I., Egensperger, R., Van Broeckhoven, C., Gierga, K., Deller, T., Rub, U., 2008. Involvement of the auditory brainstem system in spinocerebellar ataxia type 2 (SCA2), type 3 (SCA3) and type 7 (SCA7). Neuropathol Appl Neurobiol 34, 479-491.
Hruscha, A., Krawitz, P., Rechenberg, A., Heinrich, V., Hecht, J., Haass, C., Schmid, B., 2013. Efficient CRISPR/Cas9 genome editing with low off-target effects in zebrafish. Development 140, 4982-4987.
Hwang, W.Y., Fu, Y., Reyon, D., Maeder, M.L., Tsai, S.Q., Sander, J.D., Peterson, R.T., Yeh, J.R., Joung, J.K., 2013. Efficient genome editing in zebrafish using a CRISPR-Cas system. Nat Biotechnol 31, 227-229.
Jao, L.E., Wente, S.R., Chen, W., 2013. Efficient multiplex biallelic zebrafish genome editing using a CRISPR nuclease system. Proc Natl Acad Sci U S A 110, 13904-13909.
Kimmel, C.B., Ballard, W.W., Kimmel, S.R., Ullmann, B., Schilling, T.F., 1995. Stages of embryonic development of the zebrafish. Dev Dyn 203, 253-310.
Kohler, A., Schneider, M., Cabal, G.G., Nehrbass, U., Hurt, E., 2008. Yeast Ataxin-7 links histone deubiquitination with gene gating and mRNA export. Nat Cell Biol 10, 707-715.
Koudijs, M.J., den Broeder, M.J., Groot, E., van Eeden, F.J., 2008. Genetic analysis of the two zebrafish patched homologues identifies novel roles for the hedgehog signaling pathway. BMC Dev Biol 8, 15.
Koudijs, M.J., den Broeder, M.J., Keijser, A., Wienholds, E., Houwing, S., van Rooijen, E.M., Geisler, R., van Eeden, F.J., 2005. The zebrafish mutants dre, uki, and lep encode negative regulators of the hedgehog signaling pathway. PLoS Genet 1, e19.
La Spada, A.R., Fu, Y.H., Sopher, B.L., Libby, R.T., Wang, X., Li, L.Y., Einum, D.D., Huang, J., Possin, D.E., Smith, A.C., Martinez, R.A., Koszdin, K.L., Treuting, P.M., Ware, C.B., Hurley, J.B., Ptacek, L.J., Chen, S., 2001. Polyglutamine-expanded ataxin-7 antagonizes CRX function and induces cone-rod dystrophy in a mouse model of SCA7. Neuron 31, 913-927.
Labun, K., Montague, T.G., Gagnon, J.A., Thyme, S.B., Valen, E., 2016. CHOPCHOP v2: a web tool for the next generation of CRISPR genome engineering. Nucleic Acids Res 44, W272-276.
Lee, J., Willer, J.R., Willer, G.B., Smith, K., Gregg, R.G., Gross, J.M., 2008. Zebrafish blowout provides genetic evidence for Patched1-mediated negative regulation of Hedgehog signaling within the proximal optic vesicle of the vertebrate eye. Dev Biol 319, 10-22.
Lim, J., Crespo-Barreto, J., Jafar-Nejad, P., Bowman, A.B., Richman, R., Hill, D.E., Orr, H.T., Zoghbi, H.Y., 2008. Opposing effects of polyglutamine expansion on native protein complexes contribute to SCA1. Nature 452, 713-718.
London, N.J., Kessler, P., Williams, B., Pauer, G.J., Hagstrom, S.A., Traboulsi, E.I., 2009. Sequence alterations in RX in patients with microphthalmia, anophthalmia, and coloboma. Mol Vis 15, 162-167.
Macdonald, R., Barth, K.A., Xu, Q., Holder, N., Mikkola, I., Wilson, S.W., 1995. Midline signalling is required for Pax gene regulation and patterning of the eyes. Development 121, 3267-3278.
Macdonald, R., Scholes, J., Strahle, U., Brennan, C., Holder, N., Brand, M., Wilson, S.W., 1997. The Pax protein Noi is required for commissural axon pathway formation in the rostral forebrain. Development 124, 2397-2408.
Marc, R.E., Jones, B.W., 2003. Retinal remodeling in inherited photoreceptor degenerations. Molecular neurobiology 28, 139-147.
Marti, E., Bovolenta, P., 2002. Sonic hedgehog in CNS development: one signal, multiple outputs. Trends Neurosci 25, 89-96.
Martin, J.J., 2012. Spinocerebellar ataxia type 7. Handb Clin Neurol 103, 475-491.

McWilliam, H., Li, W., Uludag, M., Squizzato, S., Park, Y.M., Buso, N., Cowley, A.P., Lopez, R., 2013. Analysis Tool Web Services from the EMBL-EBI. Nucleic Acids Res 41, W597-600.
Michalik, A., Martin, J.J., Van Broeckhoven, C., 2004. Spinocerebellar ataxia type 7 associated with pigmentary retinal dystrophy. Eur J Hum Genet 12, 2-15.
Mohan, R.D., Dialynas, G., Weake, V.M., Liu, J., Martin-Brown, S., Florens, L., Washburn, M.P., Workman, J.L., Abmayr, S.M., 2014. Loss of Drosophila Ataxin-7, a SAGA subunit, reduces H2B ubiquitination and leads to neural and retinal degeneration. Genes Dev 28, 259-272.
Ota, S., Kawahara, A., 2014. Zebrafish: a model vertebrate suitable for the analysis of human genetic disorders. Congenit Anom (Kyoto) 54, 8-11.
Raymond, S.M., Jackson, I.J., 1995. The retinal pigmented epithelium is required for development and maintenance of the mouse neural retina. Curr Biol 5, 1286-1295.
Rost, F., Eugster, C., Schroter, C., Oates, A.C., Brusch, L., 2014. Chevron formation of the zebrafish muscle segments. J Exp Biol 217, 3870-3882.
Schimmenti, L.A., de la Cruz, J., Lewis, R.A., Karkera, J.D., Manligas, G.S., Roessler, E., Muenke, M., 2003. Novel mutation in sonic hedgehog in non-syndromic colobomatous microphthalmia. Am J Med Genet A 116A, 215-221.
Schneider, C.A., Rasband, W.S., Eliceiri, K.W., 2012. NIH Image to ImageJ: 25 years of image analysis. Nat Methods 9, 671-675.
Schwarz, M., Cecconi, F., Bernier, G., Andrejewski, N., Kammandel, B., Wagner, M., Gruss, P., 2000. Spatial specification of mammalian eye territories by reciprocal transcriptional repression of Pax2 and Pax6. Development 127, 4325-4334.
Sehgal, R., Karcavich, R., Carlson, S., Belecky-Adams, T.L., 2008. Ectopic Pax2 expression in chick ventral optic cup phenocopies loss of Pax2 expression. Dev Biol 319, 23-33.
Sheedlo, H.J., Nelson, T.H., Lin, N., Rogers, T.A., Roque, R.S., Turner, J.E., 1998. RPE secreted proteins and antibody influence photoreceptor cell survival and maturation. Brain Res Dev Brain Res 107, 57-69.
Shen, Y.C., Raymond, P.A., 2004. Zebrafish cone-rod (crx) homeobox gene promotes retinogenesis. Dev Biol 269, 237-251.
Sinn, R., Wittbrodt, J., 2013. An eye on eye development. Mech Dev 130, 347-358.
Skalicky, S.E., White, A.R., Grigg, J.R., et al., 2013. Microphthalmia, anophthalmia, and coloboma and associated ocular and systemic features: Understanding the spectrum. JAMA Ophthalmology 131, 1517-1524.
Stenkamp, D.L., Frey, R.A., Mallory, D.E., Shupe, E.E., 2002. Embryonic retinal gene expression in sonic-you mutant zebrafish. Dev Dyn 225, 344-350.
Stenkamp, D.L., Frey, R.A., Prabhudesai, S.N., Raymond, P.A., 2000. Function for hedgehog genes in zebrafish retinal development. Developmental Biology 220, 238-252.
Stevanin, G., Giunti, P., Belal, G.D., Durr, A., Ruberg, M., Wood, N., Brice, A., 1998. De novo expansion of intermediate alleles in spinocerebellar ataxia 7. Hum Mol Genet 7, 1809-1813.
Strauss, O., 2005. The retinal pigment epithelium in visual function. Physiol Rev 85, 845-881.
Take-uchi, M., Clarke, J.D., Wilson, S.W., 2003. Hedgehog signalling maintains the optic stalk-retinal interface through the regulation of Vax gene activity. Development 130, 955-968.
Thisse, C., Thisse, B., 2008. High-resolution in situ hybridization to whole-mount zebrafish embryos. Nat Protoc 3, 59-69.
Thurtell, M.J., Fraser, J.A., Bala, E., Tomsak, R.L., Biousse, V., Leigh, R.J., Newman, N.J., 2009. Two patients with spinocerebellar ataxia type 7 presenting with profound binocular visual loss yet minimal ophthalmoscopic findings. J Neuroophthalmol 29, 187-191.
Trousse, F., Marti, E., Gruss, P., Torres, M., Bovolenta, P., 2001. Control of retinal ganglion cell axon growth: a new role for Sonic hedgehog. Development 128, 3927-3936.
van Eeden, F.J., Granato, M., Schach, U., Brand, M., Furutani-Seiki, M., Haffter, P., Hammerschmidt, M., Heisenberg, C.P., Jiang, Y.J., Kane, D.A., Kelsh, R.N., Mullins, M.C., Odenthal, J., Warga, R.M., Allende, M.L., Weinberg, E.S., Nusslein-Volhard, C., 1996. Mutations affecting somite formation and patterning in the zebrafish, Danio rerio. Development 123, 153-164.

Vissers, L.E., van Ravenswaaij, C.M., Admiraal, R., Hurst, J.A., de Vries, B.B., Janssen, I.M., van der Vliet, W.A., Huys, E.H., de Jong, P.J., Hamel, B.C., Schoenmakers, E.F., Brunner, H.G., Veltman, J.A., van Kessel, A.G., 2004. Mutations in a new member of the chromodomain gene family cause CHARGE syndrome. Nat Genet 36, 955-957.
Wang, P., Liang, X., Yi, J., Zhang, Q., 2008. Novel SOX2 mutation associated with ocular coloboma in a Chinese family. Arch Ophthalmol 126, 709-713.
Waterhouse, A.M., Procter, J.B., Martin, D.M., Clamp, M., Barton, G.J., 2009. Jalview Version 2--a multiple sequence alignment editor and analysis workbench. Bioinformatics 25, 1189-1191.
Weiss, A.H., Kousseff, B.G., Ross, E.A., Longbottom, J., 1989. Simple microphthalmos. Archives of Ophthalmology 107, 1625-1630.
Wen, W., Pillai-Kastoori, L., Wilson, S.G., Morris, A.C., 2015. Sox4 regulates choroid fissure closure by limiting Hedgehog signaling during ocular morphogenesis. Dev Biol 399, 139-153.
Westerfield, M., 2000. The Zebrafish Book. A Guide for The Laboratory Use of Zebrafish (Danio rerio).
Wyatt, A., Bakrania, P., Bunyan, D.J., Osborne, R.J., Crolla, J.A., Salt, A., Ayuso, C., Newbury-Ecob, R., Abou-Rayyah, Y., Collin, J.R., Robinson, D., Ragge, N., 2008. Novel heterozygous OTX2 mutations and whole gene deletions in anophthalmia, microphthalmia and coloboma. Hum Mutat 29, E278-283.
Yanicostas, C., Barbieri, E., Hibi, M., Brice, A., Stevanin, G., Soussi-Yanicostas, N., 2012. Requirement for zebrafish ataxin-7 in differentiation of photoreceptors and cerebellar neurons. PLoS One 7, e50705.
Yefimova, M.G., Messaddeq, N., Karam, A., Jacquard, C., Weber, C., Jonet, L., Wolfrum, U., Jeanny, J.C., Trottier, Y., 2010. Polyglutamine toxicity induces rod photoreceptor division, morphological transformation or death in spinocerebellar ataxia 7 mouse retina. Neurobiol Dis 40, 311-324.
Yoo, S.Y., Pennesi, M.E., Weeber, E.J., Xu, B., Atkinson, R., Chen, S., Armstrong, D.L., Wu, S.M., Sweatt, J.D., Zoghbi, H.Y., 2003. SCA7 knockin mice model human SCA7 and reveal gradual accumulation of mutant ataxin-7 in neurons and abnormalities in short-term plasticity. Neuron 37, 383-401.
Yvert, G., Lindenberg, K.S., Picaud, S., Landwehrmeyer, G.B., Sahel, J.A., Mandel, J.L., 2000. Expanded polyglutamines induce neurodegeneration and trans-neuronal alterations in cerebellum and retina of SCA7 transgenic mice. Human molecular genetics 9, 2491-2506.
Zhang, X.M., Yang, X.J., 2001. Regulation of retinal ganglion cell production by Sonic hedgehog. Development 128, 943-957.
Zhao, Y., Lang, G., Ito, S., Bonnet, J., Metzger, E., Sawatsubashi, S., Suzuki, E., Le Guezennec, X., Stunnenberg, H.G., Krasnov, A., Georgieva, S.G., Schule, R., Takeyama, K., Kato, S., Tora, L., Devys, D., 2008. A TFTC/STAGA module mediates histone H2A and H2B deubiquitination, coactivates nuclear receptors, and counteracts heterochromatin silencing. Mol Cell 29, 92-101.
Zoghbi, H.Y., Orr, H.T., 2000. Glutamine repeats and neurodegeneration. Annu Rev Neurosci 23, 217-247.

DISCUSSION AND PERSPECTIVES

Chapter 4

Discussion and Perspectives

The goal of this thesis was to determine the physiological role of *atxn7* using zebrafish as a model. Given that the retina is affected in SCA7, we paid attention to the ocular morphogenesis and retinal neuron differentiation, with particular interest in the photoreceptors. Originally our general hypothesis was that *atxn7* is required for ocular development and loss-of-function of *atxn7* should result in ocular defects, indicating an organ sensitivity. This hypothesis was tested and supported in Chapter 3 (Manuscript).

We showed that *atxn7* is expressed dynamically during zebrafish development and is particularly increased in the area of the retina. *atxn7* knockdown in zebrafish resulted predominantly in a characteristic ocular malformation named coloboma, supporting our initial hypothesis. We also demonstrated that the coloboma defect was a result of an increase of the Hh signaling that altered proximo-distal patterning of the optic vesicle, including expansion of *pax2* expression and retraction of *pax6*. Finally, we showed that *atxn7* is also required for the terminal differentiation of photoreceptors through the regulation of *crx* expression.

Taken together, these results indicate that *atxn7* plays an important role in vertebrate ocular development and in the terminal differentiation of photoreceptors.

Alteration in the expression of *atxn7* causes ocular coloboma.

Ocular coloboma is an eye malformation caused by a failure in the closure of the optic fissure during embryonic development, and is the leading cause of blindness in children. The estimated prevalence of coloboma is 1 of 5000 live births (Shah et al., 2011). Multiple studies have shown that genetic perturbations of developmentally important genes and signaling pathways results in the failure of the optic fissure closure in vertebrate eye (Azuma et al., 2003; Eccles and Schimmenti, 1999; London et al., 2009; Schimmenti et al., 2003; Vissers et al., 2004; Wang et al., 2008; Wyatt et al., 2008). However, these causative genes that have been identified account for a small fraction of the clinically reported cases (Skalicky et al., 2013), highlighting the importance of looking for new causative genes that can provide a better understanding of this common defect.

In the present work, we have demonstrated a specific role of *atxn7* in regulating the choroid fissure closure. Morpholino-mediated *atxn7* downregulation caused coloboma and an altered proximo-distal patterning of the optic vesicle. We further tested and confirmed this phenotype on a mosaic *atxn7* knockout generated with CRISPR/Cas9. F0 founders already presented a coloboma phenotype. Furthermore, the analysis of different concentrations of morpholino showed the high specificity and sensibility of the ocular phenotype, since at low morpholino concentration the eye defect persisted. Finally, ectopic expression of human ATXN7 partially rescued the coloboma phenotype, demonstrating that the phenotype is specifically due to decreased *atxn7* level, and at the same time that the function of ATXN7 in the closure of the choroid fissure is likely conserved in vertebrate evolution. Furthermore, since coloboma is often associated with microphthalmia, we tested this possibility and found that indeed *atxn7* morphant eye were smaller, but in strict proportion to a smaller animal size. Therefore, coloboma in *atxn7* morphant appears to represent a structural developmental eye defect independent of microphthalmia. The role of *atxn7* in the regulation of the choroid fissure closure is consistent with the spatiotemporal expression pattern of *atxn7,* which is characterized by maternal contribution and early and persistent zygotic expression, with important expression level in the eye.

It is worth mentioning that in an earlier characterization on *atxn7* morphant phenotype by Yanicostas and collaborators (Yanicostas et al., 2012), the coloboma was not reported. The authors only described a “partially depigmented retina”, which was not further analyzed. However, the supplementary figures presented in this paper clearly show the presence of coloboma.

Atxn7 acts as a negative regulator of Hh signaling pathway

Gregory-Evans proposed a coloboma gene network composed of various coloboma-causing genes identified (Gregory-Evans et al., 2013). A central member of this network is *shh*. Multiple studies have established a relationship between the concentration levels of the Hh signal and the presence of coloboma (Ekker et al., 1995; Lee et al., 2008; Macdonald et al., 1995; Pillai-Kastoori et al., 2014; Wen et al., 2015). Mutations of many genes regulated by *shh* also lead to coloboma phenotype in vertebrates. Therefore, comparing our observations with those reported phenotypes, we hypothesized that the Hh signaling pathway might be affected in *atxn7* morphant.

We indeed found an increased level of *shha* and *twhh* in the ventral midline of the developing brain of atxn7 deficient embryos at 18 hpf. At this site and precise time point, Hh signaling controls the proximo-distal patterning of the optic vesicle by regulating the expression of two genes, *pax2a*, expressed in the optic stalk, and *pax6*, expressed in the optic vesicle (Ekker et al., 1995; Macdonald et al., 1995). Accordingly, we found that the signal of *pax2a* was abnormally extended into the area of the presumptive optic vesicle, while the expression of *pax6* was retracted in the area of the optic stalk. This specific alteration of *pax2*/*pax6* expression pattern, is consistent with deregulation of Hh pathway as reported earlier (Ekker et al., 1995; Lee et al., 2008; Macdonald et al., 1995; Pillai-Kastoori et al., 2014; Wen et al., 2015). Moreover, aberrant expression of *vax2* in the dorsal retina further support the alteration in the *shh* signaling pathway, as previously reported (Take-uchi et al., 2003).

Additional experiments are required in order to determine the mechanism(s) whereby atxn7 is regulating the Hh signaling pathway. ATXN7 is a highly conserved member of the SAGA complex that regulates transcription through GCN5-dependent histone acetylation and USP22-dependent histone deubiquitination activities (Helmlinger et al., 2006; Kohler et al., 2008; Zhao et al., 2008). As part of the SAGA co-regulator of transcription, it is possible that atxn7 could directly alter the expression of the Hh genes. However, there is yet no reports that could support this direct interaction. A second possibility could be an indirect regulation. Supporting this hypothesis, a very recent report of mouse embryos lacking enzymatic activity of the acetyltransferase of GCN5 (*Gcn5*$^{hat/hat}$) presented an increased diencephalic Shh signaling caused by a decreased diencephalic retinoic acid (RA) signaling (Wilde et al., 2017). Interestingly enough, RA pathway has also been implicated with an aberrant choroid fissure closure, resulting in a coloboma defect (Gongal et al., 2011; Lupo et al., 2011). Moreover, it is suggested that RA acts upstream of Shh (Gongal et al., 2011). Additionally, it has been reported that USP22 can act as a repressor of the *SOX2* gene (Sussman et al., 2013). Furthermore, it has been shown that *SOX2* participates in the regulation of genes of the SHH signaling pathways (Engelen et al., 2011) and that *SOX2* mutations can as well cause coloboma (Wang et al., 2008). In *Drosophila*, the absence of *atxn7* produced a global decrease in the levels of H3K9 acetylation and H2B ubiquitination (Mohan et al., 2014). Integrating all these observations to try to explain the coloboma phenotype in atxn7 deficient zebrafish, this suggest: on the one hand, the loss of atxn7 function would compromise the activity of GCN5, which would lead, according to Wilde et al 2017, to decreased RA signaling and increased SHH level, and hence to coloboma; on the other hand, the loss of atxn7 function would potentiate the activity of USP22, which would repress SOX2, leading to alteration of the Hh pathway and hence to coloboma phenotype. Therefore, we favor an indirect model of

regulation and we hypothesize that atxn7 negatively regulates the expression of Hh -and possibly *sox2*- as a consequence of alterations in the histone acetylation -and/or deubiquitination- activities of the SAGA complex.

These hypotheses can be tested in zebrafish. First, it would be worth to test by Western blot the global levels of H3K9 acetylation and H2B ubiquitination in *atxn7* deficient fish, to confirm the *drosophila* data. It would be important to study USP22 and GCN5 as well, to test whether their potential dysfunction in *atxn7* deficient fish could be related to their level of expression. Additionally, measurements of the expression level and pattern of *sox2* and its related genes could be performed either by WISH, quantitative RT-PCR or western blot. Regarding the levels of RA, we propose the use of previously reported transgenic line RGYn2. This stable transgenic zebrafish line carries a RA-inducible reporter gene that is able to localize regions of RA-mediated gene activation during zebrafish development (Perz-Edwards et al., 2001). As a final point, it would be interesting to conduct unbiased examinations such as RNA-seq or even ChIP-seq to identify more *atxn7* targets that are involved in ocular development.

Molecular rescue of the *atxn7* coloboma phenotype. (RA, crx)

To validate the upregulation of Hh pathway activity. Multiple studies have used cyclopamine, a pharmacological inhibitor of the Hh pathway that acts downstream of the Hh receptor Patched (Chen et al., 2002; Cooper et al., 1998), to suppress a coloboma phenotype (Lee et al., 2008; Pillai-Kastoori et al., 2014; Wen et al., 2015).

In theory, we would be able to perform a molecular rescue on the *atxn7* morphants, however unlike the other reports of coloboma phenotype due to an increase Hh pathway activity, here we demonstrated a parallel diminished expression of the crx gene. This is relevant since it has been demonstrated that reduced expression leads to the expansion of *pax2* into the optic vesicle and the retraction of *pax6* (Shen and Raymond, 2004). And as we have cited the expression of *crx* is independent of variations in the expression of *shh* (Stenkamp et al., 2002). Suggesting that despite a reduction in the Hh pathway activity, the coloboma defect could persist in *atxn7* morphtans due to the reduced expression of *crx*, discarding thus the possibility of a molecular rescue of the coloboma phenotype.

Double rescue combining mRNA injection to restore the wild-type level of CRX in addition to the cyclopamine in *atxn7* deficient embryos, would represent a bigger challenge. Cells are very sensitive to variations in concentrations levels of Hh. Establishing proper concentration levels for both –mRNA and cyclopamine- could be difficult.

Shh one morphogen, same response?

Hh signaling has been widely studied in various models from *Drosophila* to higher vertebrates and it has been shown that it plays essential roles in patterning of the embryo, limb buds and organs among others (Briscoe and Therond, 2013). Does this mean that *atxn7* deficiency would systematically cause coloboma through Shh deregulation in any other animal model? Not necessarily. Although Hh signals are involved in common developmental mechanisms in several organisms, it has been shown as well that alterations in the Hh signaling can produce different outcomes according to the animal model used. For example, the zebrafish *shh* mutant (syu) displays a reduction in RGC formation (Neumann and Nuesslein-Volhard, 2000), while on the contrary knocking down *shh* in chick causes an increased in RGC differentiation (Zhang and Yang, 2001). Similarly, *shh* mutations cause severe cyclopia in mouse and human (Chiang et al., 1996; Roessler et al., 1996) but not in zebrafish, likely because redundancy of Hh members (Karlstrom et al., 1999; Schauerte et al., 1998). Moreover, there are many components involved in the Hh transduction pathway, and it appears that different members of the pathway present differences among the organisms. For example, Gli1 acts as the main activator in the Hh cascade in zebrafish, but is dispensable in the mouse (Karlstrom et al., 2003). On the contrary, Gli2 appears to be the major mediator in the mouse (Park et al., 2000). This suggests that members of the cascade can be differentially recruited in different species, consequently presenting differences in phenotypes. Another important factor to take in account is the conditions used to alter the levels of Hh expression. Cells are extremely sensitive to variations in the concentration levels of Hh, hence distinct methods (pharmacological, antisense oligonucleotides, point mutation, etc.) could result in different phenotypes due to diverse degrees in inhibition. Therefore, it will be worth taking these factors in account when comparing the phenotype of different organisms where *atxn7* is inactivated. Additionally, the present results put ATXN7 as a candidate gene in human coloboma, however, this possibility shall be taken into the context of the complex Hh signaling pathway, which differs among species.

Could alterations in cell death or proliferation account for the coloboma defect in *atxn7* deficient fish?

The choroid fissure closure can be subdivided in three stages: 1) the proliferation of the retinoblasts generating enough cells that the lateral edges of the choroid fissure come in proximity; 2) the basement membrane lining in the choroid fissure is degraded facilitating

adhesion between the cells facing the opposite sides of the fissure; 3) cells on opposing sides of the fissure form adhesions that spread and thereby close the choroid fissure in the area of the ventral retina (Bazin-Lopez et al., 2015; James et al., 2016). These ocular developmental events require constant and dynamic coordination between cell proliferation, cell differentiation, and cell death. Multiple experiments have demonstrated that the Hh signaling could play a role in modulating the proliferation of progenitor cells and can also act as a survival factor (Amato et al., 2004). Furthermore, over proliferation within the retinal has been shown to lead to colobomas (Kim et al., 2007). Thus, this raises the question if the increased Hh signaling in atxn7 deficient zebrafish could influence the cell death or proliferation balance and ultimately cause the coloboma defect.

During the eye morphogenesis, two major proliferation events occur: first, during the eye field outgrowth, cell proliferation is controlled by numerous transcriptional factors including *Rx1, Six3, Lhx2,* and *Optx2* that are independent of the Hh signal (Fuhrmann, 2010; Zuber et al., 2003); second, there is proliferation of retinoblasts during retinogenesis, and in this case there is no report of direct link with the Hh signal or any of its members; so far the involved participants that have been reported belong to the (v)-ATPase complex or the Inhibitor of differentiation (Id) family (Nuckels et al., 2009; Uribe and Gross, 2010). Moreover, multiple reports of mutants with altered Hh signal similar to the one we here report have shown that over proliferation is not a main cause for coloboma defect (Lee et al., 2008; Pillai-Kastoori et al., 2014; Wen et al., 2015).

Concerning the involvement of Shh in cell death, diverse reports have demonstrated that at early stages, cell survival is not dependent of Hh signals (Neumann and Nuesslein-Volhard, 2000; Stenkamp et al., 2002); it is after the retinal differentiation that Hh plays a role in retinal cell survival (around 58 hpf). In our study, we have reported defects of shh expression at earlier stage (24 hpf), which are persistent and strong until 48 hpf (Figure 2 and S2). This suggests that the coloboma defect that we report is not a consequence of the involvement of Hh signaling in cell death. Moreover, the mutant of pax2a (*noi*), a member of the Hh pathway, had no rescue in the coloboma phenotype when exposed to an anti-apoptotic compound (Gregory-Evans et al., 2011).

Taking all this in account we consider that neither over proliferation nor increased cell death in response to the Hh signal alteration is responsible for the coloboma phenotype exhibits in *atxn7* morphants. Therefore, other cellular mechanisms such as degradation of the basement membrane or cell adhesion would be worth to preferentially analysis to further characterize the closure defect.

Alteration in the axon guidance.

Analysis of fish mutant related to the Hh pathway revealed anomalies in the axon pathfinding (Macdonald et al., 1997). Using the transgenic line SoFa1 we analyzed the axon pathfinding of *atxn7* morphants and demonstrated that the axons properly crossed the ventral midline of the diencephalon forming the optic chiasma, and ultimately innervate the contralateral tectal lobe. However, we reported that 30.76% (n=4/13) of morphant embryos presented axons that aberrantly extended toward the anterior commissure. We suggest this could be a direct consequence of a more relaxed axon bundle, as we observed in Figure7H.

However we don't discard the possibility of an axon pathfinding anomaly. To test this option we suggest cell transplants of altered *atxn7* SoFa1 donor cells placed into non injected-non transgenic acceptor embryos, this could help track the optic nerve in a properly formed axon bundle.

Reduced size in *atxn7* morphants.

Here we have presented evidence that there was no presence of microphtalmia but overall the body size was significantly reduced in *atxn7* morphants during development (Supplementary Figure S4). Interestingly, morphants appeared to be morphologically normal with a reduced 'short' body.

The underlying factors that could account for this reduction in embryo size remain to be found. We have the hypothesis that the defect could be the result of alteration of the Hh signaling pathway. There has been evidence of reduced body size in *pax6* morphants (Coutinho et al., 2011). However, comparison of the whole larva phenotype displayed in *pax6* morphants with the phenotype reported with overexpression of *shh* and the phenotype we present in this dissertation appear all to differ (Macdonald et al., 1995). Variations in the experimental methodology or as well the change in the target gene could account to the difference in the phenotype. Further experimentations, including analysis of the expression of Hh signaling involved genes by in situ hybridization in other areas besides the retina might bring light to this hypothesis.

Finally, we have discarded the possibility of an increase cell death causing the reduced size as merely a side effect of morpholino injection. It is known that morpholino major off-targeting effect is the activation of p53 apoptosis pathway (Robu et al., 2007). However, reduced size was also found in the F0 mosaic knockout of *atxn7* (not shown) and so far there are no reports of p53 induction by the system CRISPR-Cas9.

Atxn7 alters photoreceptor terminal differentiation.

Differentiated photoreceptor cells in zebrafish typically display elongated nuclei, well differentiated outer segments apposed to the RPE, and clusters of mitochondria in the intervening inner segments, directly below the outer segments. The terminal differentiation of photoreceptors involve the formation of the outer segments. We reported the requirement of *atxn7* in proper photoreceptor terminal differentiation, since most a*txn7* morphant photoreceptors exhibited lack or much shorter outer segments than normal. Other a*txn7* morphant photoreceptors were more affected with delocalized mitochondria and disorganized inner segments. These defects were likely not a secondary effect of coloboma, since it was observed in other areas of the retina apart from the extruding area.

Trying to explain this phenotype we formulated three hypotheses. 1) The alteration in the photoreceptor morphogenesis could be a response to the Hh upregulation in the midline. In this situation, we would expect alteration of the differentiation of other retinal neurons; however, this was not the case, as only the photoreceptors were affected. 2) The RPE is a known source for secreted factors, including *shh*, towards the photoreceptors for their differentiation. In this situation, only photoreceptors located in the extruded retina would be affected; however, alteration of photoreceptor morphogenesis was also observed in region where RPE appears normal. 3) Excluding the two previous hypotheses, we postulated that malformation of photoreceptors could be intrinsic to the photoreceptor cell itself, due to the lack of expression of key transcription factors known to control the terminal differentiation of photoreceptors. This hypothesis made sense since photoreceptors are the most sensitive neurons to the toxicity of mutant ATXN7 in SCA7. Furthermore, ATXN7 is proposed to directly interact with CRX allowing SAGA to execute epigenetic modifications on CRX-regulated genes (Chen et al., 2004; La Spada et al., 2001). In zebrafish, it was challenging to test the transactivation function of crx on its targeted genes in the absence of atxn7. However, by in situ hybridization we discovered that there was a significant difference in the intensity and localization of the *crx* signal in the *atxn7* deficient fish. Notably, *atxn7* morphants presented areas with complete lack of signal (Figure 8F-G) and this was not caused by a developmental delay. Importantly, it has been reported that the expression of *crx* is independent of variations in the expression of *shh* (Stenkamp et al., 2002). Therefore, the variables level of *crx* likely accounts for the variability in the photoreceptor morphogenesis seen in *atxn7* morphants. Importantly, these results indicate that there is at least two independent molecular pathways (shh and crx) that are altered in *atxn7* morphants.

This is thus the first evidence that *atxn7* could regulate *crx* expression. Whether this regulation is direct or indirect needs more investigation. Crx is not the only transcription factor involved in photoreceptor differentiation (Swaroop et al., 2010). Nrl and Nr2e3, for instance, are also involved in photoreceptor differentiation, the latter is particularly important for the cell-fate specification of cone and rod lineages. In addition, these three transcription factors are downstream in a regulatory cascade involving several upstream transcription factors, such as Otx2 or RORβ. Therefore, it would be first worth testing by *in situ* hybridization these other transcription factors involved in photoreceptor differentiation in order to identify at which step atxn7 could play a role.

The heterogenous patterns of crx and outer segment alterations that we observed in *atxn7* deficient fish likely explain the observation of Yanicostas et al., (2012), who previously reported variable level of expression of rhodopsin along the retina of similar atxn7 morphant. In this study, the underlying mechansim of rhodosin alteration was not explored. Given that atxn7 seems to play a role in the regulation of transcription factors involved in photoreceptor differentiation, and given that the cones are affected before the rods in SCA7, it would be interesting to compare the labeling of different cone subtypes and rhodopsin to determine if there is –like in the disease- any specific cone-type susceptibility to the atxn7 downregulation (Vihtelic et al., 1999).

Atxn7 and SAGA

Studies have established several molecular functions of SAGA. SAGA is a multifunctional coactivator complex containing histone acetyltransferase (HAT) and deubiquitylase (DUB) activities and it also directly interacts with the TATA-binding protein (TBP) to facilitate transcription initiation (reviewed in (Koutelou et al., 2010; Rodriguez-Navarro, 2009)).To determine the specific regulatory network of SAGA, several studies used genome-wide transcriptome analyses. Analysis of steady-state mRNA initially indicated that yeast SAGA regulates the expression of about 10% of yeast genes. This view was recently challenged by Bonnet et al (2014) who reported that SAGA is responsible for H3K9ac at promoter regions and deubiquitination of H2Bub in gene bodies of almost all transcribed genes, in both yeast and human. In addition, SAGA inactivation in yeast strongly affected Pol II recruitment at active promoters leading to a major decrease of Pol II transcription, as revealed by the analysis of newly-synthesized RNA.

If SAGA is required for the expression of all Pol II transcribed genes, how can we explain a prominent role of zebrafish *atxn7* in ocular development? One possibility is that *atxn7* and its

paralogs play different roles in SAGA to ensure the regulation of specific genetic program. Along this view, *atxn7* would specifically allow SAGA to regulate the choroid fissure closure and the terminal differentiation of photoreceptors. To address this question our initial approach was to determine the expression of the paralogs in the atxn7 morphant context by RT-PCR. We didn't find significant changes, however we don't discard the possibility of alteration in the spatial expression pattern or that alterations could be masked in this global experiment. We suggest a second approach by in situ hybridization to determine the areas of expression of each paralog and determine the presence of alterations in a more refined manner. Additionally co-injection of each paralog with atxn7 Mo could reveal a possible rescue effect.

Relationship between *atxn7* downregulation and SCA7.

In SCA7, the ubiquitously expressed mutant ATXN7 leads to selective neurodegeneration, predominantly affecting the Purkinje cells of cerebellum and the photoreceptors of retina. The mechanism underlying selective degeneration in SCA7 still remains unclear.

Here we have shown that the downregulation of *atxn7* presents a predominant ocular phenotype i.e. even at minimal concentrations of morpholino an eye specific phenotype persisted. Moreover, we showed a specific impairment of the photoreceptor cells. At minimal morpholino concentration, we notice that the brain also showed morphological alterations – although it was not characterized in this study- but no other organ. Together, our results strongly indicate a sensitive and specific function of *atxn7* in the ocular and photoreceptor development. This organ and neuronal sensitivity might account for the pathogenesis observed in the SCA7 disease, since loss of function mechanism is thought to contribute to the pathogenesis in polyQ disease. Interestingly, the SCA7 R7E transgenic mouse photoreceptors progressively lose their outer segments and cell polarity, and relapse to round cell shape suggesting the loss of photoreceptor differentiation (Yefimova et al., 2010). While the formation of OS is compromised during photoreceptor terminal differentiation in the *atxn7* morphant. Both models suggest an apparent mirror phenotype raising the question whether *atxn7* could have a function in the maintenance of the outer segment integrity in adult photoreceptors. It's worth mentioning that the OS of both rods and cones is a dynamic structure, undergoing on daily partial renewal and shedding. In order to do so there is required an important gene expression activity.

The hypothesis that *atxn7* is required for the renewal and maintenance of photoreceptor outer segment can be assessed in zebrafish. To do so, we suggest to perform a transient kockdown of *atxn7* in the retina. This can be achieved by the electrophoration of positively-charged

lissamine-tagged morpholinos in the fish adult retina as previously reported (Thummel et al., 2011).

If this function of atxn7 is confirmed, then it would be tempting to overexpress wildtype ATXN7 in the SCA7 mouse retina to preserve the photoreceptor integrity, as a preclinical trial.

Analyzing embryonic development for an adult onset disease.

All polyQ disorders are late-onset neurodegenerative disorders. Most studies in different animal models have been focused on the disease onset and progression or just prior to it. However, studies in SCA2, SCA6, and HD (Arteaga-Bracho et al., 2016; Barnat et al., 2017; Jayabal et al., 2017; Kiehl et al., 2000; Miyazaki et al., 2004; Molero et al., 2016) are challenging this view, showing that developmental anomalies could account as the biological base for the programming and the vulnerability of adult onset disorders. For example, Molero et al.(2016) showed that when mice are selectively exposed to mutant HTT 97Q until postnatal day 21, they recapitulate a HD-like phenotype including neuropathology and motor deficits. Whether in SCA7 ATXN7 dysfunction leads to developmental malformation of photoreceptors, rendering them susceptible to degeneration in adult, remains a possibility, given our finding showing the important role of zebrafish *atxn7* in photoreceptor differentiation.

Shh and SCA7

Is there any other link between the Hh signaling pathway and other tissues vulnerable in SCA7? Interestingly, it has been reported that expression of Shh is needed for differentiation of Bergmann glia. Additionally, altered expression of Shh result in an abnormal arrangement and development of Purkinje neurons (Dahmane and Ruiz i Altaba, 1999). Two of the most susceptible cell types in the SCA7 cerebellar pathology (Furrer et al., 2011; Garden et al., 2002; Palhan et al., 2005). Interestingly there have been reports of patients with Pax6 mutations presenting cerebellar ataxia (Chien et al., 2009). Yet most of the genes involved in the Hh signaling pathway have generally been studied in a developmental context. In adults, it is known that Shh continues to be expressed in the cortex and in the granule layer of the cerebellum (Traiffort et al., 1998). And that it has a role in the survival of the spinal cord (Miao et al., 1997). Finally, it has been demonstrated that increased amount of Hh signaling is linked to dedifferentiation of cells (Landsman et al., 2011), a phenotype that has been seen in the SCA7 mice. Therefore, the question deserves further consideration.

Highlights of the present work

- Atxn7 is required for proximo-distal patterning of the optic stalk and vesicle, and in choroid fissure closure.
- Atxn7 regulates the expression of Hh family members in a negative manner.
- Atxn7 is required for the morphogenesis of the photoreceptor outer segment through the control of *crx* expression.

In summary, this thesis includes a detailed examination for the requirement of *atxn7* in regulating ocular morphogenesis in zebrafish. It provides a thorough expression profile of *atxn7,* both temporally through the development and spatially in retina during early ocular morphogenesis and retinal neurogenesis stages.

Independent loss-of-function analyses conducted on *atxn7* by morpholino-knockdown and mutant Crispr-Cas9 models demonstrated a specific role of *atxn7* in regulating the choroid fissure closure. Molecular analysis of the ocular coloboma provided strong evidence that *atxn7* negatively regulates midline Hh. The elevated midline Hh activity as a result of *atxn7* deficiency caused an expanded optic stalk, reflected by the expansion of the *pax2a* signal that ultimately inhibited the choroid fissure from closing, causing a coloboma defect. This was confirmed with the corresponding retraction of the *pax6* signal and expansion of the *vax2* signal. Moreover, alteration in the angle of the somites further supports variations in the Hh signaling.

We have also provided some evidence for a requirement of *atxn7* in photoreceptor morphogenesis that appears to be independent of the Hh signaling. We are therefore eager to elucidate additional functions of *atxn7* in regulating embryonic retinal and brain neurogenesis and development.

While further analysis is required to continue identifying direct target genes of *atxn7*, our study during ocular development opens new lines of study for the involvement of atxn7 deficiency on human disease. First we demonstrate a specific eye defect which proves a clear organ sensibility to variation in the function of *atxn7* during ocular morphogenesis, second we show the involvement of *atxn7* in photoreceptor morphogenesis both which could account for SCA7 physiopathology. Moreover, the discovery of a regulatory relationship between *atxn7* and the Hh signaling pathway during ocular development provides evidence to propose *atxn7* as a causative gene of coloboma. This is relevant, since coloboma despite being a common vision condition and the leading cause of blindness in children, only a handful of causative genes have been identified, and they account a minimal fraction of the clinically reported ocular coloboma cases. Future studies will focus on the determination of the direct target(s) of *atxn7*, and how these targets affect Hh signaling activity and ocular development.

Taking this together it is reasonable to speculate that *atxn7* deficiency may be involved SCA7 retinopathy and is a novel addition for the gene coloboma network.

ANEX1

ANEX 1

Reagents

In situ hybridization.

Hybridization Mix 1 (Stored at -20°C)

5mL	Formamide (Deionized)
2.5mL	20X SSC
100µL	Heparin 5mg/mL
50µL	Tween-20 20%
92µL	Citric acid 1M
2.25mL	Ultra-pure water

Hybridization Mix 2 (Better prepare at the moment the amount needed)

10 mL	Formamide
5 mL	20X SSC
100 µL	Tween-20 20%
184 µL	Citric acid 1M
4.7 mL	Ultra-pure water

MABT (Storage at room temperature)

5 mL	Maleic Acid 1M
0.43g	NaCl
250 µL	Tween-20 20%
45 mL	Ultra-pure water

Blocking Solution 10X (Storage at -20)

1 g	Blocking reagent
10 mL	MAB (*Maleic Acid Buffer* WITHOUT Tween 20)

Preparation of BS requires to be with shaking and heating

Revelation Solution (Better prepare at the moment the amount needed)

2 mL	Tris HCL 1M
1 mL	MgCl2 1M
400µL	NaCl 5M
100µL	Tween-20 20%
16.5 mL	Ultra-pure water

Staining Solution (Better prepare at the moment the amount needed)

10 mL	Revelation Solution
45 µL	NBT solution *
35 µL	BCIP solution *

*NBT and BCIP ROCHE commercial solutions

<u>Imaging</u>

3% Methylcellulose

1.5 g	methylcellulose (Sigma M-0387) **
50 ml	PBS

** This number is important not all methylcellulose has the same viscosity

The preparation of methylcellulose can be tricky leading to cloudy/opaque solutions inadequate for imagining. The used protocol for this study:

1. Heat the PBS to 60°C in a tall beaker.
2. Add the methyl cellulose and mix with a very long glass rod.
3. Put the beaker in the freezer and stir it every half hour until it begins to freeze.
4. Put at 4° for two days.
5. To remove little specks of undissolved methyl cellulose spin at 10.000 rpm.
6. The solution should now be clear, aliquot in 1.5 ml tubes at keep at -20C.

BIBLIOGRAPHY

Bibliography

Abou-Sleymane, G., Chalmel, F., Helmlinger, D., Lardenois, A., Thibault, C., Weber, C., Merienne, K., Mandel, J.L., Poch, O., Devys, D., Trottier, Y., 2006. Polyglutamine expansion causes neurodegeneration by altering the neuronal differentiation program. Hum Mol Genet 15, 691-703.
Adler, R., Canto-Soler, M.V., 2007. Molecular mechanisms of optic vesicle development: complexities, ambiguities and controversies. Dev Biol 305, 1-13.
Ajayi, A., Yu, X., Lindberg, S., Langel, U., Strom, A.L., 2012. Expanded ataxin-7 cause toxicity by inducing ROS production from NADPH oxidase complexes in a stable inducible Spinocerebellar ataxia type 7 (SCA7) model. BMC Neurosci 13, 86.
Ajayi, A., Yu, X., Wahlo-Svedin, C., Tsirigotaki, G., Karlstrom, V., Strom, A.L., 2015. Altered p53 and NOX1 activity cause bioenergetic defects in a SCA7 polyglutamine disease model. Biochim Biophys Acta 1847, 418-428.
Alcauter, S., Barrios, F.A., Diaz, R., Fernandez-Ruiz, J., 2011. Gray and white matter alterations in spinocerebellar ataxia type 7: an in vivo DTI and VBM study. Neuroimage 55, 1-7.
Aleman, T.S., Cideciyan, A.V., Volpe, N.J., Stevanin, G., Brice, A., Jacobson, S.G., 2002. Spinocerebellar ataxia type 7 (SCA7) shows a cone-rod dystrophy phenotype. Exp Eye Res 74, 737-745.
Almeida, A.D., Boije, H., Chow, R.W., He, J., Tham, J., Suzuki, S.C., Harris, W.A., 2014. Spectrum of Fates: a new approach to the study of the developing zebrafish retina. Development 141, 1971-1980.
Amato, M.A., Boy, S., Perron, M., 2004. Hedgehog signaling in vertebrate eye development: a growing puzzle. Cell Mol Life Sci 61, 899-910.
Amberger, J.S., Bocchini, C.A., Schiettecatte, F., Scott, A.F., Hamosh, A., 2015. OMIM.org: Online Mendelian Inheritance in Man (OMIM(R)), an online catalog of human genes and genetic disorders. Nucleic Acids Res 43, D789-798.
Ambrose, C.M., Duyao, M.P., Barnes, G., Bates, G.P., Lin, C.S., Srinidhi, J., Baxendale, S., Hummerich, H., Lehrach, H., Altherr, M., et al., 1994. Structure and expression of the Huntington's disease gene: evidence against simple inactivation due to an expanded CAG repeat. Somat Cell Mol Genet 20, 27-38.
Ansorge, O., Giunti, P., Michalik, A., Van Broeckhoven, C., Harding, B., Wood, N., Scaravilli, F., 2004. Ataxin-7 aggregation and ubiquitination in infantile SCA7 with 180 CAG repeats. Ann Neurol 56, 448-452.
Armakolas, A., Stathopoulos, G.P., Nezos, A., Theos, A., Stathaki, M., Koutsilieris, M., 2012. Subdivision of molecularly-classified groups by new gene signatures in breast cancer patients. Oncol Rep 28, 2255-2263.
Arteaga-Bracho, E.E., Gulinello, M., Winchester, M.L., Pichamoorthy, N., Petronglo, J.R., Zambrano, A.D., Inocencio, J., De Jesus, C.D., Louie, J.O., Gokhan, S., Mehler, M.F., Molero, A.E., 2016. Postnatal and adult consequences of loss of huntingtin during development: Implications for Huntington's disease. Neurobiol Dis 96, 144-155.
Atanassov, B.S., Evrard, Y.A., Multani, A.S., Zhang, Z., Tora, L., Devys, D., Chang, S., Dent, S.Y., 2009. Gcn5 and SAGA regulate shelterin protein turnover and telomere maintenance. Mol Cell 35, 352-364.
Auerbach, W., Hurlbert, M.S., Hilditch-Maguire, P., Wadghiri, Y.Z., Wheeler, V.C., Cohen, S.I., Joyner, A.L., MacDonald, M.E., Turnbull, D.H., 2001. The HD mutation causes progressive lethal neurological disease in mice expressing reduced levels of huntingtin. Hum Mol Genet 10, 2515-2523.
Azuma, N., Yamaguchi, Y., Handa, H., Tadokoro, K., Asaka, A., Kawase, E., Yamada, M., 2003. Mutations of the PAX6 gene detected in patients with a variety of optic-nerve malformations. Am J Hum Genet 72, 1565-1570.

Bang, O.Y., Lee, P.H., Kim, S.Y., Kim, H.J., Huh, K., 2004. Pontine atrophy precedes cerebellar degeneration in spinocerebellar ataxia 7: MRI-based volumetric analysis. J Neurol Neurosurg Psychiatry 75, 1452-1456.
Barnat, M., Le Friec, J., Benstaali, C., Humbert, S., 2017. Huntingtin-Mediated Multipolar-Bipolar Transition of Newborn Cortical Neurons Is Critical for Their Postnatal Neuronal Morphology. Neuron 93, 99-114.
Baumer, N., Marquardt, T., Stoykova, A., Spieler, D., Treichel, D., Ashery-Padan, R., Gruss, P., 2003. Retinal pigmented epithelium determination requires the redundant activities of Pax2 and Pax6. Development 130, 2903-2915.
Bazin-Lopez, N., Valdivia, L.E., Wilson, S.W., Gestri, G., 2015. Watching eyes take shape. Curr Opin Genet Dev 32, 73-79.
Beauchemin, A.M., Gottlieb, B., Beitel, L.K., Elhaji, Y.A., Pinsky, L., Trifiro, M.A., 2001. Cytochrome c oxidase subunit Vb interacts with human androgen receptor: a potential mechanism for neurotoxicity in spinobulbar muscular atrophy. Brain Res Bull 56, 285-297.
Beitel, L.K., Alvarado, C., Mokhtar, S., Paliouras, M., Trifiro, M., 2013. Mechanisms mediating spinal and bulbar muscular atrophy: investigations into polyglutamine-expanded androgen receptor function and dysfunction. Front Neurol 4, 53.
Benton, C.S., de Silva, R., Rutledge, S.L., Bohlega, S., Ashizawa, T., Zoghbi, H.Y., 1998. Molecular and clinical studies in SCA-7 define a broad clinical spectrum and the infantile phenotype. Neurology 51, 1081-1086.
Bhaumik, S.R., 2011. Distinct regulatory mechanisms of eukaryotic transcriptional activation by SAGA and TFIID. Biochim Biophys Acta 1809, 97-108.
Bibliowicz, J., Tittle, R.K., Gross, J.M., 2011. Chapter 7 - Toward a Better Understanding of Human Eye Disease: Insights From the Zebrafish, Danio rerio, in: Chang, K.T., Min, K.-T. (Eds.), Progress in Molecular Biology and Translational Science. Academic Press, pp. 287-330.
Bonnet, J., Wang, C.Y., Baptista, T., Vincent, S.D., Hsiao, W.C., Stierle, M., Kao, C.F., Tora, L., Devys, D., 2014. The SAGA coactivator complex acts on the whole transcribed genome and is required for RNA polymerase II transcription. Genes Dev 28, 1999-2012.
Branchek, T., 1984. The development of photoreceptors in the zebrafish, brachydanio rerio. II. Function. J Comp Neurol 224, 116-122.
Brand, M., Moggs, J.G., Oulad-Abdelghani, M., Lejeune, F., Dilworth, F.J., Stevenin, J., Almouzni, G., Tora, L., 2001. UV-damaged DNA-binding protein in the TFTC complex links DNA damage recognition to nucleosome acetylation. EMBO J 20, 3187-3196.
Briscoe, J., Therond, P.P., 2013. The mechanisms of Hedgehog signalling and its roles in development and disease. Nat Rev Mol Cell Biol 14, 416-429.
Bu, P., Evrard, Y.A., Lozano, G., Dent, S.Y., 2007. Loss of Gcn5 acetyltransferase activity leads to neural tube closure defects and exencephaly in mouse embryos. Mol Cell Biol 27, 3405-3416.
Burrill, J.D., Easter, S.S., Jr., 1995. The first retinal axons and their microenvironment in zebrafish: cryptic pioneers and the pretract. J Neurosci 15, 2935-2947.
Carre, C., Szymczak, D., Pidoux, J., Antoniewski, C., 2005. The histone H3 acetylase dGcn5 is a key player in Drosophila melanogaster metamorphosis. Mol Cell Biol 25, 8228-8238.
Cattaneo, E., Rigamonti, D., Goffredo, D., Zuccato, C., Squitieri, F., Sipione, S., 2001. Loss of normal huntingtin function: new developments in Huntington's disease research. Trends Neurosci 24, 182-188.
Cattaneo, E., Zuccato, C., Tartari, M., 2005. Normal huntingtin function: an alternative approach to Huntington's disease. Nat Rev Neurosci 6, 919-930.
Chen, H.K., Fernandez-Funez, P., Acevedo, S.F., Lam, Y.C., Kaytor, M.D., Fernandez, M.H., Aitken, A., Skoulakis, E.M., Orr, H.T., Botas, J., Zoghbi, H.Y., 2003. Interaction of Akt-phosphorylated ataxin-1 with 14-3-3 mediates neurodegeneration in spinocerebellar ataxia type 1. Cell 113, 457-468.
Chen, J.K., Taipale, J., Cooper, M.K., Beachy, P.A., 2002. Inhibition of Hedgehog signaling by direct binding of cyclopamine to Smoothened. Genes Dev 16, 2743-2748.

Chen, L., Wei, T., Si, X., Wang, Q., Li, Y., Leng, Y., Deng, A., Chen, J., Wang, G., Zhu, S., Kang, J., 2013. Lysine acetyltransferase GCN5 potentiates the growth of non-small cell lung cancer via promotion of E2F1, cyclin D1, and cyclin E1 expression. J Biol Chem 288, 14510-14521.
Chen, S., Peng, G.H., Wang, X., Smith, A.C., Grote, S.K., Sopher, B.L., La Spada, A.R., 2004. Interference of Crx-dependent transcription by ataxin-7 involves interaction between the glutamine regions and requires the ataxin-7 carboxy-terminal region for nuclear localization. Hum Mol Genet 13, 53-67.
Chen, Y.C., Gatchel, J.R., Lewis, R.W., Mao, C.A., Grant, P.A., Zoghbi, H.Y., Dent, S.Y., 2012. Gcn5 loss-of-function accelerates cerebellar and retinal degeneration in a SCA7 mouse model. Hum Mol Genet 21, 394-405.
Chhetri, J., Jacobson, G., Gueven, N., 2014. Zebrafish--on the move towards ophthalmological research. Eye (Lond) 28, 367-380.
Chiang, C., Litingtung, Y., Lee, E., Young, K.E., Corden, J.L., Westphal, H., Beachy, P.A., 1996. Cyclopia and defective axial patterning in mice lacking Sonic hedgehog gene function. Nature 383, 407-413.
Chien, Y.H., Huang, H.P., Hwu, W.L., Chien, Y.H., Chang, T.C., Lee, N.C., 2009. Eye anomalies and neurological manifestations in patients with PAX6 mutations. Mol Vis 15, 2139-2145.
Chou, A.H., Chen, C.Y., Chen, S.Y., Chen, W.J., Chen, Y.L., Weng, Y.S., Wang, H.L., 2010. Polyglutamine-expanded ataxin-7 causes cerebellar dysfunction by inducing transcriptional dysregulation. Neurochem Int 56, 329-339.
Chow, R.L., Lang, R.A., 2001. Early eye development in vertebrates. Annu Rev Cell Dev Biol 17, 255-296.
Choy, S.W., Cheng, S.H., 2012. Hedgehog signaling. Vitam Horm 88, 1-23.
Chuang, J.C., Raymond, P.A., 2002. Embryonic origin of the eyes in teleost fish. Bioessays 24, 519-529.
Cooper, M.K., Porter, J.A., Young, K.E., Beachy, P.A., 1998. Teratogen-mediated inhibition of target tissue response to Shh signaling. Science 280, 1603-1607.
Coutinho, P., Pavlou, S., Bhatia, S., Chalmers, K.J., Kleinjan, D.A., van Heyningen, V., 2011. Discovery and assessment of conserved Pax6 target genes and enhancers. Genome Res 21, 1349-1359.
Crespo-Barreto, J., Fryer, J.D., Shaw, C.A., Orr, H.T., Zoghbi, H.Y., 2010. Partial loss of ataxin-1 function contributes to transcriptional dysregulation in spinocerebellar ataxia type 1 pathogenesis. PLoS Genet 6, e1001021.
Currie, P.D., Ingham, P.W., 1996. Induction of a specific muscle cell type by a hedgehog-like protein in zebrafish. Nature 382, 452-455.
Custer, S.K., Garden, G.A., Gill, N., Rueb, U., Libby, R.T., Schultz, C., Guyenet, S.J., Deller, T., Westrum, L.E., Sopher, B.L., La Spada, A.R., 2006. Bergmann glia expression of polyglutamine-expanded ataxin-7 produces neurodegeneration by impairing glutamate transport. Nat Neurosci 9, 1302-1311.
Dahmane, N., Ruiz i Altaba, A., 1999. Sonic hedgehog regulates the growth and patterning of the cerebellum. Development 126, 3089-3100.
David, G., Abbas, N., Stevanin, G., Durr, A., Yvert, G., Cancel, G., Weber, C., Imbert, G., Saudou, F., Antoniou, E., Drabkin, H., Gemmill, R., Giunti, P., Benomar, A., Wood, N., Ruberg, M., Agid, Y., Mandel, J.L., Brice, A., 1997. Cloning of the SCA7 gene reveals a highly unstable CAG repeat expansion. Nature genetics 17, 65-70.
David, G., Durr, A., Stevanin, G., Cancel, G., Abbas, N., Benomar, A., Belal, S., Lebre, A.S., Abada-Bendib, M., Grid, D., Holmberg, M., Yahyaoui, M., Hentati, F., Chkili, T., Agid, Y., Brice, A., 1998. Molecular and clinical correlations in autosomal dominant cerebellar ataxia with progressive macular dystrophy (SCA7). Hum Mol Genet 7, 165-170.
Diekmann, H., Anichtchik, O., Fleming, A., Futter, M., Goldsmith, P., Roach, A., Rubinsztein, D.C., 2009. Decreased BDNF levels are a major contributor to the embryonic phenotype of huntingtin knockdown zebrafish. J Neurosci 29, 1343-1349.

Dragatsis, I., Efstratiadis, A., Zeitlin, S., 1998. Mouse mutant embryos lacking huntingtin are rescued from lethality by wild-type extraembryonic tissues. Development 125, 1529-1539.
Dragatsis, I., Levine, M.S., Zeitlin, S., 2000. Inactivation of Hdh in the brain and testis results in progressive neurodegeneration and sterility in mice. Nat Genet 26, 300-306.
Duenas, A.M., Goold, R., Giunti, P., 2006. Molecular pathogenesis of spinocerebellar ataxias. Brain 129, 1357-1370.
Duncan, C.E., An, M.C., Papanikolaou, T., Rugani, C., Vitelli, C., Ellerby, L.M., 2013. Histone deacetylase-3 interacts with ataxin-7 and is altered in a spinocerebellar ataxia type 7 mouse model. Mol Neurodegener 8, 42.
Duyao, M.P., Auerbach, A.B., Ryan, A., Persichetti, F., Barnes, G.T., McNeil, S.M., Ge, P., Vonsattel, J.P., Gusella, J.F., Joyner, A.L., et al., 1995. Inactivation of the mouse Huntington's disease gene homolog Hdh. Science 269, 407-410.
Eccles, M.R., Schimmenti, L.A., 1999. Renal-coloboma syndrome: a multi-system developmental disorder caused by PAX2 mutations. Clin Genet 56, 1-9.
Einum, D.D., Townsend, J.J., Ptacek, L.J., Fu, Y.H., 2001. Ataxin-7 expression analysis in controls and spinocerebellar ataxia type 7 patients. Neurogenetics 3, 83-90.
Ekker, S.C., Ungar, A.R., Greenstein, P., von Kessler, D.P., Porter, J.A., Moon, R.T., Beachy, P.A., 1995. Patterning activities of vertebrate hedgehog proteins in the developing eye and brain. Curr Biol 5, 944-955.
Emamian, E.S., Kaytor, M.D., Duvick, L.A., Zu, T., Tousey, S.K., Zoghbi, H.Y., Clark, H.B., Orr, H.T., 2003. Serine 776 of ataxin-1 is critical for polyglutamine-induced disease in SCA1 transgenic mice. Neuron 38, 375-387.
Enevoldson, T.P., Sanders, M.D., Harding, A.E., 1994. Autosomal dominant cerebellar ataxia with pigmentary macular dystrophy. A clinical and genetic study of eight families. Brain 117 (Pt 3), 445-460.
Engelen, E., Akinci, U., Bryne, J.C., Hou, J., Gontan, C., Moen, M., Szumska, D., Kockx, C., van Ijcken, W., Dekkers, D.H., Demmers, J., Rijkers, E.J., Bhattacharya, S., Philipsen, S., Pevny, L.H., Grosveld, F.G., Rottier, R.J., Lenhard, B., Poot, R.A., 2011. Sox2 cooperates with Chd7 to regulate genes that are mutated in human syndromes. Nat Genet 43, 607-611.
Fadool, J.M., 2003. Development of a rod photoreceptor mosaic revealed in transgenic zebrafish. Dev Biol 258, 277-290.
Ferreiro, J.A., Powell, N.G., Karabetsou, N., Mellor, J., Waters, R., 2006. Roles for Gcn5p and Ada2p in transcription and nucleotide excision repair at the Saccharomyces cerevisiae MET16 gene. Nucleic Acids Res 34, 976-985.
Figiel, M., Szlachcic, W.J., Switonski, P.M., Gabka, A., Krzyzosiak, W.J., 2012. Mouse models of polyglutamine diseases: review and data table. Part I. Mol Neurobiol 46, 393-429.
Forsgren, L., Libelius, R., Holmberg, M., von Dobeln, U., Wibom, R., Heijbel, J., Sandgren, O., Holmgren, G., 1996. Muscle morphology and mitochondrial investigations of a family with autosomal dominant cerebellar ataxia and retinal degeneration mapped to chromosome 3p12-p21.1. J Neurol Sci 144, 91-98.
Fournier, M., Orpinell, M., Grauffel, C., Scheer, E., Garnier, J.M., Ye, T., Chavant, V., Joint, M., Esashi, F., Dejaegere, A., Gonczy, P., Tora, L., 2016. KAT2A/KAT2B-targeted acetylome reveals a role for PLK4 acetylation in preventing centrosome amplification. Nat Commun 7, 13227.
Fryer, J.D., Yu, P., Kang, H., Mandel-Brehm, C., Carter, A.N., Crespo-Barreto, J., Gao, Y., Flora, A., Shaw, C., Orr, H.T., Zoghbi, H.Y., 2011. Exercise and genetic rescue of SCA1 via the transcriptional repressor Capicua. Science 334, 690-693.
Fuhrmann, S., 2010. Eye morphogenesis and patterning of the optic vesicle. Curr Top Dev Biol 93, 61-84.
Furrer, S.A., Mohanachandran, M.S., Waldherr, S.M., Chang, C., Damian, V.A., Sopher, B.L., Garden, G.A., La Spada, A.R., 2011. Spinocerebellar ataxia type 7 cerebellar disease requires the coordinated action of mutant ataxin-7 in neurons and glia, and displays non-cell-autonomous bergmann glia degeneration. J Neurosci 31, 16269-16278.
Furukawa, T., Morrow, E.M., Li, T., Davis, F.C., Cepko, C.L., 1999. Retinopathy and attenuated circadian entrainment in Crx-deficient mice. Nat Genet 23, 466-470.

Garden, G.A., Libby, R.T., Fu, Y.H., Kinoshita, Y., Huang, J., Possin, D.E., Smith, A.C., Martinez, R.A., Fine, G.C., Grote, S.K., Ware, C.B., Einum, D.D., Morrison, R.S., Ptacek, L.J., Sopher, B.L., La Spada, A.R., 2002. Polyglutamine-expanded ataxin-7 promotes non-cell-autonomous purkinje cell degeneration and displays proteolytic cleavage in ataxic transgenic mice. J Neurosci 22, 4897-4905.

Gause, M., Eissenberg, J.C., Macrae, A.F., Dorsett, M., Misulovin, Z., Dorsett, D., 2006. Nipped-A, the Tra1/TRRAP subunit of the Drosophila SAGA and Tip60 complexes, has multiple roles in Notch signaling during wing development. Mol Cell Biol 26, 2347-2359.

Giunti, P., Stevanin, G., Worth, P.F., David, G., Brice, A., Wood, N.W., 1999. Molecular and clinical study of 18 families with ADCA type II: evidence for genetic heterogeneity and de novo mutation. Am J Hum Genet 64, 1594-1603.

Gongal, P.A., French, C.R., Waskiewicz, A.J., 2011. Aberrant forebrain signaling during early development underlies the generation of holoprosencephaly and coloboma. Biochim Biophys Acta 1812, 390-401.

Gotoh, M., Ichikawa, H., Arai, E., Chiku, S., Sakamoto, H., Fujimoto, H., Hiramoto, M., Nammo, T., Yasuda, K., Yoshida, T., Kanai, Y., 2014. Comprehensive exploration of novel chimeric transcripts in clear cell renal cell carcinomas using whole transcriptome analysis. Genes Chromosomes Cancer 53, 1018-1032.

Gouw, L.G., Digre, K.B., Harris, C.P., Haines, J.H., Ptacek, L.J., 1994. Autosomal dominant cerebellar ataxia with retinal degeneration: clinical, neuropathologic, and genetic analysis of a large kindred. Neurology 44, 1441-1447.

Gregory-Evans, C.Y., Moosajee, M., Shan, X., Gregory-Evans, K., 2011. Gene-specific differential response to anti-apoptotic therapies in zebrafish models of ocular coloboma. Mol Vis 17, 1473-1484.

Gregory-Evans, C.Y., Wallace, V.A., Gregory-Evans, K., 2013. Gene networks: dissecting pathways in retinal development and disease. Prog Retin Eye Res 33, 40-66.

Guo, R., Chen, J., Mitchell, D.L., Johnson, D.G., 2011. GCN5 and E2F1 stimulate nucleotide excision repair by promoting H3K9 acetylation at sites of damage. Nucleic Acids Res 39, 1390-1397.

Halbach, M.V., Gispert, S., Stehning, T., Damrath, E., Walter, M., Auburger, G., 2017. Atxn2 Knockout and CAG42-Knock-in Cerebellum Shows Similarly Dysregulated Expression in Calcium Homeostasis Pathway. Cerebellum 16, 68-81.

Hamel, C.P., 2007. Cone rod dystrophies. Orphanet J Rare Dis 2, 7.

Hammerschmidt, M., Bitgood, M.J., McMahon, A.P., 1996. Protein kinase A is a common negative regulator of Hedgehog signaling in the vertebrate embryo. Genes Dev 10, 647-658.

Harding, A.E., 1982. The clinical features and classification of the late onset autosomal dominant cerebellar ataxias. A study of 11 families, including descendants of the 'the Drew family of Walworth'. Brain 105, 1-28.

Harding, A.E., 1993. Clinical features and classification of inherited ataxias. Adv Neurol 61, 1-14.

He, X.H., Lin, F., Qin, Z.H., 2010. Current understanding on the pathogenesis of polyglutamine diseases. Neurosci Bull 26, 247-256.

Helmlinger, D., Abou-Sleymane, G., Yvert, G., Rousseau, S., Weber, C., Trottier, Y., Mandel, J.L., Devys, D., 2004a. Disease progression despite early loss of polyglutamine protein expression in SCA7 mouse model. The Journal of neuroscience : the official journal of the Society for Neuroscience 24, 1881-1887.

Helmlinger, D., Hardy, S., Abou-Sleymane, G., Eberlin, A., Bowman, A.B., Gansmuller, A., Picaud, S., Zoghbi, H.Y., Trottier, Y., Tora, L., Devys, D., 2006. Glutamine-expanded ataxin-7 alters TFTC/STAGA recruitment and chromatin structure leading to photoreceptor dysfunction. PLoS Biol 4, e67.

Helmlinger, D., Hardy, S., Sasorith, S., Klein, F., Robert, F., Weber, C., Miguet, L., Potier, N., Van-Dorsselaer, A., Wurtz, J.M., Mandel, J.L., Tora, L., Devys, D., 2004b. Ataxin-7 is a subunit of GCN5 histone acetyltransferase-containing complexes. Hum Mol Genet 13, 1257-1265.

Henshall, T.L., Tucker, B., Lumsden, A.L., Nornes, S., Lardelli, M.T., Richards, R.I., 2009. Selective neuronal requirement for huntingtin in the developing zebrafish. Hum Mol Genet 18, 4830-4842.
Hernandez-Bejarano, M., Gestri, G., Spawls, L., Nieto-Lopez, F., Picker, A., Tada, M., Brand, M., Bovolenta, P., Wilson, S.W., Cavodeassi, F., 2015. Opposing Shh and Fgf signals initiate nasotemporal patterning of the zebrafish retina. Development 142, 3933-3942.
Hitchcock, P.F., Raymond, P.A., 2004. The teleost retina as a model for developmental and regeneration biology. Zebrafish 1, 257-271.
Hoche, F., Seidel, K., Brunt, E.R., Auburger, G., Schols, L., Burk, K., de Vos, R.A., den Dunnen, W., Bechmann, I., Egensperger, R., Van Broeckhoven, C., Gierga, K., Deller, T., Rub, U., 2008. Involvement of the auditory brainstem system in spinocerebellar ataxia type 2 (SCA2), type 3 (SCA3) and type 7 (SCA7). Neuropathol Appl Neurobiol 34, 479-491.
Horton, L.C., Frosch, M.P., Vangel, M.G., Weigel-DiFranco, C., Berson, E.L., Schmahmann, J.D., 2013. Spinocerebellar ataxia type 7: clinical course, phenotype-genotype correlations, and neuropathology. Cerebellum 12, 176-193.
Housman, D., 1995. Gain of glutamines, gain of function? Nat Genet 10, 3-4.
Howe, K., Clark, M.D., Torroja, C.F., Torrance, J., Berthelot, C., Muffato, M., Collins, J.E., Humphray, S., McLaren, K., Matthews, L., McLaren, S., Sealy, I., Caccamo, M., Churcher, C., Scott, C., Barrett, J.C., Koch, R., Rauch, G.J., White, S., Chow, W., Kilian, B., Quintais, L.T., Guerra-Assuncao, J.A., Zhou, Y., Gu, Y., Yen, J., Vogel, J.H., Eyre, T., Redmond, S., Banerjee, R., Chi, J., Fu, B., Langley, E., Maguire, S.F., Laird, G.K., Lloyd, D., Kenyon, E., Donaldson, S., Sehra, H., Almeida-King, J., Loveland, J., Trevanion, S., Jones, M., Quail, M., Willey, D., Hunt, A., Burton, J., Sims, S., McLay, K., Plumb, B., Davis, J., Clee, C., Oliver, K., Clark, R., Riddle, C., Elliot, D., Threadgold, G., Harden, G., Ware, D., Begum, S., Mortimore, B., Kerry, G., Heath, P., Phillimore, B., Tracey, A., Corby, N., Dunn, M., Johnson, C., Wood, J., Clark, S., Pelan, S., Griffiths, G., Smith, M., Glithero, R., Howden, P., Barker, N., Lloyd, C., Stevens, C., Harley, J., Holt, K., Panagiotidis, G., Lovell, J., Beasley, H., Henderson, C., Gordon, D., Auger, K., Wright, D., Collins, J., Raisen, C., Dyer, L., Leung, K., Robertson, L., Ambridge, K., Leongamornlert, D., McGuire, S., Gilderthorp, R., Griffiths, C., Manthravadi, D., Nichol, S., Barker, G., Whitehead, S., Kay, M., Brown, J., Murnane, C., Gray, E., Humphries, M., Sycamore, N., Barker, D., Saunders, D., Wallis, J., Babbage, A., Hammond, S., Mashreghi-Mohammadi, M., Barr, L., Martin, S., Wray, P., Ellington, A., Matthews, N., Ellwood, M., Woodmansey, R., Clark, G., Cooper, J., Tromans, A., Grafham, D., Skuce, C., Pandian, R., Andrews, R., Harrison, E., Kimberley, A., Garnett, J., Fosker, N., Hall, R., Garner, P., Kelly, D., Bird, C., Palmer, S., Gehring, I., Berger, A., Dooley, C.M., Ersan-Urun, Z., Eser, C., Geiger, H., Geisler, M., Karotki, L., Kirn, A., Konantz, J., Konantz, M., Oberlander, M., Rudolph-Geiger, S., Teucke, M., Lanz, C., Raddatz, G., Osoegawa, K., Zhu, B., Rapp, A., Widaa, S., Langford, C., Yang, F., Schuster, S.C., Carter, N.P., Harrow, J., Ning, Z., Herrero, J., Searle, S.M., Enright, A., Geisler, R., Plasterk, R.H., Lee, C., Westerfield, M., de Jong, P.J., Zon, L.I., Postlethwait, J.H., Nusslein-Volhard, C., Hubbard, T.J., Roest Crollius, H., Rogers, J., Stemple, D.L., 2013. The zebrafish reference genome sequence and its relationship to the human genome. Nature 496, 498-503.
Hruscha, A., Krawitz, P., Rechenberg, A., Heinrich, V., Hecht, J., Haass, C., Schmid, B., 2013. Efficient CRISPR/Cas9 genome editing with low off-target effects in zebrafish. Development 140, 4982-4987.
Hu, M., Easter, S.S., 1999. Retinal neurogenesis: the formation of the initial central patch of postmitotic cells. Dev Biol 207, 309-321.
Huang, P., Zhu, Z., Lin, S., Zhang, B., 2012. Reverse genetic approaches in zebrafish. J Genet Genomics 39, 421-433.
Hwang, W.Y., Fu, Y., Reyon, D., Maeder, M.L., Tsai, S.Q., Sander, J.D., Peterson, R.T., Yeh, J.R., Joung, J.K., 2013. Efficient genome editing in zebrafish using a CRISPR-Cas system. Nat Biotechnol 31, 227-229.
Incardona, J.P., Gaffield, W., Kapur, R.P., Roelink, H., 1998. The teratogenic Veratrum alkaloid cyclopamine inhibits sonic hedgehog signal transduction. Development 125, 3553-3562.

James, A., Lee, C., Williams, A.M., Angileri, K., Lathrop, K.L., Gross, J.M., 2016. The hyaloid vasculature facilitates basement membrane breakdown during choroid fissure closure in the zebrafish eye. Dev Biol 419, 262-272.
Janer, A., Werner, A., Takahashi-Fujigasaki, J., Daret, A., Fujigasaki, H., Takada, K., Duyckaerts, C., Brice, A., Dejean, A., Sittler, A., 2010. SUMOylation attenuates the aggregation propensity and cellular toxicity of the polyglutamine expanded ataxin-7. Hum Mol Genet 19, 181-195.
Jao, L.E., Wente, S.R., Chen, W., 2013. Efficient multiplex biallelic zebrafish genome editing using a CRISPR nuclease system. Proc Natl Acad Sci U S A 110, 13904-13909.
Jayabal, S., Ljungberg, L., Watt, A.J., 2017. Transient cerebellar alterations during development prior to obvious motor phenotype in a mouse model of spinocerebellar ataxia type 6. J Physiol 595, 949-966.
Karlstrom, R.O., Talbot, W.S., Schier, A.F., 1999. Comparative synteny cloning of zebrafish you-too: mutations in the Hedgehog target gli2 affect ventral forebrain patterning. Genes Dev 13, 388-393.
Karlstrom, R.O., Tyurina, O.V., Kawakami, A., Nishioka, N., Talbot, W.S., Sasaki, H., Schier, A.F., 2003. Genetic analysis of zebrafish gli1 and gli2 reveals divergent requirements for gli genes in vertebrate development. Development 130, 1549-1564.
Kay, J.N., Finger-Baier, K.C., Roeser, T., Staub, W., Baier, H., 2001. Retinal ganglion cell genesis requires lakritz, a Zebrafish atonal Homolog. Neuron 30, 725-736.
Kay, J.N., Link, B.A., Baier, H., 2005. Staggered cell-intrinsic timing of ath5 expression underlies the wave of ganglion cell neurogenesis in the zebrafish retina. Development 132, 2573-2585.
Kaytor, M.D., Duvick, L.A., Skinner, P.J., Koob, M.D., Ranum, L.P., Orr, H.T., 1999. Nuclear localization of the spinocerebellar ataxia type 7 protein, ataxin-7. Hum Mol Genet 8, 1657-1664.
Kiehl, T.R., Nechiporuk, A., Figueroa, K.P., Keating, M.T., Huynh, D.P., Pulst, S.M., 2006. Generation and characterization of Sca2 (ataxin-2) knockout mice. Biochem Biophys Res Commun 339, 17-24.
Kiehl, T.R., Shibata, H., Pulst, S.M., 2000. The ortholog of human ataxin-2 is essential for early embryonic patterning in C. elegans. J Mol Neurosci 15, 231-241.
Kim, S.U., Takahashi, H., 1988. Tissue culture study of adult human retina neurons. Invest Ophthalmol Vis Sci 29, 1372-1379.
Kim, T.H., Goodman, J., Anderson, K.V., Niswander, L., 2007. Phactr4 regulates neural tube and optic fissure closure by controlling PP1-, Rb-, and E2F1-regulated cell-cycle progression. Dev Cell 13, 87-102.
Kimmel, C.B., Ballard, W.W., Kimmel, S.R., Ullmann, B., Schilling, T.F., 1995. Stages of embryonic development of the zebrafish. Dev Dyn 203, 253-310.
Kizilyaprak, C., Spehner, D., Devys, D., Schultz, P., 2011. The linker histone H1C contributes to the SCA7 nuclear phenotype. Nucleus 2, 444-454.
Kohler, A., Schneider, M., Cabal, G.G., Nehrbass, U., Hurt, E., 2008. Yeast Ataxin-7 links histone deubiquitination with gene gating and mRNA export. Nat Cell Biol 10, 707-715.
Koudijs, M.J., den Broeder, M.J., Groot, E., van Eeden, F.J., 2008. Genetic analysis of the two zebrafish patched homologues identifies novel roles for the hedgehog signaling pathway. BMC Dev Biol 8, 15.
Koudijs, M.J., den Broeder, M.J., Keijser, A., Wienholds, E., Houwing, S., van Rooijen, E.M., Geisler, R., van Eeden, F.J., 2005. The zebrafish mutants dre, uki, and lep encode negative regulators of the hedgehog signaling pathway. PLoS Genet 1, e19.
Koutelou, E., Hirsch, C.L., Dent, S.Y., 2010. Multiple faces of the SAGA complex. Curr Opin Cell Biol 22, 374-382.
Krauss, S., Concordet, J.P., Ingham, P.W., 1993. A functionally conserved homolog of the Drosophila segment polarity gene hh is expressed in tissues with polarizing activity in zebrafish embryos. Cell 75, 1431-1444.
La Spada, A.R., Fu, Y.H., Sopher, B.L., Libby, R.T., Wang, X., Li, L.Y., Einum, D.D., Huang, J., Possin, D.E., Smith, A.C., Martinez, R.A., Koszdin, K.L., Treuting, P.M., Ware, C.B., Hurley,

J.B., Ptacek, L.J., Chen, S., 2001. Polyglutamine-expanded ataxin-7 antagonizes CRX function and induces cone-rod dystrophy in a mouse model of SCA7. Neuron 31, 913-927.
Labun, K., Montague, T.G., Gagnon, J.A., Thyme, S.B., Valen, E., 2016. CHOPCHOP v2: a web tool for the next generation of CRISPR genome engineering. Nucleic Acids Res 44, W272-276.
Lan, X., Koutelou, E., Schibler, A.C., Chen, Y.C., Grant, P.A., Dent, S.Y., 2015. Poly(Q) Expansions in ATXN7 Affect Solubility but Not Activity of the SAGA Deubiquitinating Module. Mol Cell Biol 35, 1777-1787.
Landsman, L., Parent, A., Hebrok, M., 2011. Elevated Hedgehog/Gli signaling causes beta-cell dedifferentiation in mice. Proc Natl Acad Sci U S A 108, 17010-17015.
Lane, B.M., Lister, J.A., 2012. Otx but not Mitf transcription factors are required for zebrafish retinal pigment epithelium development. PLoS One 7, e49357.
Leavitt, B.R., Guttman, J.A., Hodgson, J.G., Kimel, G.H., Singaraja, R., Vogl, A.W., Hayden, M.R., 2001. Wild-type huntingtin reduces the cellular toxicity of mutant huntingtin in vivo. Am J Hum Genet 68, 313-324.
Lebre, A.S., Jamot, L., Takahashi, J., Spassky, N., Leprince, C., Ravise, N., Zander, C., Fujigasaki, H., Kussel-Andermann, P., Duyckaerts, C., Camonis, J.H., Brice, A., 2001. Ataxin-7 interacts with a Cbl-associated protein that it recruits into neuronal intranuclear inclusions. Hum Mol Genet 10, 1201-1213.
Lee, J., Willer, J.R., Willer, G.B., Smith, K., Gregg, R.G., Gross, J.M., 2008. Zebrafish blowout provides genetic evidence for Patched1-mediated negative regulation of Hedgehog signaling within the proximal optic vesicle of the vertebrate eye. Dev Biol 319, 10-22.
Lee, J.K., Mathews, K., Schlaggar, B., Perlmutter, J., Paulsen, J.S., Epping, E., Burmeister, L., Nopoulos, P., 2012. Measures of growth in children at risk for Huntington disease. Neurology 79, 668-674.
Lim, J., Crespo-Barreto, J., Jafar-Nejad, P., Bowman, A.B., Richman, R., Hill, D.E., Orr, H.T., Zoghbi, H.Y., 2008. Opposing effects of polyglutamine expansion on native protein complexes contribute to SCA1. Nature 452, 713-718.
Lin, W., Zhang, Z., Chen, C.H., Behringer, R.R., Dent, S.Y., 2008. Proper Gcn5 histone acetyltransferase expression is required for normal anteroposterior patterning of the mouse skeleton. Dev Growth Differ 50, 321-330.
Lin, Z., Yang, H., Kong, Q., Li, J., Lee, S.M., Gao, B., Dong, H., Wei, J., Song, J., Zhang, D.D., Fang, D., 2012. USP22 antagonizes p53 transcriptional activation by deubiquitinating Sirt1 to suppress cell apoptosis and is required for mouse embryonic development. Mol Cell 46, 484-494.
Link, B.A., Collery, R.F., 2015. Zebrafish Models of Retinal Disease. Annu Rev Vis Sci 1, 125-153.
Liu, H., Li, X., Ning, G., Zhu, S., Ma, X., Liu, X., Liu, C., Huang, M., Schmitt, I., Wullner, U., Niu, Y., Guo, C., Wang, Q., Tang, T.S., 2016. The Machado-Joseph Disease Deubiquitinase Ataxin-3 Regulates the Stability and Apoptotic Function of p53. PLoS Biol 14, e2000733.
London, N.J., Kessler, P., Williams, B., Pauer, G.J., Hagstrom, S.A., Traboulsi, E.I., 2009. Sequence alterations in RX in patients with microphthalmia, anophthalmia, and coloboma. Mol Vis 15, 162-167.
Lumsden, A.L., Henshall, T.L., Dayan, S., Lardelli, M.T., Richards, R.I., 2007. Huntingtin-deficient zebrafish exhibit defects in iron utilization and development. Hum Mol Genet 16, 1905-1920.
Luo, Y., Fan, Y., Zhou, B., Xu, Z., Chen, Y., Sun, X., 2012. Generation of induced pluripotent stem cells from skin fibroblasts of a patient with olivopontocerebellar atrophy. Tohoku J Exp Med 226, 151-159.
Lupo, G., Gestri, G., O'Brien, M., Denton, R.M., Chandraratna, R.A., Ley, S.V., Harris, W.A., Wilson, S.W., 2011. Retinoic acid receptor signaling regulates choroid fissure closure through independent mechanisms in the ventral optic cup and periocular mesenchyme. Proc Natl Acad Sci U S A 108, 8698-8703.

Ma, J., Brennan, K.J., D'Aloia, M.R., Pascuzzi, P.E., Weake, V.M., 2016. Transcriptome Profiling Identifies Multiplexin as a Target of SAGA Deubiquitinase Activity in Glia Required for Precise Axon Guidance During Drosophila Visual Development. G3 (Bethesda) 6, 2435-2445.
Macdonald, R., Barth, K.A., Xu, Q., Holder, N., Mikkola, I., Wilson, S.W., 1995. Midline signalling is required for Pax gene regulation and patterning of the eyes. Development 121, 3267-3278.
Macdonald, R., Scholes, J., Strahle, U., Brennan, C., Holder, N., Brand, M., Wilson, S.W., 1997. The Pax protein Noi is required for commissural axon pathway formation in the rostral forebrain. Development 124, 2397-2408.
Majaz, S., Tong, Z., Peng, K., Wang, W., Ren, W., Li, M., Liu, K., Mo, P., Li, W., Yu, C., 2016. Histone acetyl transferase GCN5 promotes human hepatocellular carcinoma progression by enhancing AIB1 expression. Cell Biosci 6, 47.
Marc, R.E., Jones, B.W., 2003. Retinal remodeling in inherited photoreceptor degenerations. Molecular neurobiology 28, 139-147.
Marita, K.G., 2011. Human cadaveric retinal cultures: an experimental tool for retinal regeneration. J Ophthalmic Vis Res 6, 69-72.
Marsh, J.L., Walker, H., Theisen, H., Zhu, Y.Z., Fielder, T., Purcell, J., Thompson, L.M., 2000. Expanded polyglutamine peptides alone are intrinsically cytotoxic and cause neurodegeneration in Drosophila. Hum Mol Genet 9, 13-25.
Marti, E., Bovolenta, P., 2002. Sonic hedgehog in CNS development: one signal, multiple outputs. Trends Neurosci 25, 89-96.
Martin, J., Van Regemorter, N., Del-Favero, J., Lofgren, A., Van Broeckhoven, C., 1999. Spinocerebellar ataxia type 7 (SCA7) - correlations between phenotype and genotype in one large Belgian family. J Neurol Sci 168, 37-46.
Martin, J.J., 2012. Spinocerebellar ataxia type 7. Handb Clin Neurol 103, 475-491.
Martinez, E., Palhan, V.B., Tjernberg, A., Lymar, E.S., Gamper, A.M., Kundu, T.K., Chait, B.T., Roeder, R.G., 2001. Human STAGA complex is a chromatin-acetylating transcription coactivator that interacts with pre-mRNA splicing and DNA damage-binding factors in vivo. Mol Cell Biol 21, 6782-6795.
Masai, I., Stemple, D.L., Okamoto, H., Wilson, S.W., 2000. Midline signals regulate retinal neurogenesis in zebrafish. Neuron 27, 251-263.
Matilla-Duenas, A., 2012. The ever expanding spinocerebellar ataxias. Editorial. Cerebellum 11, 821-827.
Matilla-Duenas, A., Ashizawa, T., Brice, A., Magri, S., McFarland, K.N., Pandolfo, M., Pulst, S.M., Riess, O., Rubinsztein, D.C., Schmidt, J., Schmidt, T., Scoles, D.R., Stevanin, G., Taroni, F., Underwood, B.R., Sanchez, I., 2014. Consensus paper: pathological mechanisms underlying neurodegeneration in spinocerebellar ataxias. Cerebellum 13, 269-302.
Mayer, E.J., Carter, D.A., Ren, Y., Hughes, E.H., Rice, C.M., Halfpenny, C.A., Scolding, N.J., Dick, A.D., 2005. Neural progenitor cells from postmortem adult human retina. Br J Ophthalmol 89, 102-106.
McCullough, S.D., Xu, X., Dent, S.Y., Bekiranov, S., Roeder, R.G., Grant, P.A., 2012. Reelin is a target of polyglutamine expanded ataxin-7 in human spinocerebellar ataxia type 7 (SCA7) astrocytes. Proc Natl Acad Sci U S A 109, 21319-21324.
McMahon, S.J., Pray-Grant, M.G., Schieltz, D., Yates, J.R., 3rd, Grant, P.A., 2005. Polyglutamine-expanded spinocerebellar ataxia-7 protein disrupts normal SAGA and SLIK histone acetyltransferase activity. Proc Natl Acad Sci U S A 102, 8478-8482.
McWilliam, H., Li, W., Uludag, M., Squizzato, S., Park, Y.M., Buso, N., Cowley, A.P., Lopez, R., 2013. Analysis Tool Web Services from the EMBL-EBI. Nucleic Acids Res 41, W597-600.
Miao, N., Wang, M., Ott, J.A., D'Alessandro, J.S., Woolf, T.M., Bumcrot, D.A., Mahanthappa, N.K., Pang, K., 1997. Sonic hedgehog promotes the survival of specific CNS neuron populations and protects these cells from toxic insult In vitro. J Neurosci 17, 5891-5899.
Michalik, A., Martin, J.J., Van Broeckhoven, C., 2004. Spinocerebellar ataxia type 7 associated with pigmentary retinal dystrophy. Eur J Hum Genet 12, 2-15.
Milne, R.L., Burwinkel, B., Michailidou, K., Arias-Perez, J.I., Zamora, M.P., Menendez-Rodriguez, P., Hardisson, D., Mendiola, M., Gonzalez-Neira, A., Pita, G., Alonso, M.R.,

Dennis, J., Wang, Q., Bolla, M.K., Swerdlow, A., Ashworth, A., Orr, N., Schoemaker, M., Ko, Y.D., Brauch, H., Hamann, U., Network, G., Andrulis, I.L., Knight, J.A., Glendon, G., Tchatchou, S., kConFab, I., Australian Ovarian Cancer Study, G., Matsuo, K., Ito, H., Iwata, H., Tajima, K., Li, J., Brand, J.S., Brenner, H., Dieffenbach, A.K., Arndt, V., Stegmaier, C., Lambrechts, D., Peuteman, G., Christiaens, M.R., Smeets, A., Jakubowska, A., Lubinski, J., Jaworska-Bieniek, K., Durda, K., Hartman, M., Hui, M., Yen Lim, W., Wan Chan, C., Marme, F., Yang, R., Bugert, P., Lindblom, A., Margolin, S., Garcia-Closas, M., Chanock, S.J., Lissowska, J., Figueroa, J.D., Bojesen, S.E., Nordestgaard, B.G., Flyger, H., Hooning, M.J., Kriege, M., van den Ouweland, A.M., Koppert, L.B., Fletcher, O., Johnson, N., dos-Santos-Silva, I., Peto, J., Zheng, W., Deming-Halverson, S., Shrubsole, M.J., Long, J., Chang-Claude, J., Rudolph, A., Seibold, P., Flesch-Janys, D., Winqvist, R., Pylkas, K., Jukkola-Vuorinen, A., Grip, M., Cox, A., Cross, S.S., Reed, M.W., Schmidt, M.K., Broeks, A., Cornelissen, S., Braaf, L., Kang, D., Choi, J.Y., Park, S.K., Noh, D.Y., Simard, J., Dumont, M., Goldberg, M.S., Labreche, F., Fasching, P.A., Hein, A., Ekici, A.B., Beckmann, M.W., Radice, P., Peterlongo, P., Azzollini, J., Barile, M., Sawyer, E., Tomlinson, I., Kerin, M., Miller, N., Hopper, J.L., Schmidt, D.F., Makalic, E., Southey, M.C., Hwang Teo, S., Har Yip, C., Sivanandan, K., Tay, W.T., Shen, C.Y., Hsiung, C.N., Yu, J.C., Hou, M.F., Guenel, P., Truong, T., Sanchez, M., Mulot, C., Blot, W., Cai, Q., Nevanlinna, H., Muranen, T.A., Aittomaki, K., Blomqvist, C., Wu, A.H., Tseng, C.C., Van Den Berg, D., Stram, D.O., Bogdanova, N., Dork, T., Muir, K., Lophatananon, A., Stewart-Brown, S., Siriwanarangsan, P., Mannermaa, A., Kataja, V., Kosma, V.M., Hartikainen, J.M., Shu, X.O., Lu, W., Gao, Y.T., Zhang, B., Couch, F.J., Toland, A.E., Tnbcc, Yannoukakos, D., Sangrajrang, S., McKay, J., Wang, X., Olson, J.E., Vachon, C., Purrington, K., Severi, G., Baglietto, L., Haiman, C.A., Henderson, B.E., Schumacher, F., Le Marchand, L., Devilee, P., Tollenaar, R.A., Seynaeve, C., Czene, K., Eriksson, M., Humphreys, K., Darabi, H., Ahmed, S., Shah, M., Pharoah, P.D., Hall, P., Giles, G.G., Benitez, J., Dunning, A.M., Chenevix-Trench, G., Easton, D.F., 2014. Common non-synonymous SNPs associated with breast cancer susceptibility: findings from the Breast Cancer Association Consortium. Hum Mol Genet 23, 6096-6111.

Miyazaki, T., Hashimoto, K., Shin, H.S., Kano, M., Watanabe, M., 2004. P/Q-type Ca2+ channel alpha1A regulates synaptic competition on developing cerebellar Purkinje cells. J Neurosci 24, 1734-1743.

Mohan, R.D., Dialynas, G., Weake, V.M., Liu, J., Martin-Brown, S., Florens, L., Washburn, M.P., Workman, J.L., Abmayr, S.M., 2014. Loss of Drosophila Ataxin-7, a SAGA subunit, reduces H2B ubiquitination and leads to neural and retinal degeneration. Genes Dev 28, 259-272.

Mohibullah, N., Hahn, S., 2008. Site-specific cross-linking of TBP in vivo and in vitro reveals a direct functional interaction with the SAGA subunit Spt3. Genes Dev 22, 2994-3006.

Molero, A.E., Arteaga-Bracho, E.E., Chen, C.H., Gulinello, M., Winchester, M.L., Pichamoorthy, N., Gokhan, S., Khodakhah, K., Mehler, M.F., 2016. Selective expression of mutant huntingtin during development recapitulates characteristic features of Huntington's disease. Proc Natl Acad Sci U S A 113, 5736-5741.

Molina-Calavita, M., Barnat, M., Elias, S., Aparicio, E., Piel, M., Humbert, S., 2014. Mutant huntingtin affects cortical progenitor cell division and development of the mouse neocortex. J Neurosci 34, 10034-10040.

Morley, J.F., Brignull, H.R., Weyers, J.J., Morimoto, R.I., 2002. The threshold for polyglutamine-expansion protein aggregation and cellular toxicity is dynamic and influenced by aging in Caenorhabditis elegans. Proc Natl Acad Sci U S A 99, 10417-10422.

Muto, A., Orger, M.B., Wehman, A.M., Smear, M.C., Kay, J.N., Page-McCaw, P.S., Gahtan, E., Xiao, T., Nevin, L.M., Gosse, N.J., Staub, W., Finger-Baier, K., Baier, H., 2005. Forward genetic analysis of visual behavior in zebrafish. PLoS Genet 1, e66.

Nakamura, Y., Tagawa, K., Oka, T., Sasabe, T., Ito, H., Shiwaku, H., La Spada, A.R., Okazawa, H., 2012. Ataxin-7 associates with microtubules and stabilizes the cytoskeletal network. Hum Mol Genet 21, 1099-1110.

Nasir, J., Floresco, S.B., O'Kusky, J.R., Diewert, V.M., Richman, J.M., Zeisler, J., Borowski, A., Marth, J.D., Phillips, A.G., Hayden, M.R., 1995. Targeted disruption of the Huntington's

disease gene results in embryonic lethality and behavioral and morphological changes in heterozygotes. Cell 81, 811-823.
Neumann, C.J., Nuesslein-Volhard, C., 2000. Patterning of the zebrafish retina by a wave of sonic hedgehog activity. Science 289, 2137-2139.
Nishida, A., Furukawa, A., Koike, C., Tano, Y., Aizawa, S., Matsuo, I., Furukawa, T., 2003. Otx2 homeobox gene controls retinal photoreceptor cell fate and pineal gland development. Nat Neurosci 6, 1255-1263.
Nopoulos, P.C., Aylward, E.H., Ross, C.A., Mills, J.A., Langbehn, D.R., Johnson, H.J., Magnotta, V.A., Pierson, R.K., Beglinger, L.J., Nance, M.A., Barker, R.A., Paulsen, J.S., Investigators, P.-H., Coordinators of the Huntington Study, G., 2011. Smaller intracranial volume in prodromal Huntington's disease: evidence for abnormal neurodevelopment. Brain 134, 137-142.
Nuckels, R.J., Ng, A., Darland, T., Gross, J.M., 2009. The vacuolar-ATPase complex regulates retinoblast proliferation and survival, photoreceptor morphogenesis, and pigmentation in the zebrafish eye. Invest Ophthalmol Vis Sci 50, 893-905.
Nusslein-Volhard, C., Wieschaus, E., 1980. Mutations affecting segment number and polarity in Drosophila. Nature 287, 795-801.
O'Kusky, J.R., Nasir, J., Cicchetti, F., Parent, A., Hayden, M.R., 1999. Neuronal degeneration in the basal ganglia and loss of pallido-subthalamic synapses in mice with targeted disruption of the Huntington's disease gene. Brain Res 818, 468-479.
Ordway, J.M., Tallaksen-Greene, S., Gutekunst, C.A., Bernstein, E.M., Cearley, J.A., Wiener, H.W., Dure, L.S.t., Lindsey, R., Hersch, S.M., Jope, R.S., Albin, R.L., Detloff, P.J., 1997. Ectopically expressed CAG repeats cause intranuclear inclusions and a progressive late onset neurological phenotype in the mouse. Cell 91, 753-763.
Oron-Karni, V., Farhy, C., Elgart, M., Marquardt, T., Remizova, L., Yaron, O., Xie, Q., Cvekl, A., Ashery-Padan, R., 2008. Dual requirement for Pax6 in retinal progenitor cells. Development 135, 4037-4047.
Ota, S., Kawahara, A., 2014. Zebrafish: a model vertebrate suitable for the analysis of human genetic disorders. Congenit Anom (Kyoto) 54, 8-11.
Palhan, V.B., Chen, S., Peng, G.H., Tjernberg, A., Gamper, A.M., Fan, Y., Chait, B.T., La Spada, A.R., Roeder, R.G., 2005. Polyglutamine-expanded ataxin-7 inhibits STAGA histone acetyltransferase activity to produce retinal degeneration. Proc Natl Acad Sci U S A 102, 8472-8477.
Park, H.L., Bai, C., Platt, K.A., Matise, M.P., Beeghly, A., Hui, C.C., Nakashima, M., Joyner, A.L., 2000. Mouse Gli1 mutants are viable but have defects in SHH signaling in combination with a Gli2 mutation. Development 127, 1593-1605.
Patel, J.H., Du, Y., Ard, P.G., Phillips, C., Carella, B., Chen, C.J., Rakowski, C., Chatterjee, C., Lieberman, P.M., Lane, W.S., Blobel, G.A., McMahon, S.B., 2004. The c-MYC oncoprotein is a substrate of the acetyltransferases hGCN5/PCAF and TIP60. Mol Cell Biol 24, 10826-10834.
Perron, M., Boy, S., Amato, M.A., Viczian, A., Koebernick, K., Pieler, T., Harris, W.A., 2003. A novel function for Hedgehog signalling in retinal pigment epithelium differentiation. Development 130, 1565-1577.
Persichetti, F., Carlee, L., Faber, P.W., McNeil, S.M., Ambrose, C.M., Srinidhi, J., Anderson, M., Barnes, G.T., Gusella, J.F., MacDonald, M.E., 1996. Differential expression of normal and mutant Huntington's disease gene alleles. Neurobiol Dis 3, 183-190.
Perutz, M.F., Finch, J.T., Berriman, J., Lesk, A., 2002. Amyloid fibers are water-filled nanotubes. Proc Natl Acad Sci U S A 99, 5591-5595.
Perz-Edwards, A., Hardison, N.L., Linney, E., 2001. Retinoic acid-mediated gene expression in transgenic reporter zebrafish. Dev Biol 229, 89-101.
Pillai-Kastoori, L., Wen, W., Wilson, S.G., Strachan, E., Lo-Castro, A., Fichera, M., Musumeci, S.A., Lehmann, O.J., Morris, A.C., 2014. Sox11 is required to maintain proper levels of Hedgehog signaling during vertebrate ocular morphogenesis. PLoS Genet 10, e1004491.
Qi, D., Larsson, J., Mannervik, M., 2004. Drosophila Ada2b is required for viability and normal histone H3 acetylation. Mol Cell Biol 24, 8080-8089.

Raymond, P.A., Barthel, L.K., Curran, G.A., 1995. Developmental patterning of rod and cone photoreceptors in embryonic zebrafish. J Comp Neurol 359, 537-550.
Raymond, S.M., Jackson, I.J., 1995. The retinal pigmented epithelium is required for development and maintenance of the mouse neural retina. Curr Biol 5, 1286-1295.
Richardson, R., Tracey-White, D., Webster, A., Moosajee, M., 2017. The zebrafish eye-a paradigm for investigating human ocular genetics. Eye (Lond) 31, 68-86.
Robu, M.E., Larson, J.D., Nasevicius, A., Beiraghi, S., Brenner, C., Farber, S.A., Ekker, S.C., 2007. p53 activation by knockdown technologies. PLoS Genet 3, e78.
Rodriguez-Navarro, S., 2009. Insights into SAGA function during gene expression. EMBO Rep 10, 843-850.
Rodriguez-Navarro, S., Fischer, T., Luo, M.J., Antunez, O., Brettschneider, S., Lechner, J., Perez-Ortin, J.E., Reed, R., Hurt, E., 2004. Sus1, a functional component of the SAGA histone acetylase complex and the nuclear pore-associated mRNA export machinery. Cell 116, 75-86.
Roessler, E., Belloni, E., Gaudenz, K., Jay, P., Berta, P., Scherer, S.W., Tsui, L.C., Muenke, M., 1996. Mutations in the human Sonic Hedgehog gene cause holoprosencephaly. Nat Genet 14, 357-360.
Ross, C.A., Poirier, M.A., 2004. Protein aggregation and neurodegenerative disease. Nat Med 10 Suppl, S10-17.
Rost, F., Eugster, C., Schroter, C., Oates, A.C., Brusch, L., 2014. Chevron formation of the zebrafish muscle segments. J Exp Biol 217, 3870-3882.
Rub, U., Brunt, E.R., Gierga, K., Seidel, K., Schultz, C., Schols, L., Auburger, G., Heinsen, H., Ippel, P.F., Glimmerveen, W.F., Wittebol-Post, D., Arai, K., Deller, T., de Vos, R.A., 2005. Spinocerebellar ataxia type 7 (SCA7): first report of a systematic neuropathological study of the brain of a patient with a very short expanded CAG-repeat. Brain Pathol 15, 287-295.
Rub, U., Brunt, E.R., Seidel, K., Gierga, K., Mooy, C.M., Kettner, M., Van Broeckhoven, C., Bechmann, I., La Spada, A.R., Schols, L., den Dunnen, W., de Vos, R.A., Deller, T., 2008. Spinocerebellar ataxia type 7 (SCA7): widespread brain damage in an adult-onset patient with progressive visual impairments in comparison with an adult-onset patient without visual impairments. Neuropathol Appl Neurobiol 34, 155-168.
Rub, U., Schols, L., Paulson, H., Auburger, G., Kermer, P., Jen, J.C., Seidel, K., Korf, H.W., Deller, T., 2013. Clinical features, neurogenetics and neuropathology of the polyglutamine spinocerebellar ataxias type 1, 2, 3, 6 and 7. Prog Neurobiol 104, 38-66.
Sanders, S.L., Jennings, J., Canutescu, A., Link, A.J., Weil, P.A., 2002. Proteomics of the eukaryotic transcription machinery: identification of proteins associated with components of yeast TFIID by multidimensional mass spectrometry. Mol Cell Biol 22, 4723-4738.
Saszik, S., Bilotta, J., Givin, C.M., 1999. ERG assessment of zebrafish retinal development. Vis Neurosci 16, 881-888.
Schauerte, H.E., van Eeden, F.J., Fricke, C., Odenthal, J., Strahle, U., Haffter, P., 1998. Sonic hedgehog is not required for the induction of medial floor plate cells in the zebrafish. Development 125, 2983-2993.
Scheel, H., Tomiuk, S., Hofmann, K., 2003. Elucidation of ataxin-3 and ataxin-7 function by integrative bioinformatics. Hum Mol Genet 12, 2845-2852.
Schimmenti, L.A., de la Cruz, J., Lewis, R.A., Karkera, J.D., Manligas, G.S., Roessler, E., Muenke, M., 2003. Novel mutation in sonic hedgehog in non-syndromic colobomatous microphthalmia. Am J Med Genet A 116A, 215-221.
Schmitt, E.A., Dowling, J.E., 1994. Early eye morphogenesis in the zebrafish, Brachydanio rerio. J Comp Neurol 344, 532-542.
Schmitt, E.A., Dowling, J.E., 1996. Comparison of topographical patterns of ganglion and photoreceptor cell differentiation in the retina of the zebrafish, Danio rerio. J Comp Neurol 371, 222-234.
Schmitt, E.A., Dowling, J.E., 1999. Early retinal development in the zebrafish, Danio rerio: light and electron microscopic analyses. J Comp Neurol 404, 515-536.
Schneider, C.A., Rasband, W.S., Eliceiri, K.W., 2012. NIH Image to ImageJ: 25 years of image analysis. Nat Methods 9, 671-675.

Scholefield, J., Greenberg, L.J., Weinberg, M.S., Arbuthnot, P.B., Abdelgany, A., Wood, M.J., 2009. Design of RNAi hairpins for mutation-specific silencing of ataxin-7 and correction of a SCA7 phenotype. PLoS One 4, e7232.
Scholefield, J., Watson, L., Smith, D., Greenberg, J., Wood, M.J., 2014. Allele-specific silencing of mutant Ataxin-7 in SCA7 patient-derived fibroblasts. Eur J Hum Genet 22, 1369-1375.
Schols, L., Amoiridis, G., Buttner, T., Przuntek, H., Epplen, J.T., Riess, O., 1997. Autosomal dominant cerebellar ataxia: phenotypic differences in genetically defined subtypes? Ann Neurol 42, 924-932.
Schols, L., Bauer, P., Schmidt, T., Schulte, T., Riess, O., 2004. Autosomal dominant cerebellar ataxias: clinical features, genetics, and pathogenesis. Lancet Neurol 3, 291-304.
Schwarz, M., Cecconi, F., Bernier, G., Andrejewski, N., Kammandel, B., Wagner, M., Gruss, P., 2000. Spatial specification of mammalian eye territories by reciprocal transcriptional repression of Pax2 and Pax6. Development 127, 4325-4334.
Sehgal, R., Karcavich, R., Carlson, S., Belecky-Adams, T.L., 2008. Ectopic Pax2 expression in chick ventral optic cup phenocopies loss of Pax2 expression. Dev Biol 319, 23-33.
Shah, S.P., Taylor, A.E., Sowden, J.C., Ragge, N.K., Russell-Eggitt, I., Rahi, J.S., Gilbert, C.E., Surveillance of Eye Anomalies Special Interest, G., 2011. Anophthalmos, microphthalmos, and typical coloboma in the United Kingdom: a prospective study of incidence and risk. Invest Ophthalmol Vis Sci 52, 558-564.
Shao, J., Diamond, M.I., 2007. Polyglutamine diseases: emerging concepts in pathogenesis and therapy. Hum Mol Genet 16 Spec No. 2, R115-123.
Sheedlo, H.J., Nelson, T.H., Lin, N., Rogers, T.A., Roque, R.S., Turner, J.E., 1998. RPE secreted proteins and antibody influence photoreceptor cell survival and maturation. Brain Res Dev Brain Res 107, 57-69.
Shen, Y.C., Raymond, P.A., 2004. Zebrafish cone-rod (crx) homeobox gene promotes retinogenesis. Dev Biol 269, 237-251.
Shkumatava, A., Fischer, S., Muller, F., Strahle, U., Neumann, C.J., 2004. Sonic hedgehog, secreted by amacrine cells, acts as a short-range signal to direct differentiation and lamination in the zebrafish retina. Development 131, 3849-3858.
Sinn, R., Wittbrodt, J., 2013. An eye on eye development. Mech Dev 130, 347-358.
Skalicky, S.E., White, A.R., Grigg, J.R., et al., 2013. Microphthalmia, anophthalmia, and coloboma and associated ocular and systemic features: Understanding the spectrum. JAMA Ophthalmology 131, 1517-1524.
Sohocki, M.M., Sullivan, L.S., Mintz-Hittner, H.A., Birch, D., Heckenlively, J.R., Freund, C.L., McInnes, R.R., Daiger, S.P., 1998. A range of clinical phenotypes associated with mutations in CRX, a photoreceptor transcription-factor gene. Am J Hum Genet 63, 1307-1315.
Sopher, B.L., Ladd, P.D., Pineda, V.V., Libby, R.T., Sunkin, S.M., Hurley, J.B., Thienes, C.P., Gaasterland, T., Filippova, G.N., La Spada, A.R., 2011. CTCF regulates ataxin-7 expression through promotion of a convergently transcribed, antisense noncoding RNA. Neuron 70, 1071-1084.
Squitieri, F., Gellera, C., Cannella, M., Mariotti, C., Cislaghi, G., Rubinsztein, D.C., Almqvist, E.W., Turner, D., Bachoud-Levi, A.C., Simpson, S.A., Delatycki, M., Maglione, V., Hayden, M.R., Donato, S.D., 2003. Homozygosity for CAG mutation in Huntington disease is associated with a more severe clinical course. Brain 126, 946-955.
Stenkamp, D.L., 2007. Neurogenesis in the fish retina. Int Rev Cytol 259, 173-224.
Stenkamp, D.L., Frey, R.A., 2003. Extraretinal and retinal hedgehog signaling sequentially regulate retinal differentiation in zebrafish. Dev Biol 258, 349-363.
Stenkamp, D.L., Frey, R.A., Mallory, D.E., Shupe, E.E., 2002. Embryonic retinal gene expression in sonic-you mutant zebrafish. Dev Dyn 225, 344-350.
Stenkamp, D.L., Frey, R.A., Prabhudesai, S.N., Raymond, P.A., 2000. Function for hedgehog genes in zebrafish retinal development. Developmental Biology 220, 238-252.
Stevanin, G., Giunti, P., Belal, G.D., Durr, A., Ruberg, M., Wood, N., Brice, A., 1998. De novo expansion of intermediate alleles in spinocerebellar ataxia 7. Hum Mol Genet 7, 1809-1813.
Strauss, O., 2005. The retinal pigment epithelium in visual function. Physiol Rev 85, 845-881.

Strom, A.L., Forsgren, L., Holmberg, M., 2005. A role for both wild-type and expanded ataxin-7 in transcriptional regulation. Neurobiol Dis 20, 646-655.
Sugars, K.L., Rubinsztein, D.C., 2003. Transcriptional abnormalities in Huntington disease. Trends Genet 19, 233-238.
Sussman, R.T., Stanek, T.J., Esteso, P., Gearhart, J.D., Knudsen, K.E., McMahon, S.B., 2013. The epigenetic modifier ubiquitin-specific protease 22 (USP22) regulates embryonic stem cell differentiation via transcriptional repression of sex-determining region Y-box 2 (SOX2). J Biol Chem 288, 24234-24246.
Swaroop, A., Kim, D., Forrest, D., 2010. Transcriptional regulation of photoreceptor development and homeostasis in the mammalian retina. Nat Rev Neurosci 11, 563-576.
Take-uchi, M., Clarke, J.D., Wilson, S.W., 2003. Hedgehog signalling maintains the optic stalk-retinal interface through the regulation of Vax gene activity. Development 130, 955-968.
Tan, J.Y., Vance, K.W., Varela, M.A., Sirey, T., Watson, L.M., Curtis, H.J., Marinello, M., Alves, S., Steinkraus, B., Cooper, S., Nesterova, T., Brockdorff, N., Fulga, T., Brice, A., Sittler, A., Oliver, P.L., Wood, M.J., Ponting, C.P., Marques, A.C., 2014. Cross-talking noncoding RNAs contribute to cell-specific neurodegeneration in SCA7. Nat Struct Mol Biol 21, 955-961.
Taroni, F., DiDonato, S., 2004. Pathways to motor incoordination: the inherited ataxias. Nat Rev Neurosci 5, 641-655.
Taylor, J., Grote, S.K., Xia, J., Vandelft, M., Graczyk, J., Ellerby, L.M., La Spada, A.R., Truant, R., 2006. Ataxin-7 can export from the nucleus via a conserved exportin-dependent signal. J Biol Chem 281, 2730-2739.
Thisse, C., Thisse, B., 2008. High-resolution in situ hybridization to whole-mount zebrafish embryos. Nat Protoc 3, 59-69.
Thoreson, W.B., 2008. The Vertebrate Retina, in: Gendelman, H.E., Ikezu, T. (Eds.), Neuroimmune Pharmacology. Springer US, Boston, MA, pp. 123-134.
Thummel, R., Bailey, T.J., Hyde, D.R., 2011. In vivo electroporation of morpholinos into the adult zebrafish retina. J Vis Exp, e3603.
Thurtell, M.J., Fraser, J.A., Bala, E., Tomsak, R.L., Biousse, V., Leigh, R.J., Newman, N.J., 2009. Two patients with spinocerebellar ataxia type 7 presenting with profound binocular visual loss yet minimal ophthalmoscopic findings. J Neuroophthalmol 29, 187-191.
Torres, M., Gomez-Pardo, E., Gruss, P., 1996. Pax2 contributes to inner ear patterning and optic nerve trajectory. Development 122, 3381-3391.
Traiffort, E., Charytoniuk, D.A., Faure, H., Ruat, M., 1998. Regional distribution of Sonic Hedgehog, patched, and smoothened mRNA in the adult rat brain. J Neurochem 70, 1327-1330.
Trang, H., Stanley, S.Y., Thorner, P., Faghfoury, H., Schulze, A., Hawkins, C., Pearson, C.E., Yoon, G., 2015. Massive CAG repeat expansion and somatic instability in maternally transmitted infantile spinocerebellar ataxia type 7. JAMA Neurol 72, 219-223.
Trottier, Y., Lutz, Y., Stevanin, G., Imbert, G., Devys, D., Cancel, G., Saudou, F., Weber, C., David, G., Tora, L., et al., 1995. Polyglutamine expansion as a pathological epitope in Huntington's disease and four dominant cerebellar ataxias. Nature 378, 403-406.
Trousse, F., Marti, E., Gruss, P., Torres, M., Bovolenta, P., 2001. Control of retinal ganglion cell axon growth: a new role for Sonic hedgehog. Development 128, 3927-3936.
Trushina, E., Dyer, R.B., Badger, J.D., 2nd, Ure, D., Eide, L., Tran, D.D., Vrieze, B.T., Legendre-Guillemin, V., McPherson, P.S., Mandavilli, B.S., Van Houten, B., Zeitlin, S., McNiven, M., Aebersold, R., Hayden, M., Parisi, J.E., Seeberg, E., Dragatsis, I., Doyle, K., Bender, A., Chacko, C., McMurray, C.T., 2004. Mutant huntingtin impairs axonal trafficking in mammalian neurons in vivo and in vitro. Mol Cell Biol 24, 8195-8209.
Tsai, H.F., Lin, S.J., Li, C., Hsieh, M., 2005. Decreased expression of Hsp27 and Hsp70 in transformed lymphoblastoid cells from patients with spinocerebellar ataxia type 7. Biochem Biophys Res Commun 334, 1279-1286.
Tse, W.K., Eisenhaber, B., Ho, S.H., Ng, Q., Eisenhaber, F., Jiang, Y.J., 2009. Genome-wide loss-of-function analysis of deubiquitylating enzymes for zebrafish development. BMC Genomics 10, 637.

Uribe, R.A., Gross, J.M., 2010. Id2a influences neuron and glia formation in the zebrafish retina by modulating retinoblast cell cycle kinetics. Development 137, 3763-3774.
van de Warrenburg, B.P., Frenken, C.W., Ausems, M.G., Kleefstra, T., Sinke, R.J., Knoers, N.V., Kremer, H.P., 2001. Striking anticipation in spinocerebellar ataxia type 7: the infantile phenotype. J Neurol 248, 911-914.
van Eeden, F.J., Granato, M., Schach, U., Brand, M., Furutani-Seiki, M., Haffter, P., Hammerschmidt, M., Heisenberg, C.P., Jiang, Y.J., Kane, D.A., Kelsh, R.N., Mullins, M.C., Odenthal, J., Warga, R.M., Allende, M.L., Weinberg, E.S., Nusslein-Volhard, C., 1996. Mutations affecting somite formation and patterning in the zebrafish, Danio rerio. Development 123, 153-164.
Van Raamsdonk, J.M., Pearson, J., Murphy, Z., Hayden, M.R., Leavitt, B.R., 2006. Wild-type huntingtin ameliorates striatal neuronal atrophy but does not prevent other abnormalities in the YAC128 mouse model of Huntington disease. BMC Neurosci 7, 80.
Verwer, R.W., Baker, R.E., Boiten, E.F., Dubelaar, E.J., van Ginkel, C.J., Sluiter, A.A., Swaab, D.F., 2003. Post-mortem brain tissue cultures from elderly control subjects and patients with a neurodegenerative disease. Exp Gerontol 38, 167-172.
Vihtelic, T.S., 2008. Teleost lens development and degeneration. Int Rev Cell Mol Biol 269, 341-373.
Vihtelic, T.S., Doro, C.J., Hyde, D.R., 1999. Cloning and characterization of six zebrafish photoreceptor opsin cDNAs and immunolocalization of their corresponding proteins. Vis Neurosci 16, 571-585.
Vissers, L.E., van Ravenswaaij, C.M., Admiraal, R., Hurst, J.A., de Vries, B.B., Janssen, I.M., van der Vliet, W.A., Huys, E.H., de Jong, P.J., Hamel, B.C., Schoenmakers, E.F., Brunner, H.G., Veltman, J.A., van Kessel, A.G., 2004. Mutations in a new member of the chromodomain gene family cause CHARGE syndrome. Nat Genet 36, 955-957.
Wan, J., Goldman, D., 2016. Retina regeneration in zebrafish. Curr Opin Genet Dev 40, 41-47.
Wang, L., Dent, S.Y., 2014. Functions of SAGA in development and disease. Epigenomics 6, 329-339.
Wang, P., Liang, X., Yi, J., Zhang, Q., 2008. Novel SOX2 mutation associated with ocular coloboma in a Chinese family. Arch Ophthalmol 126, 709-713.
Warrick, J.M., Morabito, L.M., Bilen, J., Gordesky-Gold, B., Faust, L.Z., Paulson, H.L., Bonini, N.M., 2005. Ataxin-3 suppresses polyglutamine neurodegeneration in Drosophila by a ubiquitin-associated mechanism. Mol Cell 18, 37-48.
Waterhouse, A.M., Procter, J.B., Martin, D.M., Clamp, M., Barton, G.J., 2009. Jalview Version 2--a multiple sequence alignment editor and analysis workbench. Bioinformatics 25, 1189-1191.
Weiss, A.H., Kousseff, B.G., Ross, E.A., Longbottom, J., 1989. Simple microphthalmos. Archives of Ophthalmology 107, 1625-1630.
Wen, W., Pillai-Kastoori, L., Wilson, S.G., Morris, A.C., 2015. Sox4 regulates choroid fissure closure by limiting Hedgehog signaling during ocular morphogenesis. Dev Biol 399, 139-153.
Westerfield, M., 2000. The Zebrafish Book. A Guide for The Laboratory Use of Zebrafish (Danio rerio).
Whitney, A., Lim, M., Kanabar, D., Lin, J.P., 2007. Massive SCA7 expansion detected in a 7-month-old male with hypotonia, cardiomegaly, and renal compromise. Dev Med Child Neurol 49, 140-143.
Wilde, J.J., Siegenthaler, J.A., Dent, S.Y., Niswander, L.A., 2017. Diencephalic Size Is Restricted by a Novel Interplay Between GCN5 Acetyltransferase Activity and Retinoic Acid Signaling. J Neurosci 37, 2565-2579.
Wyatt, A., Bakrania, P., Bunyan, D.J., Osborne, R.J., Crolla, J.A., Salt, A., Ayuso, C., Newbury-Ecob, R., Abou-Rayyah, Y., Collin, J.R., Robinson, D., Ragge, N., 2008. Novel heterozygous OTX2 mutations and whole gene deletions in anophthalmia, microphthalmia and coloboma. Hum Mutat 29, E278-283.
Wyce, A., Henry, K.W., Berger, S.L., 2004. H2B ubiquitylation and de-ubiquitylation in gene activation. Novartis Found Symp 259, 63-73; discussion 73-67, 163-169.

Wyce, A., Xiao, T., Whelan, K.A., Kosman, C., Walter, W., Eick, D., Hughes, T.R., Krogan, N.J., Strahl, B.D., Berger, S.L., 2007. H2B ubiquitylation acts as a barrier to Ctk1 nucleosomal recruitment prior to removal by Ubp8 within a SAGA-related complex. Mol Cell 27, 275-288.
Xiao, H., Yu, Z., Wu, Y., Nan, J., Merry, D.E., Sekiguchi, J.M., Ferguson, D.O., Lieberman, A.P., Dressler, G.R., 2012. A polyglutamine expansion disease protein sequesters PTIP to attenuate DNA repair and increase genomic instability. Hum Mol Genet 21, 4225-4236.
Xu, W., Edmondson, D.G., Evrard, Y.A., Wakamiya, M., Behringer, R.R., Roth, S.Y., 2000. Loss of Gcn5l2 leads to increased apoptosis and mesodermal defects during mouse development. Nat Genet 26, 229-232.
Yang, H., Liu, S., He, W.T., Zhao, J., Jiang, L.L., Hu, H.Y., 2015. Aggregation of Polyglutamine-expanded Ataxin 7 Protein Specifically Sequesters Ubiquitin-specific Protease 22 and Deteriorates Its Deubiquitinating Function in the Spt-Ada-Gcn5-Acetyltransferase (SAGA) Complex. J Biol Chem 290, 21996-22004.
Yanicostas, C., Barbieri, E., Hibi, M., Brice, A., Stevanin, G., Soussi-Yanicostas, N., 2012. Requirement for zebrafish ataxin-7 in differentiation of photoreceptors and cerebellar neurons. PLoS One 7, e50705.
Yefimova, M.G., Messaddeq, N., Karam, A., Jacquard, C., Weber, C., Jonet, L., Wolfrum, U., Jeanny, J.C., Trottier, Y., 2010. Polyglutamine toxicity induces rod photoreceptor division, morphological transformation or death in spinocerebellar ataxia 7 mouse retina. Neurobiol Dis 40, 311-324.
Yin, Y.W., Jin, H.J., Zhao, W., Gao, B., Fang, J., Wei, J., Zhang, D.D., Zhang, J., Fang, D., 2015. The Histone Acetyltransferase GCN5 Expression Is Elevated and Regulated by c-Myc and E2F1 Transcription Factors in Human Colon Cancer. Gene Expr 16, 187-196.
Yoo, S.Y., Pennesi, M.E., Weeber, E.J., Xu, B., Atkinson, R., Chen, S., Armstrong, D.L., Wu, S.M., Sweatt, J.D., Zoghbi, H.Y., 2003. SCA7 knockin mice model human SCA7 and reveal gradual accumulation of mutant ataxin-7 in neurons and abnormalities in short-term plasticity. Neuron 37, 383-401.
Yu, X., Ajayi, A., Boga, N.R., Strom, A.L., 2012. Differential degradation of full-length and cleaved ataxin-7 fragments in a novel stable inducible SCA7 model. J Mol Neurosci 47, 219-233.
Yu, Y., Teng, Y., Liu, H., Reed, S.H., Waters, R., 2005. UV irradiation stimulates histone acetylation and chromatin remodeling at a repressed yeast locus. Proc Natl Acad Sci U S A 102, 8650-8655.
Yvert, G., Lindenberg, K.S., Devys, D., Helmlinger, D., Landwehrmeyer, G.B., Mandel, J.L., 2001. SCA7 mouse models show selective stabilization of mutant ataxin-7 and similar cellular responses in different neuronal cell types. Hum Mol Genet 10, 1679-1692.
Yvert, G., Lindenberg, K.S., Picaud, S., Landwehrmeyer, G.B., Sahel, J.A., Mandel, J.L., 2000. Expanded polyglutamines induce neurodegeneration and trans-neuronal alterations in cerebellum and retina of SCA7 transgenic mice. Human molecular genetics 9, 2491-2506.
Zagozewski, J.L., Zhang, Q., Eisenstat, D.D., 2014. Genetic regulation of vertebrate eye development. Clin Genet 86, 453-460.
Zander, C., Takahashi, J., El Hachimi, K.H., Fujigasaki, H., Albanese, V., Lebre, A.S., Stevanin, G., Duyckaerts, C., Brice, A., 2001. Similarities between spinocerebellar ataxia type 7 (SCA7) cell models and human brain: proteins recruited in inclusions and activation of caspase-3. Hum Mol Genet 10, 2569-2579.
Zeitlin, S., Liu, J.P., Chapman, D.L., Papaioannou, V.E., Efstratiadis, A., 1995. Increased apoptosis and early embryonic lethality in mice nullizygous for the Huntington's disease gene homologue. Nat Genet 11, 155-163.
Zhang, X.M., Yang, X.J., 2001. Regulation of retinal ganglion cell production by Sonic hedgehog. Development 128, 943-957.
Zhang, X.Y., Pfeiffer, H.K., Thorne, A.W., McMahon, S.B., 2008a. USP22, an hSAGA subunit and potential cancer stem cell marker, reverses the polycomb-catalyzed ubiquitylation of histone H2A. Cell Cycle 7, 1522-1524.
Zhang, X.Y., Varthi, M., Sykes, S.M., Phillips, C., Warzecha, C., Zhu, W., Wyce, A., Thorne, A.W., Berger, S.L., McMahon, S.B., 2008b. The putative cancer stem cell marker USP22 is a

subunit of the human SAGA complex required for activated transcription and cell-cycle progression. Mol Cell 29, 102-111.
Zhao, Y., Lang, G., Ito, S., Bonnet, J., Metzger, E., Sawatsubashi, S., Suzuki, E., Le Guezennec, X., Stunnenberg, H.G., Krasnov, A., Georgieva, S.G., Schule, R., Takeyama, K., Kato, S., Tora, L., Devys, D., 2008. A TFTC/STAGA module mediates histone H2A and H2B deubiquitination, coactivates nuclear receptors, and counteracts heterochromatin silencing. Mol Cell 29, 92-101.
Zoghbi, H.Y., Orr, H.T., 2000. Glutamine repeats and neurodegeneration. Annu Rev Neurosci 23, 217-247.
Zuber, M.E., Gestri, G., Viczian, A.S., Barsacchi, G., Harris, W.A., 2003. Specification of the vertebrate eye by a network of eye field transcription factors. Development 130, 5155-5167.

Résumé de la thèse

Résumé de la thèse

Introduction

L'ataxie spinocérébelleuse de type 7 (SCA7) est une maladie neurodégénérative à transmission autosomale dominante caractérisée par une perte progressive des neurones du cervelet et des structures associées, conduisant à une ataxie cérébelleuse, une dysarthrie et une dysphagie (David et al., 1998). SCA7 appartient à un groupe de désordres liés à une expansion CAG/polyglutamine (polyQ), incluant d'autres ataxies spinocérébelleuses (SCA1-3, 6 et 17), la maladie de Huntington (HD), l'atrophie musculaire spinobulbaire (SBMA) et l'atrophie dentatorubrale-pallidoluysienne (DRPLA). Pour ces maladies, une expansion du nombre de répétitions CAG traduites dans différents gènes causatifs conduit à l'expansion du triplet polyQ dans les protéines mutées correspondantes. Le seuil précis de répétitions conduisant à la maladie varie au sein de celle ci (David et al., 1997 ; Zoghbi et Orr, 2000). Des preuves cumulatives indiquent qu'un gain de fonction toxique des protéines mutées et la perte de fonction de la protéine normale sont à l'origine de la pathogenèse polyQ ((Lim et al., 2008; Zoghbi and Orr, 2000). Ainsi, déterminer la fonction normale des protéines à polyQ contribuerait à une meilleure compréhension des mécanismes pathologiques à l'origine de ces maladies.

Deux caractéristiques distinctes de SCA7 sont : la présence d'une forte anticipation par laquelle une apparition précoce ainsi qu'une une sévérité plus grande des symptômes sont observés au cours des générations successives de familles atteintes et la perte de l'acuité visuelle causée par la dégénérescence des photorécepteurs en cônes et en bâtonnets retrouvée chez 83% des patients (Benton et al., 1998; David et al., 1998; Hoche et al., 2008; Stevanin et al., 1998). Les dystrophies des cônes et des bâtonnets (CRD ; prévalence : 1/40 000) sont des maladies héréditaires de la rétine caractérisées par une implication primaire des cônes avec une diminution progressive de l'acuité visuelle et de la vision en couleur, suivie d'une détérioration des bâtonnets, de la perte de la vision périphérique et d'une cécité nocturne (Hamel, 2007). Selon l'Organisation mondiale de la santé (OMS), jusqu'en 2014 285 millions de personnes étaient atteintes par la détérioration visuelle et la cécité, dont 39 millions d'aveugles et 246 millions ayant une vue faible. Les organismes modèles ayant une physiologie similaire à celle de l'Homme sont indispensables à la compréhension des processus développementaux, à l'identification de potentiels gènes causatifs des maladies humaines et au développement de thérapies.

SCA7 est causée par une augmentation du nombre normal de répétitions polyQ (4-35 répétitions) localisées en N-terminal de la protéine ataxine-7 (ATXN7), une protéine de 892 acides aminés conservée au cours de l'évolution (Michalik et al., 2004). ATXN7 est un membre

hautement conservé du complexe multiprotéique Spt-Ada-Gcn5 Acetyltransferase (SAGA) régulant la transcription via l'acétylation de l'histone H3 par la sous-unité GCN5-dépendante et la déubiquitination de H2B par la sous-unité USP22, deux activités enzymatiques essentielles au fonctionnement normal de la cellule (Helmlinger et al., 2006; Kohler et al., 2008; Zhao et al., 2008).

Les rétines post-mortem des patients SCA7 présentent une perte quasi totale des photorécepteurs cônes et bâtonnets (Michalik et al., 2004). Les modèles murins de SCA7 montrent pour leur part une perte progressive de la morphologie typique des photorécepteurs, avec notamment la disparition de leurs segments externes conduisant à leur dysfonctionnement. Ces observations suggèrent qu'une perte de la maintenance des photorécepteurs en état différencié précède leur mort (Abou-Sleymane et al., 2006; Yefimova et al., 2010).

Le rôle physiologique de l'ATXN7 reste encore inconnu et il n'existe pas de modèle murin déficient en ATXN7 disponible pour étudier la fonction de la protéine dans le développement de la rétine et la différenciation des photorécepteurs. Le poisson-zèbre émerge donc comme un modèle alternatif puisqu'il possède le gène orthologue atxn7 possédant 51,74% d'identité avec le gène humain ATXN7. Ce modèle présente une popularité croissante pour les études du développement des vertébrés et leur génétique du fait de la transparence de ses embryons qui se développent ex-utero, rendant possible la visualisation d'évènements du développement. De plus, le poisson-zèbre est un meilleur modèle pour notre étude puisque contrairement aux rongeurs et de façon similaire aux humains, cet animal est diurne et sa rétine est riche en cônes de divers sous-types, en plus des bâtonnets. Finalement, la morphogenèse de l'œil du poisson-zèbre se déroule par étapes comme chez l'homme et la souris, mais est 20 fois plus rapide et déjà hautement caractérisée (Bibliowicz et al., 2011).

Objectif

L'objectif principal de ma thèse est de déterminer le rôle de l'ATXN7 au cours du développement de l'œil chez les vertébrés, en utilisant le poisson-zèbre comme modèle animal.

Bien que les maladies à expansion de polyglutamine se développent principalement à l'âge adulte des résultats récents, notamment pour la maladie de Huntington, montrent que des anomalies précoces au cours du développement des animaux modèles pourraient rendre les neurones adultes vulnérables à la dégénérescence. Dans ce contexte, notre approche devrait

aussi enrichir notre compréhension des mécanismes pathologiques sous-jacents à SCA7 qui reste encore aujourd'hui une maladie incurable.

Méthodes

Pour déterminer le rôle de l'*atxn7* chez le poisson-zèbre, j'ai réduit l'expression du gène atxn7 dans la lignée poisson-zèbre usuelle AB en utilisant deux types d'oligonucléotides anti-sens morpholinos: l'un ciblant le codon initiateur AUG (*atxn7* Mo1), ce qui prévient la synthèse protéique de l'atxn7, l'autre ciblant un site d'épissage (*atxn7* Mo2) ce qui mène à la production d'ARN messagers aberrants codant pour un codon de terminaison précoce. La caractérisation des poisson-zèbres inactivés pour l'*atxn7* (ci-après appelés morphants) s'est faite en combinant différentes techniques d'imagerie incluant la microscopie optique conventionnelle, la microscopie électronique et la microscopie confocale et des techniques d'hybridation *in situ* et de RT-PCR pour tester l'expression de certains gènes. De plus, j'ai inactivé l'*atxn7* dans la lignée transgénique innovante SoFa1 qui code pour différentes protéines fluorescentes dans chaque couche de la rétine, permettant ainsi de mettre en image en microscopie confocale 3 dimensions (3D) la différenciation neuronale sur le même poisson. Enfin, j'ai utilisé la technologie innovante CRISPR-Cas9 pour valider les observations faites sur les poissons-zèbre morphants.

Résultats

Dysmorphogenèse de l'œil

L'inactivation du gène *atxn7* dans les embryons de poisson-zèbre AB à l'aide de l'*atxn*7 Mo1 a conduit à des anomalies importantes du développement de l'œil. Le premier signe d'un défaut oculaire a été détecté très tôt au stade 10 somites (14 heures post-fertilisation, hpf), lorsque l'évagination de la vésicule optique se produit formant une crête horizontale. A ce stade les embryons morphants présentent une crête anormale et ce défaut persiste et est nettement plus visible à 48 hpf, où la région ventrale de l'œil montre un manque de pigmentation et une fermeture incomplète de la fissure optique de la rétine, défaut connu sous le nom de colobome chez l'humain.

Le colobome fait partie d'un spectre des malformations oculaires pouvant inclure la microphtalmie et l'anophtalmie, qui peuvent être présents de façon unilatérale ou bilatérale; lorsqu'elles sont bilatérales ces malformations peuvent survenir dans n'importe quelle combinaison. Pour quantifier des différences potentielles dans la taille des yeux qui pourraient suggérer la présence d'une microphtalmie, la longueur antérieur-postérieur de l'œil a été mise

en rapport avec la longueur du corps de chaque larve. Le ratio œil/corps est fondamentalement la mesure normalisée d'un œil. Ces analyses ont révélé une absence significative de changement dans le ratio œil/corps des embryons morphants comparés aux contrôles, montrant une absence de microphtalmie.

A 5 jours post-fertilisation (dpf), les morphants présentent un trou dans l'épithélium pigmentaire rétinien (RPE) postérieur lorsqu'orientés en position latérale, et une extrusion du RPE dans le cerveau lorsqu'orientés de façon dorsale. Ces anomalies apparaissent de façon progressive au cours du développement et ont pu être observées de façon régulière avec les deux morpholinos ciblant le gène *atxn7*, de façon concentration-dépendante, mais jamais en présence du morpholino contrôle. Nos observations montrent pour la première fois que la protéine atxn7 est impliquée dans la morphogenèse de l'œil.

Afin de déterminer plus précisément la nature du tissu qui extrude vers la région du cerveau, des sections histologiques de rétine ont été analysées au microscope. Nous avons observé une interruption du RPE dans la partie postérieure de la rétine, ce qui expliquerait l'absence de pigmentation dans cette région lorsqu'observée en position latérale au macroscope. De plus, nous avons trouvé que le tissu extrudant dans le cerveau comprend aussi bien le RPE que la rétine neurale.

Tenant compte de la forte interdépendance entre le RPE et les photorécepteurs pour leur développement et leur fonction, nous avons plus particulièrement étudié ces 2 types cellulaires par microscopie électronique. Nous avons trouvé que les segments externes des photorécepteurs sont absents ou plus courts chez les morphants par rapport aux contrôles, indépendamment de la présence ou non du RPE. La perte de fonction de l'*atxn7* du poisson-zèbre cause donc un effet similaire à l'expression de l'ATXN7 mutante chez la souris: la quasi absence de segments externes des photorécepteurs.

Altération du programme génétique de développement de l'œil

Au cours de la morphogenèse de la cupule optique, les couches de la vésicule optique migrent de façon ventrale au niveau de la fissure de la choroïde le long de l'axe proximo-distal de sorte que la rétine et le RPE sont confinés *in fine* dans la cupule. L'échec de cette fermeture conduit aux colobomes, qui sont caractérisés par la persistance d'un trou à l'arrière de l'œil tel qu'observé chez les morphants atxn7. Les voies hedgehog (Hh) sont des régulateurs clés de la morphogenèse de la cupule optique et une altération de ces voies conduit à un phénotype de colobome parce que la tige optique en développement est anormalement étendue dans la rétine et entrave la rencontre et la fusion des bordures de la fissure de la choroïde. La longueur

appropriée de la tige optique est contrôlée par le facteur de transcription *pax2*. L'expression de *pax2* est induite par la voie Sonic hedgehog (*shh*), mais restreinte à la tige grâce à l'effet répressif du facteur de transcription pax6; en effet pax6 forme une limite précise entre la tige optique et la rétine neurale en devenir afin de restreindre pax2 à son territoire d'expression. La surexpression du facteur *Shh* suffit à induire une expression aberrante de *pax2* dans les territoires plus distaux de la vésicule optique d'où il est normalement absent, i.e. empiétant sur le territoire de *pax6*, causant ainsi le colobome.

Afin de comprendre les bases moléculaires des phénotypes oculaires des morphants, nous avons réalisé des hybridations *in situ* pour étudier l'expression de ces voies. Nous avons mis en évidence une sur-expression de 2 membres de la famille Hh, *shh* et *twhh*, associée à une expression aberrante de *pax2* au-delà de ses limites et une réduction de la zone d'expression de pax6, ce qui est cohérent avec les conséquences connues de la sur-activation de la voie Hh. Ces résultats montrent que l'agencement des motifs proximo-distaux de la vésicule optique est déterioré chez les embryons morphants *atxn7* par l'altération de la voie de signalisation Hh, conduisant ainsi au colobome.

De façon intéressante, le gène *vax2* qui code pour un facteur de transcription qui participe à la fermeture de la fissure optique et qui est également régulé par la voie Hh montre un niveau d'expression aberrant, en accord avec le développement du colobome . Pris tous ensemble, ces résultats nous permettent de proposer un modèle dans lequel *atxn7* joue un rôle dans le développement de l'œil en agissant en amont de la voie de signalisation Hh, conduisant au colobome, à l'extrusion de la rétine neurale et à l'interruption du RPE que nous avons rapportés.

Des études antérieures ont rapporté qu'une interruption de la voie Hh conduit à une altération de la formation des somites dans le corps du poisson-zèbre, présentant un angle plus obtus. Afin d'appuyer nos observations concernant l'altération de la voie Hh, nous avons mesuré l'angle des somites chez les morphants. Nous avons mis en évidence la présence de somites en forme de chevron chez les morphants, avec un phénotype des somites ayant un angle moyen de 118°, comparé à 91° pour les contrôles, indiquant une dérégulation des voies de signalisation Hh en absence d'atxn7.

Altération de la différenciation de la rétine neurale

Les défauts des segments externes chez les morphants suggèrent que la différenciation des photorécepteurs est incomplète, ce qui nous a conduit à explorer plus globalement le processus de différenciation de la rétine neurale. La différenciation des neurones rétiniens du

neuro-épithélium se propage progressivement en au moins 3 vagues parallèles menant aux trois couches de la rétine. Afin d'étudier ce processus complexe, nous avons décidé d'utiliser la lignée transgénique SoFa1 qui permet d'imager la différenciation neuronale en 4D sur le même poisson par microscopie confocale. À 5 jours, lorsque la rétine est entièrement formée, le colobome devient alors visible au niveau cellulaire.À ce niveau de résolution, nous avons pu observer que les cellules ganglionnaires de la rétine (RGCs) projettent leurs axones formant le nerf optique qui lui même inerve le tectum optique En particulier, l'imagerie 3D a révélé que les axones des RGCs des morphants ne sont pas correctement regroupés au niveau du nerf optique, ce qui conduit à une subdivision du nerf optique. Les axones traversent correctement la ligne médiane ventrale du diencéphale formant le chiasme optique, et vont ultérieurement innerver le lobe tectal contre-latéral. Cependant, 30,76% (n=4/13) des embryons morphants Mo1 présentent des axones étendus de façon aberrante vers la commissure antérieure, suggérant un empaquement axonal plus lâche. Ces anomalies sont vraisemblablement une conséquence du colobome.

Altération de la morphogenèse des photorécepteurs chez les morphants Mo1

L'interaction entre les photorécepteurs et le RPE est nécessaire pour une fonction visuelle appropriée (Strauss, 2005). De plus, le développement de chacune de ces 2 structures est corrélé à celui de l'autre (Raymond and Jackson, 1995; Sheedlo et al., 1998). De façon remarquable, les premières analyses morphologiques des photorécepteurs des morphants Mo1 ont révélé la présence de photorécepteurs différenciés dans des zones dépourvues de pigmentation.

L'analyse des zones présentant un RPE non interrompu a été réalisée en vue de déterminer si les différences observées dans les segments externes(OS) chez les morphants Mo1 étaient dues aux anomalies dans l'architecture de la rétine expulsée. Cette analyse a révélé la présence de photorécepteurs morphologiquement similaires à ceux rencontrés dans les zones dépourvues de pigmentation. De façon intéressante, d'autres zones de la rétine présentent des photorécepteurs avec des segments internes (IS) non affectés mais totalement dépourvus de segments externes, confirmant l'indépendance du RPE dans la morphogenèse des photorécepteurs chez les morphants Mo1. Additionnellement, nous avons observé une absence de segments externes et une désorganisation des segments internes chez certains photorécepteurs, pour lesquels l'ellipsoïde distinct ne présentait pas les mitochondries caractéristiques de la région la plus apicale. Il est important de souligner qu'en dépit des altérations morphologiques des photorécepteurs décrites ci-dessus, aucun signe apparent de mort cellulaire n'a pu être mis en évidence dans les différentes régions observées de la rétine.

Ces observations nous ont permis de poser l'hypothèse selon laquelle des facteurs intrinsèques aux photorécepteurs interviendraient dans l'altération de la différenciation des photorécepteurs chez les morphants Mo1. En vue de valider cette hypothèse, des expériences d'hybridation *in situ* pour *crx* ont été réalisées à 48 hpf sur des poisson-zèbres contrôles ou morphants Mo1. Le choix de ce gène pour l'étude s'est fait selon 2 critères clé : premièrement, il a été montré que l'expression de *crx* est essentielle à une différenciation correcte des photorécepteurs (Shen and Raymond, 2004), et deuxièmement des études antérieures ont rapporté une interaction entre atxn7 et crx (Chen et al., 2004; La Spada et al., 2001).

Les morphants Mo1 présentent une localisation et une intensité de crx significativement différente des contrôles. Notamment, les morphants Mo1 montrent des zones avec une absence totale de signal. Ce défaut n'est pas dû à un retard de développement des morphants.

Ces résultats pris en compte, il ressort que la diminution des niveaux d'*atxn7* conduit à une altération de l'expression de *crx*, un gène important pour la différenciation terminale des photorécepteurs. Il serait possible que le phénotype des photorécepteurs décrit dans notre étude résulte au moins partiellement de l'altération de l'expression de ce gène. Il est intéressant de noter que des études ont rapporté que l'expression de *crx* est indépendante des variations de *shh* (Stenkamp et al., 2002), suggérant que plus d'une voie de signalisation serait affectée chez les morphants Mo1.

Atxn7 et ses paralogues

Afin de comprendre le lien entre l'inactivation d'atxn7 et la dérégulation de différents acteurs régulant la morphogenèse de l'œil, nous avons réalisé 2 expériences différentes:

Les analyses bio-informatiques ont identifié la famille des gènes *SCA7* composée de 4 paralogues chez les vertébrés (*atxn7, L1*, *L2* et *L3b*). L'alignement de tous les membres de la famille des atxn7 du poisson-zèbre a révélé l'existence de 3 blocs d'homologie; de façon intéressante, le premier bloc n'est pas conservé pour le paralogue atxn7L1 et le 3^{e} bloc ne comprend pas atxn7L3 ; de plus, le paralogue atxn7L2 est dupliqué chez le poisson-zèbre. En vue de déterminer une potentielle altération de l'expression des paralogues *atxn7* dans le contexte du morphant qui pourrait expliquer les changements moléculaires que nous avons observés, nous avons effectué des RT-PCR à différents temps et nous n'avons trouvé aucune différence d'expression des paralogues entre contrôles et morphants. Cependant, des études supplémentaires sont nécessaires afin de déterminer l'éventuelle contribution des paralogues dans le contexte d'absence d'atxn7.

Spécificité du phénotype

Les anti-sens morpholino sont des outils flexibles et rapides d'utilisation pour inhiber l'expression de gène. Cependant ils peuvent, comme plusieurs outils similaires, causer des effets non-spécifiques qui brouillent l'analyse des résultats. Afin de confirmer la spécificité des phénotypes des morphants générés par l'atxn7Mo^{aug}, nous avons effectué 3 expériences différentes. Dans un premier temps nous avons généré un second morpholino non chevauchant dirigé contre un site d'épissage de l'ARN de l'atxn7, l'atxn7Mo^{spl}. Ce dernier a conduit à une altération de l'épissage de l'ARN, et à un défaut de fermeture de la choroïde similaire à celui produit par le premier morpholino atxn7Mo^{aug}. Nous avons ensuite effectué une expérience de « sauvetage » du phénotype de l'œil des morphants Mo1 en surexprimant l'ARN messager de l'ATXN7 sauvage humaine (contenant 10 glutamines). L'ATXN7 humaine a permis d'augmenter de 2.5x le nombre de poissons présentant un œil normal et de diminuer de 2x la présence de phénotype sévère de l'œil des morphants. Ce résultat montre d'une part que le phénotype de l'œil est bien relié à des variations du niveau d'ATXN7, et d'autre part que la fonction de l'ATXN7 dans le développement de l'œil semble conservée au cours de l'évolution. Enfin, nous avons ensuite développé une toute autre approche pour inactiver l'atxn7 en utilisant le système CRISPR-Cas9. Deux ARN guides (sgRNA) ont été conçus pour cibler la région codante entre les exons 1 et 4, et ont été injectés avec la protéine Cas9 dans les embryons afin d'étudier la population d'embryons F0 résultants. Cette population a présenté un colobome dans 24.48 % des cas (12/49). En revanche, aucun des embryons injectés avec le guide ou la protéine Cas9 seul ne présentent ce défaut. L'analyse des séquences ciblées ont confirmé que des indels ont été générés dans les embryons atteints. Pris ensemble, les résultats obtenus avec les deux morpholinos et le CRISPR-Cas9 appuient fortement la spécificité du phénotype de colobome lorsque l'atxn7 est inactivée.

Conclusion

En résumé, ces travaux de thèse incluent un examen détaillé de la nécessité d'atxn7 dans la régulation de la morphogenèse oculaire chez le poisson-zèbre. Ils fournissent un profil d'expression minutieux d'atxn7, aussi bien sur le plan temporel au cours du développement que sur le plan spatial dans la rétine au cours de la morphogenèse oculaire et des différents stages de la neurogénèse de la rétine.

Les analyses indépendantes de perte de fonction d'*atxn7* réalisées par utilisation de morpholinos inactivant *atxn7* et de modèles mutés par CRISPR/Cas9 ont montré un rôle spécifique d'atxn7 dans la régulation de la fermeture de la fissure choroïde. L'analyse moléculaire du colobome oculaire a fortement mis en évidence que l'atxn7 régule

négativement la ligne médiane Hh. L'activité élevée de Hh de la ligne médiane comme conséquence du déficit en atxn7 a conduit à une tige optique étendue, reflétée par l'expansion du signal pax2a qui empêche la fermeture de la fissure choroïde, causant le colobome. Ceci a été confirmé par la rétraction correspondante du signal de pax6 et l'expansion du signal de vax2. De plus, l'altération de l'angle des somites supporte également l'hypothèse ?des variations dans la signalisation Hh.

Nous avons également démontré qu'atxn7 est indispensable à la morphogenèse complète des photorécepteurs qui semble indépendante de la voie de signalisation Hh. Nous prévoyons donc désormais d'élucider les fonctions additionnelles d'atxn7 dans la régulation du développement et de la neurogénèse embryonnaire de la rétine et du cerveau.

Bien que des études supplémentaires soient nécessaires à l'identification de gènes partenaires directs d'atxn7, notre étude réalisée au cours du développement oculaire ouvre de nouvelles voies pour l'étude du déficit en atxn7 dans la maladie chez l'Homme. Premièrement, nous avons démontré un défaut spécifique à l'œil prouvant une nette sensibilité de l'organe aux variations de la fonction d'atxn7 au cours de la morphogénèse oculaire. Dans un second temps, nous avons montré l'implication d'atxn7 dans la morphogenèse des photorécepteurs qui pourrait aider à expliquer la physiopathologie SCA7. De plus, la découverte d'un mécanisme de régulation entre atxn7 et la voie de signalisation Hh au cours du développement oculaire permet de désigner l'atxn7 comme le gène potentiellement causatif du colobome. Ceci serait pertinent dans la mesure où seuls quelques gènes causatifs du colobome ont été identifiés. Des études supplémentaires permettront de déterminer la ou les cible(s) directe(s) d'atxn7, et comment ces cibles affectent l'activité de la voie de signalisation Hh et le développement oculaire.

Pris tous ensemble, ces résultats permettent de suggérer que le déficit en atxn7 serait impliqué dans la rétinopathie SCA7 et serait un gène additionnel dans le réseau de gènes à l'origine de colobomes.

Références

Abou-Sleymane, G., Chalmel, F., Helmlinger, D., Lardenois, A., Thibault, C., Weber, C., Merienne, K., Mandel, J.L., Poch, O., Devys, D., Trottier, Y., 2006. Polyglutamine expansion causes neurodegeneration by altering the neuronal differentiation program. Hum Mol Genet 15, 691-703.

Benton, C.S., de Silva, R., Rutledge, S.L., Bohlega, S., Ashizawa, T., Zoghbi, H.Y., 1998. Molecular and clinical studies in SCA-7 define a broad clinical spectrum and the infantile phenotype. Neurology 51, 1081-1086.

Bibliowicz, J., Tittle, R.K., Gross, J.M., 2011. Chapter 7 - Toward a Better Understanding of Human Eye Disease: Insights From the Zebrafish, Danio rerio, in: Chang, K.T., Min, K.-T. (Eds.), Progress in Molecular Biology and Translational Science. Academic Press, pp. 287-330.

Chen, S., Peng, G.H., Wang, X., Smith, A.C., Grote, S.K., Sopher, B.L., La Spada, A.R., 2004. Interference of Crx-dependent transcription by ataxin-7 involves interaction between the glutamine regions and requires the ataxin-7 carboxy-terminal region for nuclear localization. Hum Mol Genet 13, 53-67.

David, G., Abbas, N., Stevanin, G., Durr, A., Yvert, G., Cancel, G., Weber, C., Imbert, G., Saudou, F., Antoniou, E., Drabkin, H., Gemmill, R., Giunti, P., Benomar, A., Wood, N., Ruberg, M., Agid, Y., Mandel, J.L., Brice, A., 1997. Cloning of the SCA7 gene reveals a highly unstable CAG repeat expansion. Nature genetics 17, 65-70.

David, G., Durr, A., Stevanin, G., Cancel, G., Abbas, N., Benomar, A., Belal, S., Lebre, A.S., Abada-Bendib, M., Grid, D., Holmberg, M., Yahyaoui, M., Hentati, F., Chkili, T., Agid, Y., Brice, A., 1998. Molecular and clinical correlations in autosomal dominant cerebellar ataxia with progressive macular dystrophy (SCA7). Hum Mol Genet 7, 165-170.

Hamel, C.P., 2007. Cone rod dystrophies. Orphanet J Rare Dis 2, 7.

Helmlinger, D., Hardy, S., Abou-Sleymane, G., Eberlin, A., Bowman, A.B., Gansmuller, A., Picaud, S., Zoghbi, H.Y., Trottier, Y., Tora, L., Devys, D., 2006. Glutamine-expanded ataxin-7 alters TFTC/STAGA recruitment and chromatin structure leading to photoreceptor dysfunction. PLoS Biol 4, e67.

Hoche, F., Seidel, K., Brunt, E.R., Auburger, G., Schols, L., Burk, K., de Vos, R.A., den Dunnen, W., Bechmann, I., Egensperger, R., Van Broeckhoven, C., Gierga, K., Deller, T., Rub, U., 2008. Involvement of the auditory brainstem system in spinocerebellar ataxia type 2 (SCA2), type 3 (SCA3) and type 7 (SCA7). Neuropathol Appl Neurobiol 34, 479-491.

Kohler, A., Schneider, M., Cabal, G.G., Nehrbass, U., Hurt, E., 2008. Yeast Ataxin-7 links histone deubiquitination with gene gating and mRNA export. Nat Cell Biol 10, 707-715.

La Spada, A.R., Fu, Y.H., Sopher, B.L., Libby, R.T., Wang, X., Li, L.Y., Einum, D.D., Huang, J., Possin, D.E., Smith, A.C., Martinez, R.A., Koszdin, K.L., Treuting, P.M., Ware, C.B., Hurley, J.B., Ptacek, L.J., Chen, S., 2001. Polyglutamine-expanded ataxin-7 antagonizes CRX function and induces cone-rod dystrophy in a mouse model of SCA7. Neuron 31, 913-927.

Lim, J., Crespo-Barreto, J., Jafar-Nejad, P., Bowman, A.B., Richman, R., Hill, D.E., Orr, H.T., Zoghbi, H.Y., 2008. Opposing effects of polyglutamine expansion on native protein complexes contribute to SCA1. Nature 452, 713-718.

Michalik, A., Martin, J.J., Van Broeckhoven, C., 2004. Spinocerebellar ataxia type 7 associated with pigmentary retinal dystrophy. Eur J Hum Genet 12, 2-15.

Raymond, S.M., Jackson, I.J., 1995. The retinal pigmented epithelium is required for development and maintenance of the mouse neural retina. Curr Biol 5, 1286-1295.

Sheedlo, H.J., Nelson, T.H., Lin, N., Rogers, T.A., Roque, R.S., Turner, J.E., 1998. RPE secreted proteins and antibody influence photoreceptor cell survival and maturation. Brain Res Dev Brain Res 107, 57-69.

Shen, Y.C., Raymond, P.A., 2004. Zebrafish cone-rod (crx) homeobox gene promotes retinogenesis. Dev Biol 269, 237-251.

Stenkamp, D.L., Frey, R.A., Mallory, D.E., Shupe, E.E., 2002. Embryonic retinal gene expression in sonic-you mutant zebrafish. Dev Dyn 225, 344-350.

Stevanin, G., Giunti, P., Belal, G.D., Durr, A., Ruberg, M., Wood, N., Brice, A., 1998. De novo expansion of intermediate alleles in spinocerebellar ataxia 7. Hum Mol Genet 7, 1809-1813.

Strauss, O., 2005. The retinal pigment epithelium in visual function. Physiol Rev 85, 845-881.

Yefimova, M.G., Messaddeq, N., Karam, A., Jacquard, C., Weber, C., Jonet, L., Wolfrum, U., Jeanny, J.C., Trottier, Y., 2010. Polyglutamine toxicity induces rod photoreceptor division, morphological transformation or death in spinocerebellar ataxia 7 mouse retina. Neurobiol Dis 40, 311-324.

Zhao, Y., Lang, G., Ito, S., Bonnet, J., Metzger, E., Sawatsubashi, S., Suzuki, E., Le Guezennec, X., Stunnenberg, H.G., Krasnov, A., Georgieva, S.G., Schule, R., Takeyama, K., Kato, S., Tora, L., Devys, D., 2008. A TFTC/STAGA module mediates histone H2A and H2B deubiquitination, coactivates nuclear receptors, and counteracts heterochromatin silencing. Mol Cell 29, 92-101.

Zoghbi, H.Y., Orr, H.T., 2000. Glutamine repeats and neurodegeneration. Annu Rev Neurosci 23, 217-247.

Samantha CARRILLO-ROSAS

Etude du rôle de l'Ataxine-7 dans le développement de l'œil et son impact dans la compréhension des pathologies de l'œil et de l'ataxie spinocérébelleuse de type 7.

Résumé

L'ataxie spinocérébelleuse de type 7 (SCA7) est une maladie neurodégénérative à transmission autosomale dominante, causée par une expansion toxique de polyglutamine (polyQ) dans la protéine Ataxine-7. Elle se caractérise par une dégénérescence des photorécepteurs en cônes et en bâtonnets, ainsi que des cellules cérébelleuses de Purkinje et granuleuses. La nature sélective de cette dégénérescence reste peu claire, l'expression d'Ataxine-7 étant ubiquitaire. Dans ce contexte, nous avons exploré la fonction de l'orthologue d'Ataxine-7 chez le poisson-zèbre au cours du développement de l'œil. L'inactivation d'*atxn7* chez le poisson-zèbre – par des approches utilisant des oligonucléotides anti-sens ou par CRISPR/Cas9 – résulte principalement en un colobome, malformation structurelle de l'œil causée par un défaut de fermeture de la fissure choroïde. Les morphants *atxn7* présentent une altération du motif proximo-distal de la vésicule optique causée par une élévation de la signalisation Hedgehog (Hh). Une étude minutieuse des photorécepteurs révèle un défaut de la morphogénèse des segments externes. La sensibilité de l'œil aux variations de fonction d'atxn7 pourrait expliquer la phyiopathologie SCA7. Notre étude suggère également qu'une perte de fonction d'*atxn7* contribuerait au développement du colobome chez l'Homme.

Mots-clés : Ataxie spinocérébelleuse de type 7, rétine, photorécepteurs, colobome, poisson-zèbre.

Résumé en anglais

Spinocerebellar ataxia type 7 (SCA7) is an autosomal-dominant neurodegenerative disorder caused by a toxic polyglutamine (polyQ) expansion in Ataxin-7 which leads to degeneration of cone and rod photoreceptors and cerebellar Purkinje and granule cells. The selective nature of degeneration remains unclear since Ataxin-7 is ubiquitously expressed. Here, we have explored the function of the Ataxin-7 ortholog in zebrafish during eye development. Inactivation of *atxn7* in zebrafish –through antisense oligonucleotides or crispr/cas9 approaches- primarily resulted in a coloboma defect, a structural malformation of the eye caused by failure of the choroid fissure to close. *atxn7* morphants displayed altered proximo-distal patterning of the optic vesicle, caused by elevated Hedgehog (Hh) signaling. Careful examination of the photoreceptors reveals a defect in the morphogenesis of the outer segments. The eye sensitivity to variations in atxn7 function could account for SCA7 physiopathology. Our study also suggests that *atxn7* loss of function may contribute to the development of human coloboma.

Key words: Spinocerebellar Ataxia type 7, retina, photoreceptor, coloboma, zebrafish